UTILIZATION OF GEOCELL-REINFORCED RAP MATERIAL BASE LAYER IN FLEXIBLE PAVEMENTS: EXPERIMENTAL AND NUMERICAL STUDIES

by

ANU MUTHUMALA GEORGE

Presented to the Faculty of the Graduate School of

The University of Texas at Arlington

in Partial Fulfillment of the Requirements

for the Degree of

DOCTOR OF PHILOSOPHY

THE UNIVERSITY OF TEXAS AT ARLINGTON

December 2018

This work is dedicated to my daughter, my lovely husband, and my beloved parents.

ACKNOWLEDGMENTS

This dissertation would not have been possible without the guidance and the help of several individuals who in one way or another contributed and extended their valuable assistance in the preparation and completion of this study.

First and foremost, I would like to express my utmost gratitude to my research advisor, Dr. Anand J Puppala for offering me the opportunity to pursue my doctoral research under his esteemed guidance. I am especially thankful to him for providing me with excellent research facilities and a very friendly working environment. I am indebted to him forever for his excellent guidance, invaluable remarks, motivation, and wholehearted support during the entire period of this research.

I would also like to convey my gratitude to Dr. Laureano R. Hoyos, Dr. Xinbao Yu and Dr. Erick Jones Sr. for their willingness to serve on my dissertation committee. I would like to thank them for their valuable advice and insightful comments.

Furthermore, I would like to thank the Department of Civil Engineering for their financial support through the GRA scholarships and graduate assistantships. I would also like to thank the University of Texas at Arlington. The work described in this dissertation was funded by the NSF I/UCRC and Texas Department of Transportation (TxDOT). Their financial support is gratefully acknowledged.

I would like to express my thanks to my colleagues Dr. Aravind Pedarla, Dr. Aritra Banerjee, Dr. Tom Taylor, Dr. Jasaswee Das, Dr. Sayantan Chakraborty, Dr. Ali Shafikhani, Dr. Santiago, Dr. Minh Hai, Dr. Sarath, Dany, Leila, Puneet, Rinu, and Manikanta for their sincere support and encouragement during this research work.

I would also like to express my heartfelt gratitude to my parents, George Kurian and Gracy George, for their love and inspiration all along. My sincere thanks are also extended to my brother and my in-laws for their continuous support and encouragement. A very special thanks to my husband, Thomson Varghese, for his unwavering support and encouragement throughout this work. Above all, I would like to thank God Almighty without whose blessings nothing would have been possible.

December 4, 2018

ABSTRACT

UTILIZATION OF GEOCELL-REINFORCED RAP MATERIAL BASE LAYER IN FLEXIBLE PAVEMENTS: EXPERIMENTAL AND NUMERICAL STUDIES

Anu Muthumala George

The University of Texas at Arlington, 2018

Supervising Professor: Dr. Anand J. Puppala

Reclaimed asphalt pavement (RAP) materials have been considered as one of the most sustainable and cost-effective options in the pavement industry. The use of RAP materials in pavement construction reduces natural resources depletion and the volume of construction debris discarded into the landfills. However, the low shear strength and high permanent deformation (PD) of RAP materials often limit their application in road bases. Utilization of mechanical stabilizers, such as geocell, for stabilizing RAP bases, have found to be effective in improving the pavement performance. The main objective of this study is to assess the efficacy of high-density polyethylene (HDPE) geocell reinforcements in enhancing the strength and stiffness properties of RAP bases and for mitigating PD behavior.

In this dissertation research, several large-scale static and repeated load tests were performed on the unreinforced RAP base (URB) and geocell-reinforced RAP bases (GRRB) over clay subgrade. The performance of the geocell reinforcement was evaluated based on various parameters including bearing capacity (q), elastic deformation (ED), PD, resilient modulus (M_r), traffic benefit ratio (TBR), and rut depth reduction (RDR). Test results showed that the HDPE geocell layer increased the M_r and reduced the PD of the RAP base layer when compared to URB.

Numerical models of the GRRB sections were developed to assess the load transfer mechanism of geocell reinforcement under static and dynamic loading. These models were developed in *FLAC*^{3D} software by employing finite-difference (FD) approach. The unreinforced and reinforced FD models were validated with experimental results and a good agreement between both was observed. The validated FD model was then used to perform parametric studies to assess the factors affecting the performance of geocell-reinforced bases.

Additionally, a life-cycle assessment (LCA) and life-cycle cost analysis (LCCA) were performed to estimate the current and future cost of the pavement section with GRRB. This analysis considered agency, user, environmental, and health impact costs incurred during the service life of the pavement section. Finally, an LCA-LCCA framework was developed to assess the sustainability of the pavement infrastructure using a sustainability index. The results showed that the GRRB can be successfully used as a sustainable and cost-effective replacement for virgin aggregate bases.

The findings from this research would aid in the development of design charts for assessing the response of geocell-reinforced pavement bases under static and repeated loading.

TABLE OF CONTENTS

LIST OF ILLUSTRATIONS

LIST OF TABLES

Chapter 1

INTRODUCTION

1.1 General

The scarcity of high-quality natural aggregates resulted in an ever-increasing demand for alternative recycled materials in the pavement construction such as quarried materials, reclaimed asphalt pavement (RAP) materials, and crushed concrete. Moreover, the rapidly increasing demand for fossil fuels and virgin raw materials is causing many environmental problems pertaining to the looming crisis of climate change from greenhouse gas (GHG) emissions (Yang and Wang 2015) necessitates an alternative option in pavement materials. Among the recycled alternatives, RAP is one of the most widely used sustainable and cost-effective option in the pavement industry (Papp *et al.* 1998).

RAP is the reprocessed pavement material obtained through pavement milling processes which generally contains asphalt and aggregates (Mulheron and O'Mahony 1990, Thakur *et al.* 2012a). The utilization of RAP in pavements construction preserve the natural aggregates, reduces the pavement construction costs, and also reduces the amount of pavement debris dumped into landfills (Williams *et al.* 2018). Efforts have been made by various DOTs and other federal agencies to increase the use of RAP materials in highway construction and rehabilitation projects to mitigate issues regarding storage and to encourage the use

of sustainable construction materials (Mokwa and Peebles 2005). According to Hansen and Copeland (2017), more than 76.9 million tons of RAP was put to use in new pavements in the United States during the year 2016.

The practice of utilizing an increased percentage of RAP in pavements can significantly decrease the release of greenhouse gas (GHGs) by reducing the energy required to manufacture the raw materials for the virgin mix (NAPA 2009). Also, the recycling of RAP curtails the amount of debris to be discarded and reduces the cost of construction materials by replacing the virgin aggregates. However, unbounded RAP is not suggested be used as a substitute for natural aggregates in pavement base layer due to its source-variability and inadequate strength and stiffness characteristics (Maher *et al.* 1997, Wilburn and Goonam 1998, Taha *et al.* 1999, Rana 2004, Kazmee *et al.* 2017). This necessitates the adoption of a cost-effective chemical or mechanical stabilization method for employing RAP in pavement bases.

Several researchers in the past have been studying the improvement in performance of pavement sections using RAP bases by mixing it with virgin aggregates or by treating it with chemical stabilizers such as lime, cement, and fly ash (Clary *et al.* 1997, Taha *et al.* 1999, 2002a, Bennert *et al.* 2000, Gnanendran, C. T., and Woodburn 2003, Potturi 2006, Potturi *et al.* 2007, Li *et al.* 2007, Attia and Abdelrahman 2010, Puppala, Hoyos, *et al.* 2011, Puppala *et al.* 2017, Hoyos *et al.* 2011, Mohammadinia *et al.* 2015, Avirneni *et al.* 2016, LaHucik *et al.* 2016).

These research studies confirmed that the virgin aggregate-RAP mix stabilized with cementitious additive can be effectively used in pavement base layer. However, blending RAP with virgin aggregates still consumes natural resources and the chemical treatment of RAP is not necessarily eco-friendly (Sambodh 2017). This necessitates the adoption of a sustainable and cost-effective mechanical stabilizer such as geogrid or geocell to enhance the performance of RAP bases.

Geosynthetic reinforcements, primarily geocell, have been widely used in pavements to provide structural support and stability to the pavement layers. The use of geocell in reinforcing base materials has been proven to increase the performance of the pavements by virtue of its three-dimensional honeycomb structure which offers lateral confinement to the infill material (Al-Qadi and Hughes 2000, Dash *et al.* 2007, Zhang, Zhao, *et al.* 2010, Han *et al.* 2011). Additionally, previous studies on stabilization of base materials using geocell indicate that geocell reinforcement enhances the performance of the RAP material by improving the strength and stiffness behavior (Pokharel *et al.* 2011, Bortz *et al.* 2012b, Thakur *et al.* 2012a).

However, most of these researches were limited to experimental studies on creep and permanent deformation behavior of geocell (novel polymeric alloy) reinforced RAP. Also, the source variability of RAP and the limited experimental studies on the resilient behavior of geocell-reinforced RAP bases (GRRB) demands an in-depth study in this area. Moreover, the lack of studies on the load transfer

mechanism of geocell-reinforced bases necessitates additional numerical studies to analyze the confining and beam bending mechanism of geocell reinforcement under static and repeated loading. This study also attempts the development of numerical prediction models based on the finite-difference (FD) approach for the geocell-soil system that can be used in the design and analysis of geocell-reinforced systems.

1.2 Problem Statement and Research Objectives

An extensive study to evaluate the effectiveness of high-density polyethylene (HDPE) geocell reinforcement in improving the strength and deformation properties of RAP bases was attempted by using experimental and numerical methods. The performance improvement of the RAP base due to geocell reinforcement was quantified in terms of bearing capacity (q), resilient modulus (M_r), permanent deformation (PD), and reduction in the required base thickness of the pavement section. The experimental evidence contemplated from this research pertaining to the utilization of GRRB in pavement infrastructure would enable the future development of design charts for geocell-reinforced pavements.

The major objective of this research is therefore to quantify the structural support offered by the geocell reinforcement by conducting a series of large-scale static and repeated load tests on unreinforced RAP base (URB) and GRRB sections. Numerical analysis of the geocell-reinforced bases was also carried out using an FD approach to assess the load transfer mechanism of the geocell reinforcement under static and dynamic loading. The FD based numerical models were validated

with the experimental findings to demonstrate a realistic approach for modeling geocell-reinforced pavements. The scope of the work also includes the development of an integrated life-cycle assessment and life-cycle cost analysis (LCA-LCCA) framework to assess the sustainability of the geocell-reinforced pavement infrastructure.

The dissertation is divided into six major tasks. The first task includes literature review, base and subgrade material selection and to perform preliminary tests on pavement base and subgrade materials. Simultaneously, the large-scale repeated load box test setup was designed and fabricated to successfully to perform repeated load tests. The large-scale box test setup was then calibrated and repeatability tests were performed to check for boundary effects and accurate functioning of the test setup under repeated loading. Preliminary tests including sieve analysis, specific gravity, Atterberg's limit, Proctor and modified compaction and the engineering tests including consolidated drained (CD) test and repeated load triaxial tests (RLTT) were also performed on the base and subgrade materials.

The second task involves a series of static and repeated load box tests on URB and GRRB over clay subgrade to assess the performance of GRRB. Parametric studies were also performed by varying the height of geocell, gradation of RAP, location of loading, and magnitude of loading to evaluate the effect of these parameters on the resilient behavior of GRRB.

The third task was to develop a numerical model to simulate the conditions within the large-scale experimental setup under the static and repeated loading conditions using an FD approach. Both unreinforced and geocell-reinforced test sections were modeled using an FD based software $FLAC^{3D}$ and these models were validated using the experimental results from the second task. The load transfer mechanism of the geocell reinforcement under static and repeated loading was analyzed using the numerical model. Parametric studies were also performed to evaluate the factors influencing the performance of geocell-reinforced RAP system.

The fourth task includes the performance assessment of GRRB under static loads in terms of bearing capacity and repeated loads in terms of M_r and PD, required pavement base thickness, and rutting and fatigue life of the designed pavement. The fifth and final task comprised of the development of an LCA-LCCA framework for assessing the sustainability of the pavement infrastructure.

Figure 1.1 illustrates the flow chart for the major tasks involved in the implementation of research methodology.

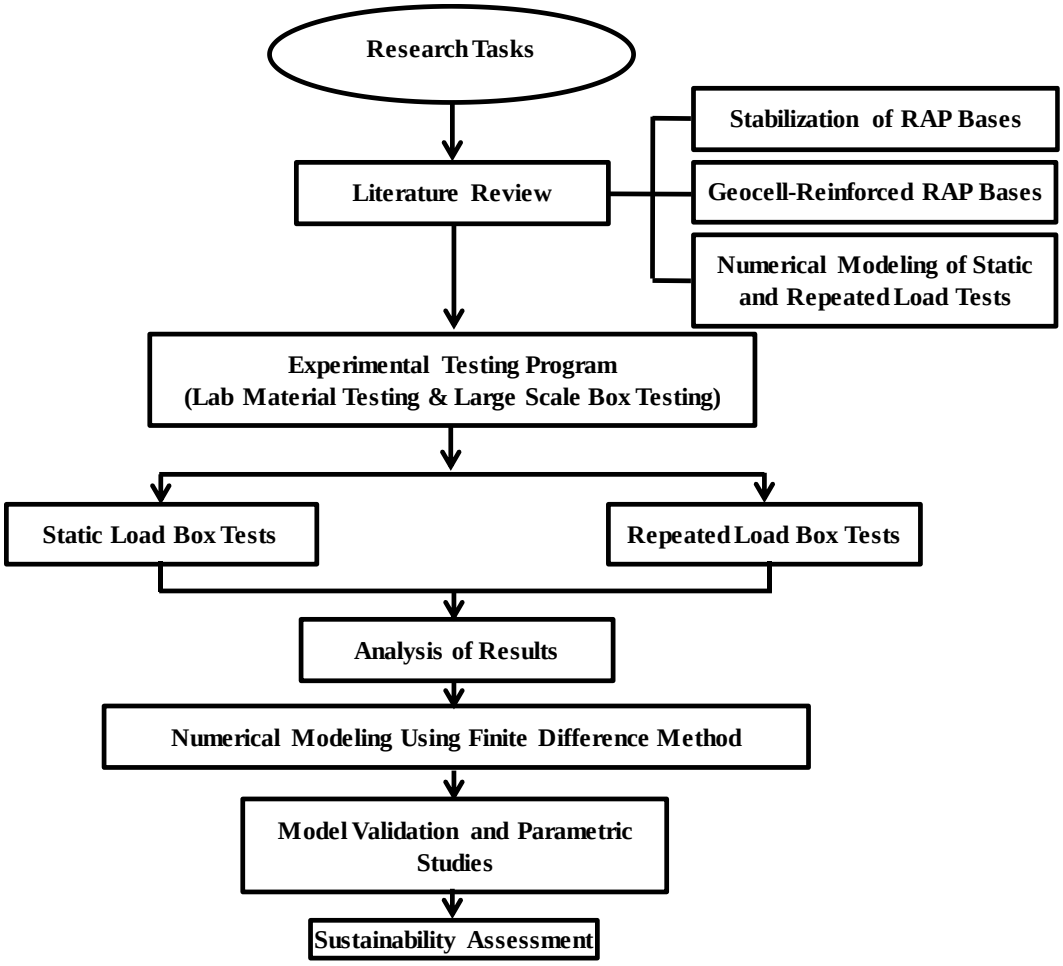

Figure 1.1 Flowchart for the major tasks involved in the research

1.3 Organization of Dissertation

The dissertation is divided into seven chapters.

The first chapter deals with the introduction to the necessity of using RAP in the pavement bases and describes the significance of stabilizing RAP with a mechanical stabilizer such as geocell. Also, the primary research objective and the

major tasks performed for implementing the research methodology are also discussed in this chapter.

Chapter 2 comprises a brief summary of the requirement for RAP usage in the United States and the potential issues of its usage in untreated or unstabilized form. The chapter also gives an overview of the studies on reclaimed asphalt pavement (RAP) materials primarily emphasizing on the properties and stabilization methods adopted by previous researchers. It also includes the prior studies on the geosynthetic reinforcement especially geocell reinforcement under static and repeated loading. A review of the literature was also conducted on the analytical and numerical models of geocell reinforcement in the foundations and pavements.

Chapter 3 includes a detailed description of the basic and engineering laboratory studies performed on the base and subgrade materials, such as sieve analysis, Atterberg's limit, Proctor and modified compaction, unconfined compressive strength test (UCS), CD test, and RLTTs. This chapter also discusses the equipment design and installation of large-scale laboratory testing for performing static and repeated load testing on unreinforced bases and GRRB.

Chapter 4 deals with the model development of large-scale laboratory box test setup using an FD approach for performing static and repeated load testing. The models were developed in *FLAC*^{3D} software and were validated using the experimental data. The validated model was used to analyze the load transfer

mechanism of the geocell reinforcement. Parametric studies were also carried out to investigate the factors influencing the improvement in performance of geocell reinforcement under static and repeated loads.

Chapter 5 discusses the performance improvement of geocell-reinforced footing in terms of bearing capacity and pavements in terms M_r, PD, reduction in pavement base thickness, and fatigue and rutting life of the designed pavement section.

Chapter 6 caters to the development of an integrated LCA-LCCA framework for analyzing the sustainability of pavements in terms of a sustainability index. A one-mile test section at Venus, Texas was selected for the study. Both LCA and LCCA of the pavement sections were evaluated separately to estimate the total cost of the pavement section including user, agency, health impact, and environmental impact costs. Finally, a sustainability index was developed to analyze the sustainability of the pavement section among other alternatives.

Chapter 7 provides a summarizes the major conclusions obtained from the research and offer recommendations for future research in the field of mechanically stabilized pavements using geocell reinforcement.

Chapter 2

LITERATURE REVIEW

2.1 Introduction

In recent years, the reclaimed asphalt pavement (RAP) material and geosynthetic reinforcement have been extensively used in pavement construction as a sustainable and cost-effective alternative for the conventional natural aggregates. The use of geosynthetic reinforcement, especially, geocells enhance the performance of the RAP base by improving the strength and deformation characteristics. Thereby, reducing the required base thickness and prolonging the pavement service life.

This chapter provides a detailed of the literature on reclaimed asphalt pavement material, use of geosynthetic reinforcement especially geocells in pavement base/subbase applications, and the large-scale static and repeated load box tests studies on geocell-reinforced base sections. The previously developed numerical, empirical, and damage models for predicting the performance of geocell-reinforced test sections in terms of bearing capacity, M_r, PD, and thickness reduction of the reinforced base layer are also reviewed. The chapter also focuses on the recent studies on life-cycle assessment (LCA) and life-cycle cost analysis (LCCA) methods used in the pavement infrastructure. Moreover, the findings and limitations of the previous researches are also examined in this chapter.

2.2 Reclaimed Asphalt Pavement Material

With the changes in the economics of pavement construction materials, stringent environmental guidelines, and an emphasis on sustainable pavement practices, the Federal Highway Administration (FHWA) is now highly favoring the use of a higher percentage of RAP material in asphalt pavement applications (Copeland 2011). The asphalt materials removed from the existing pavements during the rehabilitation and reconstruction activities are processed and reused as reclaimed asphalt pavement (RAP) materials. RAP materials are most commonly used as a sustainable and cost-effective substitute for conventional virgin aggregates in pavement construction.

The use of RAP material in pavements curtails the use of virgin aggregate in the pavement construction, which may not be locally available. Also, the reuse of RAP in the pavement bases significantly lower the construction debris dumped into the landfills, and it also prevents the depletion of nonrenewable natural resources. Ultimately, recycling asphalt pavement material develops a sustainable asphalt pavement industry by building a cycle of reuse that optimizes the natural resource consumption (Copeland 2011).

2.2.1 *Current Production and Use of RAP*

Recycling of materials from asphalt pavements dates to 1915s, however, it started getting prominence in the early 1970s when Arab Oil Embargo caused inflation of asphalt binder prices in 1973 (Kandhal and Mallick 1997). Today, the

asphalt industry is one of the most diligent industry, reusing more than 99% of RAP material back into pavement applications (Williams *et al.* 2018). The average estimated tonnage of RAP usage in asphalt pavements in 2017 was 76.2 million tons (Williams *et al.* 2018). Figure 2.1 show the average percentage of RAP material reused in the pavement construction during the year 2017. In Texas, the RAP use is about 15-19% due to the restrictions of using 100% unstabilized RAP material in the pavement bases.

A study by Collins and Ciesielski (1994) reported the use of unbound RAP materials in pavement applications, with grading as the limiting factor for usage. The study also graded the performance of pavement with RAP base or subbase course as satisfactory to excellent. A similar study by Saeed 2007 reported that some of the US DOTs allow 100% unstabilized RAP material in pavement bases. The comparison of the amount of RAP accepted, used for hot mix asphalt (HMA) and base/subbase applications, and the amount of RAP landfilled is shown in Figure 2.2.

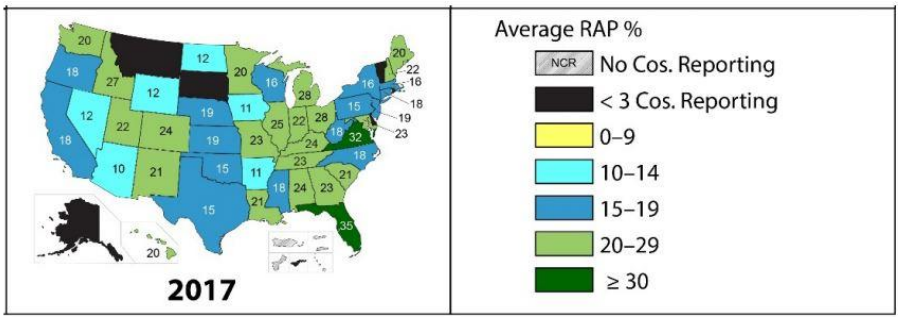

Figure 2.1 Average percentage of RAP used in pavement construction during the year 2017 (NAPA 2018)

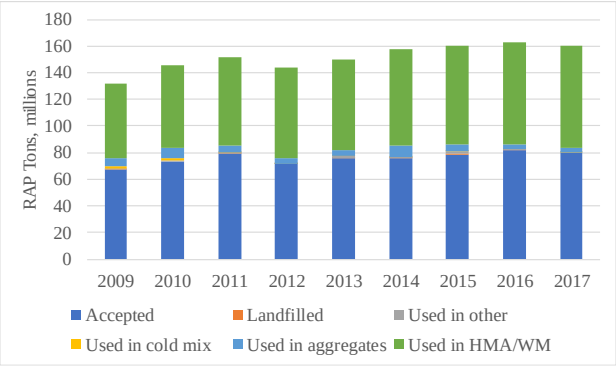

Figure 2.2 Comparison of RAP accepted, used and landfilled (Million Tons) (modified from NAPA 2018)

The utilization of recycled construction materials in pavement infrastructure has become a sustainable means for environmental benefits and economic savings (Kennedy *et al.* 1998, Wright, Jr. 2001). A significant economic saving in the pavement construction was reported by many state DOTs with the use of RAP bases (Page and Murphy 1987, Ayers 1992, Munzenmaier 1994). The use of RAP in highways and other pavement infrastructures aids in sustainable and cost-effective pavement construction, reduce the usage of conventional virgin aggregates in pavement bases, and minimize the volume of construction debris disposed into the landfills.

2.2.2 *Characteristics of RAP*

The performance of the pavement with RAP bases depends on the physical, chemical, and mechanical properties of the RAP material used in pavement base/subbase. The aggregate type, asphalt binder content and grade, type of pavement, service life of the asphalt pavement from which the RAP was milled,

method of recovery at the site, and method of processing are the main factors that determine the behavior of RAP material. In this section, a comprehensive review of the literature on the physical, chemical, and mechanical properties of RAP material is presented.

2.2.2.1 Physical Properties of RAP Material

The physical properties of RAP material are susceptible to the behavior of RAP reclaimed from the existing pavement section. These include particle gradation, specific gravity, asphalt content, unit weight, and moisture content of the RAP material (Kassim *et al.* 2005, Al-Qadi *et al.* 2007, Arulrajah *et al.* 2014). The RAP gradation is similar to the conventional crushed aggregates, though it is dependent on the milling and stockpiling operations during reclamation. The crushing and milling operations performed on reclaimed RAP material result in degradation of the aggregates. Milled RAP material contains more fines and binder content which results in higher density compared to the virgin aggregates (Chesner *et al.* 1998).

The unit weight of RAP is susceptible to variation in moisture content and aggregate type used in the pavement from which the RAP is reclaimed. From the literature, the unit weight of RAP material (milled or crushed) was found to be 9.4 to 23 kN/m^3 (Smith 1980, Kassim *et al.* 2005). The amount of in-situ rainfall and the duration of RAP storage affects the moisture content of RAP significantly and can vary from 5% to 8% (Smith 1980, Decker and Young 1996). RAP exhibit a

higher permeability than conventional virgin aggregates (Edil *et al.* 2012) and the permeability of RAP blends increased with the increased percentage of asphalt millings (Mokwa and Peebles 2005).

Research studies to estimate the asphalt content and viscosity of the asphalt binder reclaimed from the RAP reported that the asphalt content of the RAP material is about 2.2% to 12.9% for the milled RAP and 5.1% to 7.2% for the crushed RAP (Sandin 2008, Cosentino *et al.* 2012). The penetration resistance and viscosity of asphalt binder recovered from the RAP are susceptible to the age of pavement from which the RAP material is reclaimed. Generally, the viscosity of asphalt binder varies from 4,000 to 25,000 poises, and the penetration resistance of asphalt binder is approximately 80 (Epps 1990, Chesner *et al.* 1998).

2.2.2.2 Chemical Properties of RAP Material

The chemical properties of the RAP material influence the performance of the pavement with RAP bases. The major chemical properties of RAP include pH, chemical reactivity, chloride level, solubility, and surface charge. The major constituent of RAP is aggregate which amounts to 93% to 97% by weight and the remaining asphalt cement constitutes about 3% to 7%. Asphalt cement consists of asphaltenes and maltenes that contain aliphatic and polycyclic hydrocarbon compounds (Chesner *et al.* 1998). Asphaltenes are produced during the oxidation of aged asphalt cement. This will result in hardening of asphalt cement over time which will, in turn, increase the viscosity of the asphalt cement (Noureldin and

Wood 1989; Roberts *et al.* 1996). These changes in chemical properties of RAP material will modify the base layer stiffness and possibly reduce the resistance to rutting and fatigue cracking of the HMA layer (Hoppe *et al.* 2015).

2.2.2.3 Mechanical Properties of RAP Material

The mechanical properties of RAP mainly include compacted unit weight, M_r, and California bearing ratio. These properties generally susceptible to the pavement type from which the RAP is milled, the milling process adopted for reclaiming the RAP material, and the method used to process the RAP material (Senior *et al.* 1994). From the literature, the maximum dry density varies from 1600-2000 kg/m^3, and the California bearing ratio (CBR) is approximately 20-25% for the RAP material(Hanks and Magni 1989, Senior *et al.* 1994).

The asphalt binder on the RAP material minimizes the required moisture content to attain the desired dry density. (Stroup-Gardiner and Wattenberg-Komas 2013). Several studies on the effect of RAP percent in the RAP-aggregate blend on the maximum dry density (MDD) and optimum moisture content (OMC) showed that the MDD and OMC of the blend increased with increase in RAP percent (Guthrie *et al.* 2007; Locander 2009). These studies also concluded that the OMC required to achieve the desired compaction reduced with an increase in the percentage of RAP in the RAP-aggregate blend.

Unbounded RAP material possesses exceptional M_r as compared to conventional virgin aggregates. Though the stiffness of RAP is higher than the

dense-graded virgin aggregates, the amount of PD developed on unbounded RAP material was found to be excessive in contrast to the dense-aggregates (Bennert *et al.* 2000). The contradiction between the resilient and permanent deformation behavior of unbounded RAP can be attributed to the continuous breakage of asphalt binder when the RAP material is subjected to the repeated loading (Bennert *et al.* 2000, Dong and Huang 2014). The subsequent studies on RAP material to evaluate the influence of a higher RAP percent on CBR ratio showed a reduction in CBR ratio (Ayan *et al.* 2014).

The literature study on the physical, chemical and mechanical properties of the RAP material revealed that the unbounded RAP possesses a contrasting behavior of superior M_r with excessive PD behavior in contrast to the dense-graded aggregates. The exceptional M_r of the RAP material allows the use of RAP material as a pavement base course, provided that the PD is regulated within the allowable limits. This demands the adoption of some stabilization techniques to improve the PD behavior of the RAP bases. The utilization of RAP in pavement bases and the stabilization techniques adopted by previous researchers for achieving this are discussed in detail in the subsequent sections.

2.2.3 *Performance of RAP as a Pavement Base Material*

The demand for sustainable and environment-friendly pavements resulted in the utilization of recycled materials such as RAP in pavement layers, especially as surface and base layer. Recycled materials have seen increasingly used in the

pavement construction in the past years and several state DOTs have performed numerous investigations to evaluate the performance of these materials under traffic loading (Mokwa and Peebles 2005). Since most agencies do not allow a higher percentage of RAP material in the surface layer, and to avoid issues with storage of RAP for an extended period, many studies were conducted on the utilization of RAP in pavement base/subbase applications. Mainly, three stabilization methods are adopted for utilizing RAP materials in pavement bases such as blending with aggregates, chemical stabilization, and mechanical stabilization. The stabilization methods for RAP material is discussed in detail in the following sections.

2.2.3.1 Blended RAP-Aggregate Bases

Properly processed RAP, blended with conventional aggregates has proven to perform satisfactorily as pavement base for more than 20 years and is currently adopted as a standard practice in the United States. Studies have been performed to evaluate the effectiveness of RAP material as a pavement base course by constructing actual pavement sections at Lincoln Avenue (Garg and Thompson 1996). The tests demonstrated the successful application of RAP as an alternative to conventional crushed stone aggregate bases.

The effect of RAP material on the layer and drainage coefficients of the base aggregates were studied by performing M_r and permeability tests, respectively (MacGregor *et al.* 1999). No significant change in the permeability of the base

course was observed with the addition of RAP, whereas an increase in M_r was observed with higher RAP content. Similar improvements in the M_r of the base layer were also observed by various researchers on using blends of RAP and aggregates (Bennert *et al.* 2000, Cosentino *et al.* 2003, 2012, Attia and Abdelrahman 2010). The M_r of RAP material was observed to be higher than the conventional crushed stone aggregates.

The studies attempted to assess the shear strength parameters including cohesion and friction angle of the unbounded RAP and blended RAP-aggregate specimens reported a friction angle around 44° to 52° for unstabilized RAP material. The cohesive strength of the unstabilized RAP was in the range 0 to 130 kPa (Garg and Thompson 1996, Cosentino *et al.* 2003, Bennert and Maher 2005, Kim and Labuz 2007, Attia and Abdelrahman 2010). The cohesion observed for the RAP material was associated with asphalt binder content present in the RAP material that holds the aggregates together in the mixture (Thakur and Han 2015). Furthermore, the increased RAP percent contributed to increased PD behavior of the RAP-aggregate blend that can also be associated with the presence of increase asphalt binder content (Thakur and Han 2015).

The results from the laboratory studies on RAP-aggregate blend reported the feasibility of using the RAP-aggregate blend as an alternative to conventional aggregate in road base/subbases (Taha *et al.* 1999). The results also showed a decrease in CBR ration at higher RAP percent. The study encouraged to limit the

utilization of RAP material in pavement construction to 10% when blended with virgin aggregates (Taha *et al.* 1999). Similar studies on the RAP-aggregate blends reported CBR values of 11-33% for unstabilized RAP and concluded that it can be effectively used as a pavement base course (Bennert and Maher 2005, Cosentino *et al*. 2012, and Guthrie *et al.* 2007).

Several studies on the application of RAP-aggregate blends in pavement bases recommended that the 100% RAP material cannot be permitted in the pavement bases due to its excessive PD behavior (McGarrah 2007; Dong and Huang 2014). A reduction in the shear strength of RAP-aggregate blend was observed with an increase in RAP content. McGarrah suggested limiting the RAP content in pavement bases by 25% and employing a mixing plant for blending the aggregate and RAP material. Similar studies by Schaefer *et al.* (2008) suggested a limiting value of 20% to 50% RAP content in the pavement bases.

More recent studies on blended RAP-aggregate showed the feasibility of using RAP in the pavement base layer, where the stiffness and strength properties of the RAP is higher than unbound conventional base aggregates (Locander 2009). These studies also showed that the usage of RAP in pavement base applications are beneficial and no major environmental concerns appeared to be related to using unbound RAP without chemical stabilization agents (Hoppe *et al.* 2015). However, the method involves the addition of natural aggregates to the RAP material still utilizes non-renewable resources and the availability of numerous low-cost

stabilization techniques using chemical stabilizers lead the way to use these methods in stabilizing RAP base. A detailed literature of the chemically stabilized RAP bases in pavements is presented in the following section.

2.2.3.2 Chemically Stabilized RAP Bases

The chemical stabilization methods have been successfully used for treating clayey soils for various applications, including pavement subgrade and slopes, for decades (Mohammad *et al.* 1995, Puppala *et al.* 2003, 2013, 2014, Puppala and Cerato 2009, Pedarla *et al.* 2011, Puppala, Manosuthkij, *et al.* 2011, Sirivitmaitrie *et al.* 2011, Caballero *et al.* 2016, He *et al.* 2018). The initial studies on chemically stabilized RAP bases were undertaken by constructing pavement sections with a fly ash stabilized RAP bases on Kansas Route 27 and the performance was monitored periodically using Falling Weight Deflectometer Wu (1999). The results from the study showed that fly ash stabilization reduced the rutting behavior of the pavement section significantly as compared to untreated RAP section.

Laboratory studies on RAP treated with cement and the RAP-aggregate blend using Type I Portland cement reported an increase in OMC, MDD, and the compressive strength of RAP material with an increase in cement and aggregate proportions (Taha *et al.* 2002b). Longer curing period yielded higher strength results. In a subsequent study using cement kiln dust as the stabilizer, similar trends were observed with respect to improvement in strength and deformation behavior. (Taha 2003).

Several engineering tests were performed by Gnanendran, C. T., and Woodburn (2003) on chemical stabilized RAP material to assess the effectiveness of chemical stabilization in terms of resilient and elastic modulus. RLTTs on cement and polyethylene fiber treated RAP aggregates from Dallas region, showed a steady increase in modulus of the RAP from 200 MPa to 350 MPa (Ordonez 2006; Potturi *et al.* 2007; Puppala *et al.* 2009; Hoyos *et al*. 2011; Puppala *et al.* 2011). The test results from 7, 14, and 21 days cured fly ash stabilized RAP specimens also reported a direct correlation between M_r and the curing period of the samples (Li *et al.* 2007, Wen *et al.* 2008, 2010, Camargoa *et al.* 2013).

The results from the laboratory evaluation of reconstituted coal ash (RCA) and RAP stabilized with coal fly ash and coal bottom ash showed a higher CBR value for soaked samples compared to unsoaked samples. The study suggested the use of reconstituted coal ash stabilized RAP proportion of 40%RCA + 60%RAP and 10%RCA + 90%RAP with a CBR of 66-60% (soaked for 24 hours) for base/subbase applications in pavement construction (Osinubi and Edeh 2011).

In a subsequent study, Osinubi et al. (2012) evaluated the characteristics of RAP stabilized with sawdust ash and was found to be effective for base/subbase applications. Studies on 2–3% cement stabilized RAP material reported an upsurge in the creep strength of RAP material (Bleakley and Cosentino 2013). Similar research studies on the strength and deformation properties of fly ash stabilized RAP-aggregate blend confirmed the feasibility of using fly ash stabilized RAP in

low-volume roads (Saride *et al.* 2010, George and Saride 2014a, 2014b, Saride, Avirneni, *et al.* 2015, Saride, George, Avirneni, *et al.* 2017).

Long-term durability investigation on geopolymer and cement stabilized RAP material as pavement bases showed a minimal reduction in strength of stabilized RAP material and recommended the utilization of stabilized RAP in pavement base/subbase applications (Ganne 2009, Avirneni et al. 2016). A similar research by Puppala et al. (2017) on cement/fly ash treated RAP material exhibited a low volumetric change and good retaining strength after 3^{rd}, 7^{th}, and 14^{th} cycles of durability test. The leachate tests on stabilized RAP mix demonstrated that the leaching of chemical stabilizers from treated RAP cannot affect the long-term efficiency of pavement bases (Puppala et al. 2017).

The main concern with the use of chemical additives in stabilizing RAP material is the environmental impacts such as contamination of water bodies, increases pH on the surrounding area, and limited vegetation (Chang *et al.* 2015, Sambodh 2017). The chemically treated RAP base can contaminate the water bodies and can increase the pH on the surrounding area. To overcome this issue, a stabilization method utilizing geosynthetic reinforcements such as geogrid and geocell were adopted for improving the performance of RAP material. The following sections briefly discuss the previous studies on geosynthetic reinforcements especially geocells and its application in stabilizing RAP bases.

2.3 Geosynthetic Reinforcement

Geosynthetic materials have been progressively used for reinforcing pavement base/subbase layers in recent years. One of the earliest uses of geosynthetic materials in pavement construction dates to 1920s when a woven cotton fabric was used to stabilize the subgrade of an unpaved road in South Carolina (Beckham and Mills 1935, Koerner 2016). The use of geosynthetics placed at the interface of the base layer and subgrade can increase the service life and reduce the required thickness of the pavement (Giroud and Han 2004a, 2004b). The widely used geosynthetic reinforcements in pavement bases are geogrid and geocell. A comprehensive review of previous research on the planar geosynthetics is presented in this section.

There had been extensive and wide research on implementation of planar reinforcement in various areas such as embankments, pavements, slopes, retaining walls and railroads by various researchers (Das *et al.* 1996, Adams and Collin 1997, Gabr *et al.* 1998, Alawaji 2001, Kumar and Saran 2001, Shin *et al.* 2002, Yamamoto and Otani 2002, De Merchant *et al.* 2002, Boushehrian and Hataf 2003, Michalowski 2004, Patra *et al.* 2005, Brown *et al.* 2007, Indraratna *et al.* 2013, Nair and Latha 2014, Miyata *et al.* 2015, Tafreshi *et al.* 2016, Tavakoli Mehrjardi *et al.* 2016, Wang *et al.* 2016, Das 2016, Suku *et al.* 2017, Cardile *et al.* 2017, Esmaeili *et al.* 2017). The use of first non-biodegradable geosynthetic reinforcement started in the mid of 1960s by the invention of reinforced earth technique by the French

architect Henri Vidal for the construction of retaining walls. Horizontal metal strips were used for reinforcing the granular backfill which resulted in a significant reduction of the lateral earth pressure on the retaining wall (Holtz 2004, 2017).

Several model tests on strip and square footings reinforced with aluminum foils/strips on the homogeneous sand reported an increased bearing capacity with an increase in the reinforced layers (Akinmusuru and Akinbolade 1981; Binquet and Lee 1976). The study also suggested a cover thickness of 0.05 times the width of the footing to maximize the performance of a reinforced bed (Akinmusuru and Akinbolade 1981). Similar laboratory model studies on rectangular steel footing over sand, reinforced with aluminum strips concluded that the bearing capacity is independent of sand density at higher settlement ratios (>10%). The study also recommended an optimum length of 7B (B is the width footing) for the aluminum strips (Fragaszy and Lawton 1984). The bearing capacity improvement studies on geogrid reinforced earth slabs reported a higher bearing capacity spacing between consecutive geogrid/geotextile reinforcements are minimum. The increase in bearing capacity was directly proportional to the tensile strength of tensile strength and aperture opening size of the geogrid reinforcement (Guido et al. 1986)

Similar model box tests were performed over sand subgrade reinforced vertically with galvanized rods and the results concluded that the bearing capacity was found to be a function of length and spacing of the reinforcement (Verma and Char 1986). Similar studies on the ultimate bearing capacity of the strip and square

footings over geogrid reinforced sand beds suggested a maximum width of 8B for geogrid layers. The critical depth of geogrid reinforcement was found to be 1.4B-2B (Omar et al. 1993, Pincus et al. 1993). Despite all the studies on geogrid reinforcement, to the author's knowledge, there is no available literature on geogrid-reinforced RAP material for the pavement base applications. This might be due to the advancement of three-dimensional geosynthetic reinforcements that can provide additional lateral confinement to the infill material thereby improving the performance of the infill material significantly. The following section discusses in detail about the geocell reinforcement and its applications in pavement infrastructure.

2.4 Geocell and its Application in Pavements

With the studies on planar geosynthetics proving its mettle, the studies on a three-dimensional honeycombed geosynthetic structure namely geocell are introduced considering the lateral confinement as the major reinforcement mechanism for ground improvement. The notion of a cellular confinement system was first adopted and implemented by the U.S. Army Corps of Engineers in the late 1970s (Webster 1979a). From then on, the cellular confinement systems or geocell reinforcements has been progressively used for reinforcing base layer to confine the infill material in roadway construction.

The predominant mechanisms of geocell reinforcement include lateral resistance effect, vertical stress distribution, and membrane mechanism as in Figure

2.3 (Sitharam and Hegde 2013, George 2015, Saride, George, V, *et al.* 2017a). Hoop stresses are mobilized in the geocell pockets under traffic loading which confine the infill material resulting in an increase in the strength and stiffness of the soil-geocell composite (Sitharam and Hegde 2013). In addition, the geocell-reinforced base layer acts as a stiff mattress under vertical loading and distribute the stresses developed laterally over a wider area. This result in the reduction of stresses transferred to the subgrade thereby increasing the bearing capacity (Dash 2011).

The falling weight deflectometer results on the geocell-reinforced field test sections showed a reduction of 30% in vertical stresses at the bottom of geocell layer, 15% reduction in vertical deformation, and 10 % increase in the layer modulus when reinforced with geocell (Emersleben and Meyer 2008, 2010). The test results also showed an increase in the M_r of the pavement base by two times as compared to unreinforced test section due to the additional confinement imparted by the geocell reinforcement. (Al-Qadi and Hughes 2000). A comprehensive literature study on the geocell-reinforced pavement bases is the key focus of this section. The section is subdivided into three sub-sections namely experimental studies on geocell-reinforced bases under static load condition, experimental studies on geocell-reinforced bases under dynamic load condition, and experimental studies on GRRB.

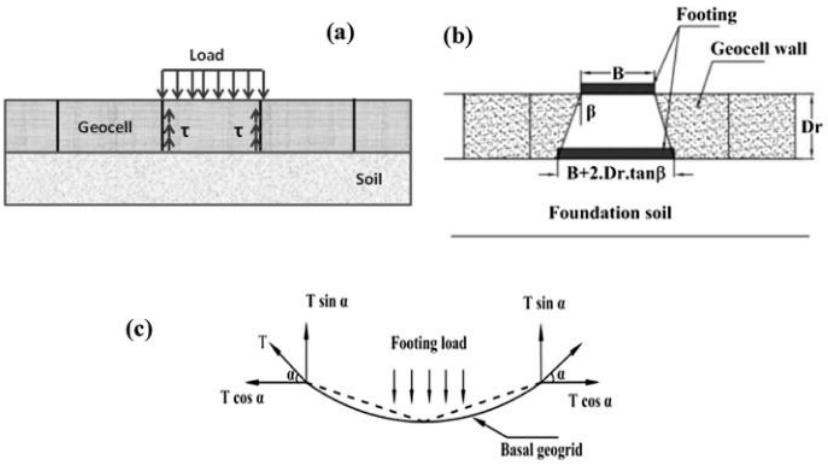

Figure 2.3 Load transfer mechanism of geocell reinforcement (a) lateral resistance effect, (b) vertical stress distribution, and (c) membrane mechanism (Source: Hegde and Sitharam 2013)

2.4.1 *Experimental Studies on Geocell-Reinforced Bases Under Static Loading*

Webster and Watkins (1977) carried out tests on unpaved test sections to assess various reinforcement techniques and found that the sand base layer reinforced with plastic cellular confinement performed better in terms of reduction in rut depth than the unreinforced crushed stone base section under traffic loading. The plastic and aluminum cells used in this study are shown in Figure 2.4. Later, full-scale field tests were carried out to examine the factors affecting the performance of these cellular confinements using aluminum grid of different shapes namely rectangular, square, and hexagonal (Webster 1979). The results concluded that the pavement base reinforced with hexagonal aluminum grid performed better than the square and rectangular grids.

Figure 2.4 Plastic and aluminum cellular confinements used at Waterways Experiment Station, Vicksburg (Source: Presto Geosystems)

Laboratory tests performed to evaluate the factors influencing the behavior of three-dimensional interconnected geogrid-cells reinforced sand showed that the dimensions and material of the grid, stiffness of subgrade, compaction, and type of loading has a major role in improving the performance of the reinforced test section. The researchers observed that the optimum h/d ratio (geocell height to pocket diameter ratio) was approximately 2.25. The study also suggested an optimum footing diameter to the cell width ratio of 1.5 to 2 (Rea and Mitchell 1978).

Large-scale plate load tests on strip footing over geocell-reinforced soft marine clay to evaluate the pressure-settlement characteristics of reinforced soil showed an increase in bearing capacity with an increase in geocell pocket diameter at the cost of the higher settlement. Geotextile was used to form the three-dimensional geocell pockets in this study (Mandal and Gupta 1994). The study recommended the use of smaller geocell size for low settlement structures (paved roads) and larger geocell size for large settlement structures (unpaved roads).

Triaxial test results on sand samples reinforced with single and multiple hand-made geocells made of woven and non-woven geotextiles showed that the soil specimen reinforced with geocell reinforcement has developed a higher apparent cohesion due to the confinement offered by the geocell reinforcement. The results of the study also recommended that the use of a minimum of three interconnected geocell pockets during testing to accurately evaluate the apparent cohesion due to geocell reinforcement. The study also provided a simplified method to estimate the apparent cohesive in terms of geometric and material properties of the geocell (Rajagopal et al. 1999). The significance of individual parameters such as size of the geocell pocket, material stiffness of geocell, and type of infill material on the improvement in performance of the embankments was investigated by several researchers by performing laboratory tests. These studies confirmed the beneficial effects of geocell reinforcement in enhancing the bearing pressure and minimizing the deformation of the embankment (Krishnaswamy et al. 2000, Latha et al. 2006).

Static load tests on strip footing over geocell-reinforced sand exhibited a substantial increase in the bearing capacity of the foundation (Dash et al. 2001). The results from the subsequent model studies on a circular footing also showed an increased bearing pressure and minimal surface heaving with the geocell reinforcement. The study also observed an enhancement in the strength and stiffness of the test bed with the presence of geogrid reinforcement below the

geocell layer (Dash et al. 2003). Similar studies on the square footing over geosynthetic reinforced foundation beds reported a rise in bearing capacity of the infill material by 3 times and nearly 30% vertical stress reduction on the subgrade surface with geocells (Biswas et al. 2016, Latha and Somwanshi 2009, Emersleben and Meyer 2008).

The test results from several large-scale static load box tests on a circular foundation suggested the use of an additional planar geosynthetic reinforcement such as geogrid to serve as an additional support to the geocell-reinforced test section (Sitharam et al. 2005, Sireesh et al. 2009). A continuation study by Sitharam et al. (2007) on geocell-reinforced weak clay also showed a substantial improvement in the performance of geocell-reinforced foundation system. Researchers observed approximately 40% reduction in the settlement and 3000% increment in subgrade reaction coefficient with the geocell-reinforced sand on soft subgrade (Zhou and Wen 2008). The load-deformation behavior of multiple geocell pockets under the uniaxial loading reported an increase in strength and stiffness properties of the geocell-soil composite with a reduction in geocell pocket diameter (Wesseloo et al. 2009).

The static load model tests performed by Pokharel et al. (2009a) to evaluate the effectiveness of geocell-reinforced pavement bases showed an increase in the bearing capacity of the geocell-reinforced base layer by a factor of 1.78 as compared to the unreinforced case. In a subsequent research by Pokharel et al.

(2009b) to examine the factors influencing geocell-reinforced sand and observed a higher performance with the circular shaped geocell as compared to the elliptical shaped geocell. A similar study on the strip footing over geocell-reinforced sand beds concluded that the geocell reinforcement under the combination of static and repeated loading offer a substantial increase in the performance over the geotextile reinforcement (Tafreshi and Dawson 2010).

Lambert et al. (2011) assessed the response of a wire netted geocell to uniaxial compression loading in the presence of different infill material namely sand, scrap tire, and the mixture of sand and scrap tire. It was observed that the axial load carrying capacity was governed by the interaction between the geocell reinforcement and the infill material. The researchers found that the contracting infill materials (scrap tire) significantly reduce the effective confinement of the geocell reinforcement. The study also demonstrated the significance of the volumetric behavior of the infill material in designing the geocell foundation system.

More recent studies on laboratory box tests on square footing over geocell-reinforced sand and clay subgrades reported an increase in ultimate bearing capacity in both cases (Sitharam and Hegde 2013). The subsequent study on the effect of infill material and different types of cellular confinement systems on the behavior of geocell-reinforced clay bed showed an increase in bearing capacity of the geocell-reinforced bed by 13, 11, and 10 times for aggregate, sand, and red soil

infill material, respectively (Hegde and Sitharam 2015b, 2017a). The three-different confining systems adopted by the researcher in this study are shown in Figure 2.5. Similar studies by Shadmand et al. (2018) on square footing over geocell-reinforced sand revealed an increase in bearing pressure and a reduction in settlement and surface heaving of the footing with an increase in number of reinforcement layers.

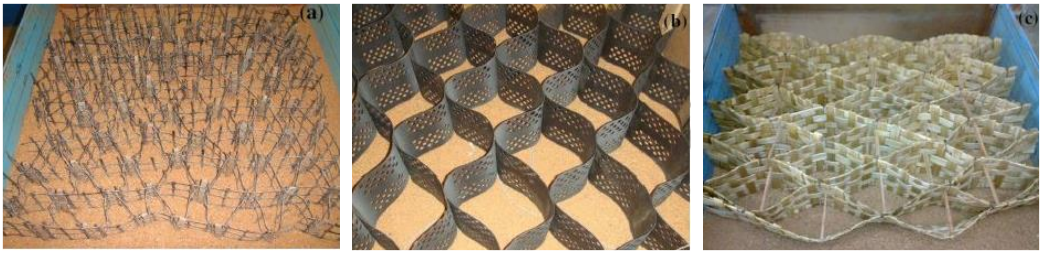

Figure 2.5 Thee different confining systems used by Hegde and Sitharam for bearing capacity studies (a) geogrid cell (b) geocell (c) bamboo cell (Source: Hegde and Sitharam 2017)

2.4.2 *Experimental Studies on Geocell-Reinforced Bases Under Dynamic Loading*

The concept of the cellular confining system was implemented by the U.S. Army Corps of Engineers by performing full-scale tests on pavement sections in the 1970s (Webster 1979). Since then, cellular reinforcement has been recognized as an effective mechanical stabilization method for improving the performance of the pavements under traffic loading. Kazerani and Jamnejad (1987) studied pavement test sections with different infill materials and reported that the influence of geocell reinforcement is more prominent with the low-quality base/subbase materials.

The performance of geocell reinforcement on railroad bases was investigated by applying a repeated load on the test section and the results revealed the effectiveness of geocell in reducing the deformation of the railroad over a subgrade with low bearing capacity (Sekine *et al.* 1994). Large-scale model laboratory tests by Mhaiskar and Mandal (1994) confirmed the performance improvement of the geocell-reinforced base under repeated loading. The study also reported the perks of utilizing geocell reinforcement in reducing deformation under repeated load condition.

The field studies on geocell reinforcement in combination with geogrids and geotextiles reported an increase in geocell confinement and a rise in the M_r of base course by two times (Al-Qadi and Hughes 2000). Model tests were performed by researchers on the unreinforced embankment and embankment reinforced with geocell to assess the feasibility of geocell in enhancing the performance of the ballast. Geocell made of high-density polyethylene (HDPE) was used as reinforcement. Experimental results demonstrated that the geocell reinforcement is effective in improving strength and minimizing the deformation of the ballast (Leshchinsky 2011, Leshchinsky and Ling 2013).

Studies on accelerated pavement testing (APT) to assess the effectiveness of NPA geocells in unpaved pavement sections exhibited a significant improvement in the stability of the pavement and also a reduction in the PD of pavement bases (Yang *et al.* 2010, 2012). Full-scale traffic testing on the NPA geocell-reinforced

bases over clay subgrade exhibited significant improvement in the performance of crushed limestone and RAP sections with respect to rut dept reduction and stress distribution angle. (Pokharel *et al.* 2011). The test results from the subsequent study demonstrated that the geocell reinforcement can be used for reinforcing granular bases for reducing the PD and increasing the elastic deformation (Pokharel *et al.* 2018).

The repeated loading studies on the strip footing over geocell-reinforced sand concluded that the settlement rate reduces significantly with an increase in width and height of geocell for a given amplitude of repeated loading cycles (Tafreshi and Dawson 2010, 2012). Similar studies on the rutting and resilient properties of the sub-base layer over soft subgrades indicated that geocell reinforcement increased the confinement which leads to an increase in M_r (Tanyu et al. 2013). The study also showed the effectiveness of geocells reducing the plastic deflections, improving the subgrade modulus by approximately two times, and the M_r by 40–50% over weak subgrade.

Recent studies on cyclic and repeated load tests to assess resilient and PD characteristics of geocell-soil composite showed a reduction in the required thickness and rut depth of pavement base with the geocell (Saride et al. 2015; Suku *et al.* 2016, 2017). These experimental and field studies confirmed the effectiveness of geocell reinforcement in enhancing the performance of the pavement bases. The

following section presents a brief review of the literature on the experimental studies on GRRB.

2.4.3 *Experimental Studies on Geocell-Reinforced RAP bases*

Limited studies are available on RAP pavement bases reinforced with geocell. An increased elastic deformation and reduced surface and base deformation were observed when the GRRB layer was subjected to cyclic loading (Acharya 2011). A similar improvement was also reported by Han et al. (2011) with the GRRB sections subjected to full-scale moving wheel load tests. The results also showed the effectiveness of geocell reinforcement in improving the stress distribution angle by distributing the load laterally through the interconnected geocell pockets.

Later, a few researchers experimentally studied the effectiveness of geocell reinforcement in RAP bases subjected to cyclic loading and reported an increase in strength and stiffness behavior as well as a reduction in PD of the base course (Thakur *et al.* 2012a, 2012b, Thakur and Han 2015). Furthermore, the studies on the creep strength of RAP revealed that the geocell reinforcement can be effectively used to minimize the creep rate of RAP base by 6 to 60% (Thakur *et al.* 2013). A subsequent study of the full-scale traffic load tests on pavement sections with GRRB recommended the adoption of a higher base layer thickness for both unreinforced and geocell-reinforced RAP cases when thin HMA is used as the surface layer (Bortz *et al.* 2012a, 2012b, Bortz and Hossain 2016).

Limited studies are available on the geocell-reinforced RAP test sections and the source variability of RAP material calls for a more detailed research on GRRB including static and repeated load laboratory tests. Moreover, all the researches of GRRB were performed with NPA geocell. To the best of authors knowledge, no previous researches have been performed on HDPE GRRB to evaluate the M_r behavior of the geocell-RAP composite. The methodologies for the performance evaluation of geocell in pavement base sections using the experimental data are discussed in the following section.

2.5 Performance Assessment of Geocell-Reinforced Bases

Performance of geocell-reinforced pavement was assessed based on the effectiveness of geocell reinforcement under static and repeated loading. In this section, performance assessment methodologies based on bearing capacity used by the previous researchers were briefly discussed. Moreover, the pavement design methodologies dependent on M_r and PD are also presented in this section.

2.5.1 *Bearing Capacity*

Bush et al. (1990) developed a method to design an embankment supported by geocell mattress over a soft ground based on slip-line fields. According to this method, the lateral thrust developed below the embankment is resisted by the tensile stress developed on the geocell mattress. This approach assumes plastic failure of the material instead of slip circle failure. The study concluded that the presence of the geocell mattress altered the direction of principal stress and maximum shear

stress to push the failure surface deep into the subgrade. The analysis results also showed that the geocell mattress promoted inward shear stresses underneath the geocell mattress and was able to generate the ultimate bearing capacity with full base friction in the foundation soil.

Bathurst and Karpurapu (1993) proposed equations to determine the effect of geocell confinement using elastic membrane theory developed by Henkel and Gilbert in 1952. The increase in confining pressure ($\Delta\sigma_3$) due to stresses developed in the geocell material is given by,

$$\Delta\sigma_3 = \frac{2M\varepsilon_c}{d}\left(\frac{1}{1-\varepsilon_a}\right) \quad (2.1)$$

where M is geocell material modulus (kN/m), ε_a is the axial strain, and d is the original diameter of the specimen, and ε_c is the circumferential strain given by,

$$\varepsilon_c = \left(\frac{1-\sqrt{1-\varepsilon_a}}{1-\varepsilon_a}\right) \quad (2.2)$$

The study also proposed a method to estimate the enhanced shear strength of the geocell-soil composite in terms of apparent cohesion (c_r) using the Mohr circle method and is given as,

$$c_r = \frac{\Delta\sigma_3}{2}\tan\left(\frac{\pi}{4}+\frac{\phi}{2}\right) \quad (2.3)$$

where ϕ is the angle of internal friction of the infill material. Mohr circle construction for the estimation of equivalent cohesion for geocell-soil composite is shown in Figure 2.6.

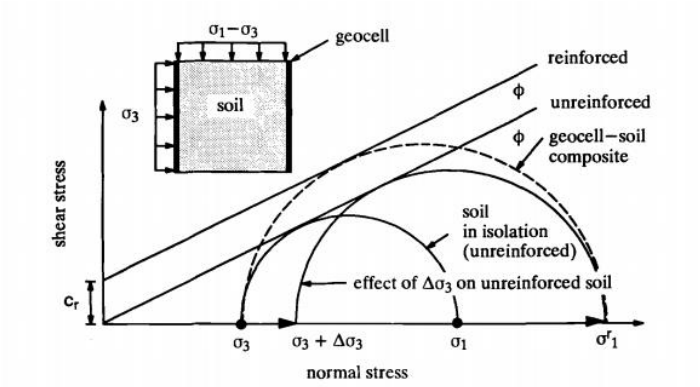

Figure 2.6 Mohr circle construction for calculating equivalent cohesion for geocell-soil composite (Source: Bathurst and Karpurapu 1993)

A bearing capacity equation was proposed by Koerner (1998) to estimate the bearing capacity of the geocell-reinforced soil beds. The study attributed the improvement in the bearing capacity of the footing bed to the relative shear strength (τ) between infill material and geocell wall. Additionally, the study assumes the buildup of an active earth pressure condition inside the geocell pockets which resulted in an improvement in bearing capacity of the reinforced footing bed. Bearing capacity failure mechanism of sand without and with the geocell is given in Figure 2.7.

The increase in bearing capacity (Δq) with geocell is given by,

$$\Delta q = 2\tau \tag{2.4}$$

$$\tau = \sigma_h \tan\delta = PK_a \tan\delta \tag{2.5}$$

where σ_h is the average horizontal pressure on the geocell wall, P is the applied pressure acting on the geocell reinforcement, δ is the angle of shearing resistance

between the infill and the geocell wall material, and K_a is the active earth pressure coefficient.

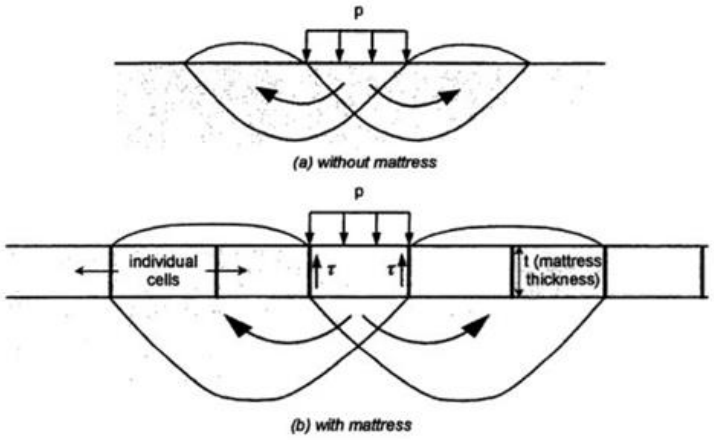

Figure 2.7 Bearing capacity failure mechanism of sand without and with the geocell (Source: Koerner 1998)

The general bearing capacity equation for geocell-reinforced bed is given as,

$$q_r = 2\tau + cN_c\zeta_c + qN_q\zeta_q + 0.5\gamma BN_\gamma\zeta_\gamma \quad (2.6)$$

where q_r is the ultimate bearing capacity of geocell-reinforced bed, c is the cohesion of the soil bed, q is the overburden pressure, γ is the infill unit weight, B is the width of the loading area, N_c, N_q, and N_γ are bearing capacity factors, and ζ_c, ζ_q, and ζ_γ are shape factors.

An alternative bearing capacity calculation method was proposed by Zhang et al. (2010) for the geocell-reinforced embankment over weak soil. The study considered the stress dispersion effect and the membrane effect as shown in Figure 2.8 as the major contributing factors for the improved bearing capacity with geocell reinforcement.

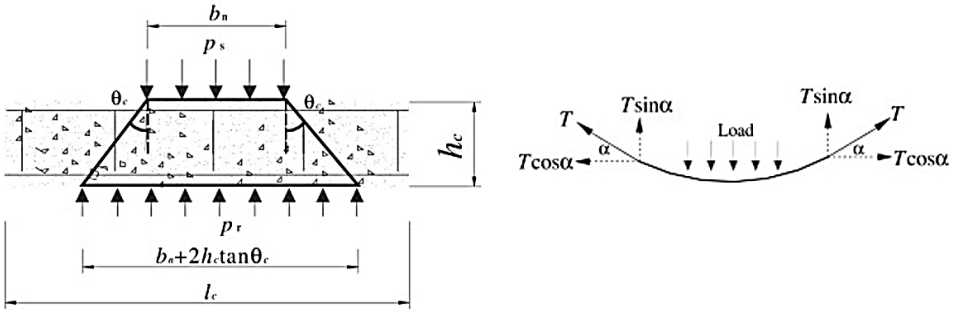

Figure 2.8 Stress dispersion mechanism and membrane mechanism of geocell-reinforced layer (Source: Zhang et al. 2010)

Increase in bearing capacity as a result of vertical stress distribution (Δp_1) is given by,

$$\Delta p_1 = \frac{2h_c \tan\theta_c}{b_n} p_s \tag{2.7}$$

And the increase in bearing capacity as a result of membrane effect (Δp_2) is given by,

$$\Delta p_2 = \frac{2T\sin\alpha}{b_n} \tag{2.8}$$

where h_c, θ_c, and T are height, dispersion angle and the tension on the geocell, p_s is the bearing capacity of untreated foundation soil, b_n is the diameter of the uniform load p_s. The final improved bearing capacity of the reinforced soil will be the sum of p_s, Δp_1, and Δp_2.

Neto et al. (2013) developed a methodology for estimating the bearing capacity of geocell-reinforced foundations. This method assumed a load dispersion angle equal to one pocket width, *d*, on each side of the load as shown in Figure 2.9. According to this method, the vertical stress on the subgrade (p^*) was estimated

initially using the force equilibrium method by considering the reinforcement mechanism (vertical stress dispersion mechanism and the confining mechanism) of geocell reinforcement. The improvement in bearing capacity (Δp) was then calculated by deducting the subgrade vertical stress from the applied stress (p). Thus, the bearing capacity of geocell-reinforced soil (p_r) is given by,

$$p_r = p_u + 4\left(\frac{h}{d}\right) k_0 pe \tan\delta + (1-e)p \tag{2.9}$$

$$\mathrm{e} = \frac{BL}{(B+2d)(L+2d)} \tag{2.10}$$

where p_u is the subgrade bearing capacity, h and d are height and width of geocell reinforcement, respectively, δ is the interface shear angle between the cell wall and infill material, k_0 is the earth pressure coefficient at rest, and L and B are length and width of the footing, respectively.

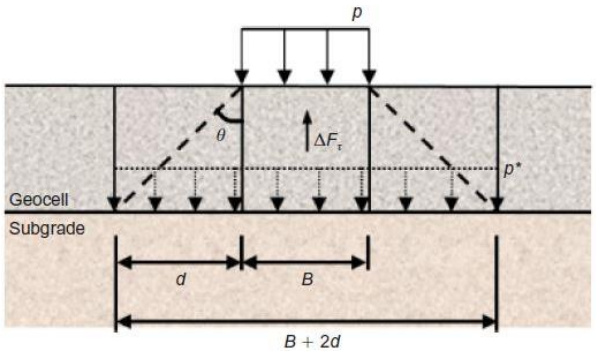

Figure 2.9 Vertical stress distribution angle calculation (Source: Neto et al. 2013)

A simple bearing capacity equation was formulated by Sitharam and Hegde (2013) for geocell-reinforced embankment. The proposed method considered vertical stress dispersion mechanism and lateral resistance of geocell

reinforcement. The membrane effect was also considered for the planar geogrid reinforcement placed at the bottom of geocell reinforcement for separation and additional strength. According to this method, the lateral resistance effect component (ΔP_1) is given as,

$$\Delta P_1 = 2\tau = 2(P_r \tan^2(45 - \phi/2) \tan\delta) \quad (2.11)$$

Vertical pressure reduction with geocell reinforcement is given by,

$$\Delta P_2 = P_r \left(1 - \frac{B}{(B + 2D_r \tan\beta)}\right) \quad (2.12)$$

Bearing capacity increase because of membrane effect is given as,

$$\Delta P_3 = \frac{2T \sin\alpha}{B} \quad (2.13)$$

where τ is the shear strength between infill material and geocell, P_r is the applied pressure, ϕ is the infill material friction angle, δ is the angle of shearing resistance between infill material and geocell, D_r is the depth of geocell reinforcement, B is the footing diameter, T is the geogrid tensile strength. Finally, the improvement in bearing capacity was quantified as the summation of bearing pressure from all the three mechanisms.

2.5.2 *Pavement Design models*

A design method was developed by Mengelt et al. (2000) to analyze the effectiveness of geocell reinforcement in flexible pavements using KENLAYER program. The study assumed that the maximum possible benefit can be obtained by placing geocell on the surface of the subgrade. Mengelt developed design charts

correlating the unreinforced and geocell-reinforced pavement life. The unreinforced design life was calculated using KENLAYER and the corresponding design life for the geocell-reinforced case was estimated from the design chart.

The design method was formulated by Pokharel (2010) for estimating the required base thickness of pavements reinforced with geocell reinforcement (Giroud and Han 2004a, 2004b). The approach was a modified form of Giroud and Han's design method for planar reinforcements. A modulus improvement factor and a *k* factor to account for the improvement in the base modulus due to confinement and the decrement rate of vertical stress distribution angle, respectively, were considered in this method (Han et al. 2007). The design formula was validated by the experimental results.

2.5.3 *Resilient Modulus* (M_r)

Limited literature is available for analytical models to assess the M_r of geocell-reinforced bases. Yang (2010) modeled a 3-D response model in $FLAC^{3D}$ to evaluate the resilient response of geocell-reinforced pavement bases. The study considered the effect of compaction induced horizontal stresses and the residual stresses accumulated in the geocell reinforcement.

2.5.4 *Permanent Deformation* (*PD*)

Damage models for estimating the PD response of geocell-reinforced pavement bases is very limited. A PD response model (Damage analysis model) was also proposed by Yang (2010) to estimate the rut depth of a pavement

corresponding to the number of wheel loads. Thakur developed and calibrated PD models for pavement bases reinforced with geocell (Thakur 2013). The empirical models proposed were based on a power model and the log-normal model and mechanistic-empirical model was based on Tseng and Lytton model.

Empirical studies on the geocell-reinforced bases can be used to predict the performance of the geocell-RAP composite in terms of bearing capacity, M_r, and PD. However, numerical studies using finite element (FE) or finite-difference (FD) approaches are required to analyze the load transfer mechanism of geocell reinforcement under the static and repeated loading conditions and also to carry out parametric studies to evaluate the parameters affecting the performance of the geocell-RAP composite. In the following section, the previous studies on numerical modeling of geocell-reinforced bases under static and repeated load cases are discussed.

2.6 Numerical Modeling of Geocell-Reinforced Pavement Bases

Numerical modeling of geocell reinforcement has always been a challenge because of its three-dimensional cellular structure. Previously, researchers used equivalent composite approach for modeling the geocell-reinforced pavements or embankments (Mhaiskar and Mandal 1996, Bathurst and Knight 1998, Madhavi Latha *et al.* 2008, Madhavi Latha and Somwanshi 2009, Chen *et al.* 2013, Mehdipour *et al.* 2017). According to this method, the geocell-reinforced layer is considered as an equivalent composite layer with enhanced strength and stiffness

properties. This method was a primitive method and it failed to capture the soil-geocell interaction which is the major mechanism responsible for the improvement in the performance of the pavement base layer when geocell is used as the reinforcement. Additionally, the equivalent composite approach failed to capture the bending mechanism of the geocell reinforcement under loading (Mehdipour *et al.* 2013).

The three-dimensional geocell reinforcement was first modeled by Han et al. (2008) using an FD software *FLAC*^{3D}. A single geocell with sand as the infill material was used in the study. The geocell was modeled as a diamond-shaped cell because of the difficulties in modeling the honeycomb structure of the geocell. The Mohr-Coulomb failure criterion was used to model sand. The linear elastic geogrid element in *FLAC*^{3D} was adopted for geocell. The study found that the maximum displacement and the maximum tension within the geocell was accumulated close to the bottom of the cell, possibly due to the small height of the geocell.

Similar studies on geocell-reinforced sand and clay bed were carried out by Saride et al. (2009) using *FLAC*^{3D} with square-shaped geocell pockets. The study concluded that the geocell mattress enhanced the performance of the footing by distributing the vertical pressure exerted by the footing over a wider area. Moreover, researchers also reported the performance improvement of the reinforced test bed with an increase in height of the geocell reinforcement.

Yang et al. (2010) modeled the actual three-dimensional structure of the geocell reinforcement using the *FLAC*^{3D} software. The geocell reinforcement was photographed during the laboratory testing and the photograph was digitized to achieve the accurate shape of the geocell pocket. Duncan-Chang material model was used in this study to model sand. The *FLAC*^{3D} model developed for this study is shown in Figure 2.10. The study concluded that the results obtained from the numerical studies matched well with the laboratory results.

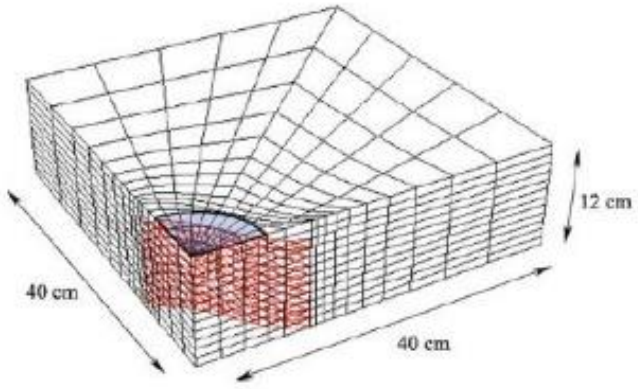

Figure 2.10 *FLAC*^{3D} model developed for simulating the actual shape of geocell (Source: Yang et al. 2010)

Leshchinsky and Ling (2013) carried out the modeling of the geocell-reinforced railway ballast structure using 3-D finite element software *ABAQUS*. The base of the ballast was reinforced with a layer of geocell reinforcement. The rhomboidal shape was adopted for geocells. The results showed that the lateral spreading of the ballast material reduced substantially with the geocell

reinforcement. In addition, the uniform distribution of stresses and the reduction in the surface deformations were also reported.

Hegde and Sitharam (2015a) adopted the honeycomb shape of geocell and performed numerical simulations on geocell-reinforced sand beds using FD software *FLAC*^{3D}. It was observed that the geocell modulus, geocell pocket diameter, and geocell height are the predominant factors responsible for the improved performance of the foundation bed. The subsequent study performed in the geocell-reinforced clay beds reported the effectiveness of geocell reinforcement in distributing the stresses laterally over a wider area (Hegde and Sitharam 2015c).

George (2015) and Saride et al. (2017c) modeled homogeneous and layered sand beds in *FLAC*^{3D} to assess the confining mechanism of geocell reinforcement. The confining stress developed in the geocell walls during static loading was quantified and validated using the experimental studies. Oliaei and Kouzegaran (2017) performed similar numerical simulations on reinforced footing subjected to static loading using an FD software *FLAC*^{3D}. The model was validated using experimental data from both single and multiple geocell test sections. The study also compared the performance of cellular geosynthetics with planar geosynthetic reinforcements.

A summary of the previous numerical researches on geocell-reinforced test sections was provided in this segment. The available literature on numerical modeling of geocell-reinforced sections are mainly on static loading condition and

no previous studies are available on GRRB. This demands numerical analysis of GRRB subjected to static and repeated load cases to assess the confining and load distribution efficiency of GRRB under the traffic loading.

Along with the experimental and numerical assessment of the performance of GRRB, the sustainability assessment is also considered as a deciding criterion for selecting the pavement base alternatives for the pavement construction. The previous studies on sustainability assessment of geocell-reinforced bases were mainly based on the performance of the reinforced pavements pertaining to PD. To the best of authors knowledge, no studies are available on the sustainability assessment of geocell-reinforced pavement sections. The following section briefly presents the methodologies adopted by previous researchers to evaluate the sustainability aspects of unreinforced pavements.

2.7 Integrated LCA-LCCA Framework for Sustainability Assessment

The pavement sustainability is typically quantified in terms of performance assessment of pavement system or by performing LCCA or LCA (Muench and Dam 2014). Most of the DOTs and federal agencies in the United States use LCCA which considers only agency and user costs as an aid in decision making related to pavements (FHWA 2002, Caltrans 2011). The costs related to the health and environmental impacts of raw material production, construction, maintenance, rehabilitation, and usage of the pavements are usually ignored. However, recent studies recommended that the costs incurred due to environmental impacts from

roadway construction, operation, and maintenance account for approximately 10% of the user costs (Chester and Horvath 2009, Santero *et al.* 2011). It was also established that the environmental and communal effects from pavements extend far beyond the acqusition and production of raw material (Santero and Horvath 2009, Santero *et al.* 2011).

Limited literature is available on the integrated LCA-LCCA framework. Chan (2007) and Zhang et al. (2010) considered the environmental costs due to increasing concerns about environmental impacts. Inti (2016), Lu et al. (2018), and Santos and Costa (2017) formulated LCA-LCCA frameworks for the selection of sustainable pavement alternative and for identifying optimal maintenance and rehabilitation strategies. However, most of the research was limited to the estimation of the environmental impact factors from energy consumption and greenhouse gases (GHG) emission. The social and health impacts due to air, noise, and water pollution were not considered in these studies. Moreover, the vehicle operating cost due to traffic delay, detour, and accidents were not addressed.

2.8 Summary

This chapter reviewed the necessity of recycled materials on the pavement infrastructure especially RAP material. The current production and usage of RAP and the mechanical, physical, and chemical properties of RAP material were discussed briefly. Various stabilization methods such as blending of RAP with natural aggregates, chemical stabilization, and mechanical stabilization were also

discussed. A brief literature on the history of geocell reinforcement, mechanism of geocell reinforcement, large-scale experimental testing and numerical studies conducted on geocell-reinforced pavement system subjected to static and repeated load were performed. The following are the outcomes of the literature study:

(a) RAP material can be successfully used as a sustainable and cost-effective base/subbase alternative in pavement applications if the RAP material is properly stabilized either by blending with natural aggregates or by using chemical or mechanical stabilizers.

(b) RAP-aggregate blend showed a higher M_r with increased RAP percent. For treated RAP, the M_r increased with a higher percent of stabilizer and curing time of the sample.

(c) RAP-aggregate blend and GRRB showed an increase in PD with loading cycles. The increase in RAP content in the blend increases the PD whereas a higher percent of stabilizer decreased the PD of the treated RAP. The PD rate decreased with the number of load cycles for both cases.

(d) The use of RAP in pavement construction preserves the natural resources, reduces the debris disposed into the landfill, and reduces the greenhouse gas emission.

(e) Geocell can be effectively used as a mechanical stabilizer to improve the performance of RAP bases in pavements. The performance improvement is attributed to the load carrying mechanism of geocell-reinforced systems

which includes confinement effect, and tension membrane effect. The improvement in performance also depends on the material of the geocell reinforcement, loading area, type of infill material, and the geometry of geocell reinforcement.

(f) A stress-dependent model must be considered for simulating the interaction between infill material and geocell in the numerical modeling of geocell-reinforced pavement bases. The equivalent composite approach for modeling geocell-reinforced bases failed to replicate the soil-structure interaction between geocell and infill material.

(g) Numerical modeling of geocell-reinforced bases under repeated and cyclic loading adopting an elasto-plastic material model is tedious and cumbersome.

(h) No literature is available on the sustainability of pavements with mechanically stabilized RAP bases. Furthermore, no LCA or LCCA studies have been done on geocell-reinforced pavements. Most of the research in this area was limited to chemical stabilization of pavements.

However, the literature study also highlighted some of the issues, concerns and grey areas of the GRRB. Majority of the previous research studies on GRRB confined only to laboratory studies by focusing on the improvement in PD behavior and creep behavior. Many important parameters for assessing the performance such as M_r, required base thickness, fatigue, and rutting life have not been studied. The

effect of gradation of RAP material, the magnitude of repeated loading, and the location of loading were also not considered in the previous studies. Furthermore, no numerical and analytical models have been developed for GRRB to analyze the load transfer mechanism under static and repeated load cases. Additionally, the absence of sustainability studies on the GRRB necessitates a more comprehensive study in this area. In the present dissertation, these issues have been addressed by performing additional experimental and numerical investigations on GRRB.

Chapter 3

LARGE-SCALE LABORATORY BOX TESTS UNDER STATIC AND REPEATED LOADS

3.1 Introduction

The load-deformation behavior of the geocell-reinforced RAP bases (GRRB) over clay subgrade subjected to static and repeated loading conditions have been investigated and presented in this chapter. The large-scale static and repeated load box tests conducted as a part of this study are listed in Table 3.1. The following sections discuss the material testing and characterization, equipment design and installation, test-section preparation and instrumentation, performance monitoring and reliability check, static load box tests, and repeated load box tests.

Table 3.1 Large-scale laboratory tests conducted for this study

Sl. #	Type of Test	# of Tests	Variable Parameter	Constant Parameter
1	Static load test	2	Unreinforced RAP	-
2	Static load test	4	Height of geocell reinforcement: 10-cm and 15-cm	Type of RAP: RAP 1 Location of applied load: at center
3	Repeated load test	2	Unreinforced RAP	-
4	Repeated load test	4	Height of geocell reinforcement: 10-cm and 15-cm	Type of RAP: RAP 1 Location of applied load: at center
5	Repeated load test	4	Gradation of RAP: RAP1(coarse-grained without fines), and RAP2 (with fines)	Height of geocell: 10-cm Location of applied load: at center
6	Repeated load test	4	Location of applied load: Loading at center, and Loading at joint	Height of geocell: 10-cm Type of RAP: RAP 2

3.2 Material Testing and Characterization

This section presents the detailed characterization of the base, subgrade, and geosynthetic reinforcement materials used in this research. The RAP material and clay were used as the base layer and subgrade, respectively. Geocells made of high-density polyethylene (HDPE)were used as the base reinforcement. Non-woven geotextile was used as a separator, at the interface of base course and subgrade, in all the laboratory box tests. The reported physical and engineering properties of the materials were determined in agreement with the TxDOT, ASTM and AASHTO specifications.

3.2.1 *Geocell Reinforcement*

HDPE geocell, manufactured by Geo Products, LLC was used as the reinforcement to impart confinement to the RAP material. The geocell mattress employed in the large-scale laboratory box testing is shown in Figure 3.1. Geocell with two different heights, 10 cm and 15 cm, were adopted in this research. The properties of HDPE geocell including cell size, cell depth, polymer density, and seam peel strength, provided by the manufacturer, are listed in Table 3.2.

Figure 3.1 Geocell section used in this study

Table 3.2 Properties of geocell material used in this study (Source: Envirogrid Cellular Confinement Systems)

Material Properties	Values
Nominal Expanded cell size (cm)	32 × 29
Nominal Expanded cell area (cm^2)	460
Cell depth (cm)	10.16
Seam Peel strength (N)	1423.43
Polymer Density (kg/m^3)	935.5 - 964.3
Carbon black content (% minimum by weight)	1.5
Nominal sheet thickness after texturing (mil)	60 (–5%, +10%)

3.2.2 *Geotextile*

The contamination of RAP bases by clay particles can degrade the performance of the base layer by reducing the M_r. The degradation of the base layer can result in premature failure of asphalt pavements. This can be prevented by placing a non-woven geotextile between the subgrade and the base layer, as a separator, to minimize the intrusion of clay particles into the RAP base. The

geotextile used in this study is shown in Figure 3.2. Table 3.3 summarizes the material properties of geotextile, as provided by the manufacturer.

Figure 3.2 Non-woven geotextile used in this study

Table 3.3 Properties of geotextile material (Source: GeoSolutions, Inc.)

Material Properties	Values
Grab tensile strength (N)	1110
Elongation (%)	50
Tear (N)	450
CBR puncture resistance	3110
Apparent Opening Size, AOS (microns)	150
Permittivity (s^{-1})	1.0
UV resistance (at 500 hrs.)	70%
Flow rate ($l/min/m^2$)	3056

3.2.3 *Reclaimed Asphalt Pavement Material*

The RAP material used in this research was collected from the Texas Department of Transportation (TxDOT) stockpile in Arlington, Texas (West of Dallas) and Grandview, Texas, respectively. The RAP stockpile at Grandview,

Texas is shown in Figure 3.3. Preliminary laboratory tests were carried out initially to characterize the RAP material. This include sieve analysis, standard Proctor compaction, specific gravity, UCS, CD test, and RLTTs.

Figure 3.3 RAP stockpile at Grandview, Texas

The particle size distribution of RAP material was determined based on TxDOT test procedure Tex-110E (1999). The coefficient of uniformity, C_u and the coefficient of curvature, C_c was observed to be 11.2 and 2.0, respectively. Effective diameter (D_{10}) of the RAP material is 0.50 mm and average grain size (D_{50}) of the RAP material is 4.2 mm. The gradation curve of the RAP material is shown in Figure 3.4. Accordingly, the RAP material was classified as a well-graded soil, based on the gradation curve and by using the USCS classification method. Hydrometer analysis was not performed in this study as 98% of RAP material was retained in No. 200 sieve.

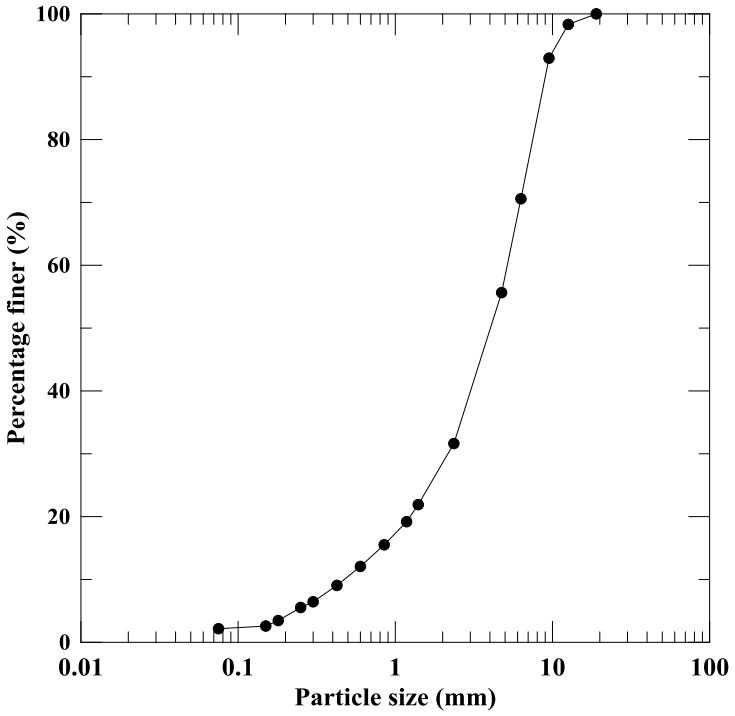

Figure 3.4 Gradation curve of the curve of RAP material

The specific gravity test was conducted as per ASTM D 854 (2014). The test method uses particles passing through 4.75-mm sieve and the determination of specific gravity was done using a pycnometer. The average specific gravity observed for the RAP material was about 2.49. Modified Proctor compaction test, based on TxDOT procedure Tex-113E (2011), was performed to obtain the maximum dry density (MDD) corresponding to the optimum moisture content (OMC) of the RAP material. The maximum theoretical dry density of the RAP material was determined to be 1958 kg/m^3 (122.3 pcf) at an OMC of 7.9% as shown in Figure 3.5.

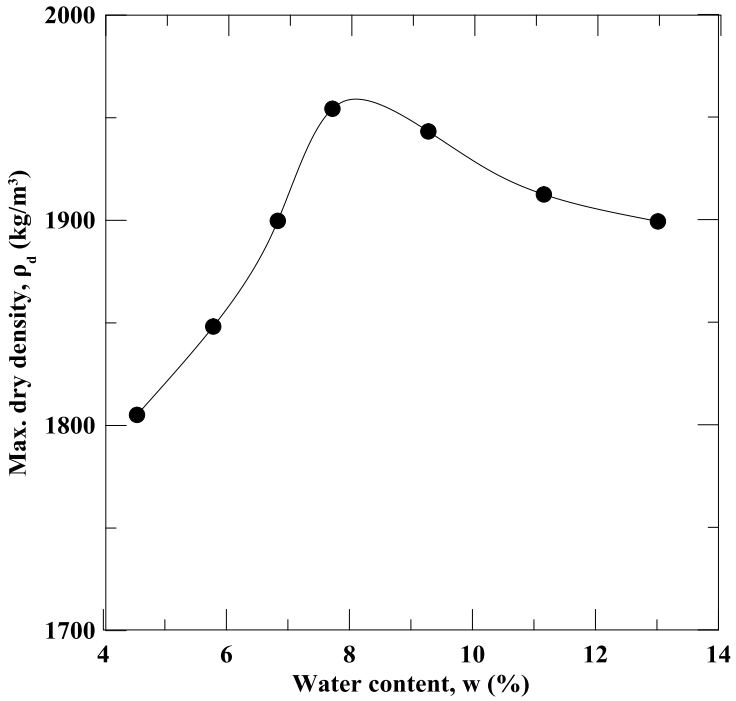

Figure 3.5 Compaction curve of the RAP material

UCS test was performed in accordance with ASTM D2166 (2016), on RAP specimens, to evaluate the unconfined compressive strength of the RAP material. The specimen for UCS was prepared at 95% MDD as per Tex 113-E (2011) procedure with a dimension of 14.2-cm (5.6-in. high) and 7.1-cm (2.8-in.) diameter. The equipment used to perform the UCS test is shown in Figure 3.6. The result from the UCS is plotted in Figure 3.7. It was observed that the RAP material has a secant modulus, E_s of 22 MPa and an unconfined compressive strength of 131 kPa.

Figure 3.6 Equipment setup to perform UCS test on RAP sample

To estimate the shear strength parameters of the RAP material, compacted at 95% MDD, CD tests were performed as per ASTM D-7181 (2011). The shearing rate of the of the specimens was maintained at a low value to account for proper equilibration within the specimen during the monotonic shearing (Banerjee and Puppala 2015, Banerjee *et al.* 2018, Patil *et al.* 2018). Three tests were performed by varying the initial confining stresses as 50 kPa, 100 kPa, and 200 kPa. The variation of axial strain with the deviator stress for all the three confining pressures is shown in Figure 3.8. A friction angle of 32° and cohesion of 98 kPa were obtained for the RAP material.

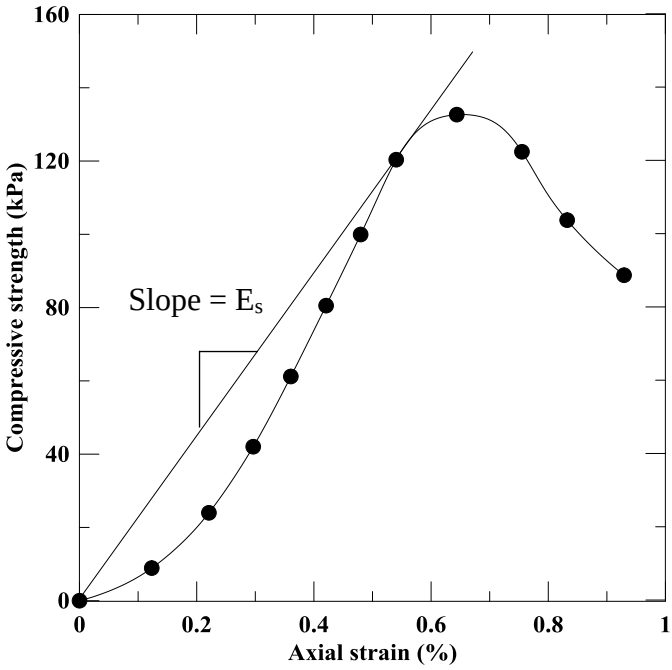

Figure 3.7 UCS test result of the RAP material

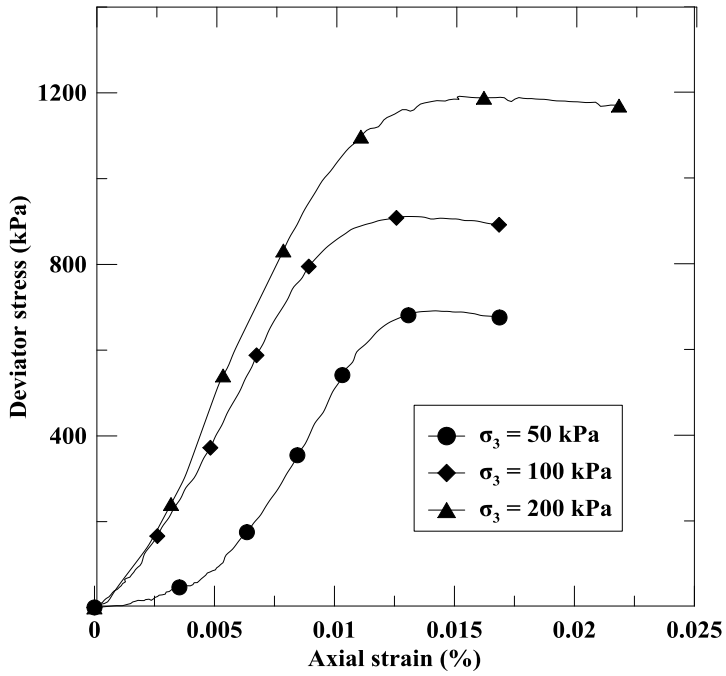

Figure 3.8 CD triaxial test results of the RAP material

The RLTTs were performed to evaluate the M_r of the RAP material using the cyclic triaxial test equipment. The 14.2 cm (5.6i n.) high and 7.1 cm (2.8 in.) diameter specimens were prepared at 95% MDD by maintaining water content at OMC. Repeated cyclic loading was applied to the RAP specimens in accordance with NCHRP 01-28A (2004). The NCHRP testing sequence employed for the unbound base/subbase material to estimate M_r is shown in Table 3.4. The variation of the M_r with the deviator stress is shown in Figure 3.9. Since the overburden pressure was expected to be moderate during the testing, the M_r of 159 MPa corresponding to 27.6 kPa deviator stress and 41.4 kPa confining pressure was adopted for the unreinforced RAP base (URB) in this research.

Table 3.4 NCHRP testing sequence to determine M_r for base/subbase materials

Sl. #	Confining Pressure		Max. Axial Stress		Cyclic Stress		Contact Stress		No. of Load Cycles
	kPa	psi	kPa	psi	kPa	psi	kPa	psi	
0	103.5	15	227.7	33.0	207.0	30.0	20.7	3.0	1000
1	20.7	3	14.5	2.1	10.4	1.5	4.1	0.6	100
2	41.4	6	29.0	4.2	20.7	3.0	8.3	1.2	100
3	69.0	10	48.3	7.0	34.5	5.0	13.8	2.0	100
4	103.5	15	72.5	10.5	51.8	7.5	20.7	3.0	100
5	138.0	20	96.6	14.0	69.0	10.0	27.6	4.0	100
6	20.7	3	24.8	3.6	20.7	3.0	4.1	0.6	100
7	41.4	6	49.7	7.2	41.4	6.0	8.3	1.2	100
8	69.0	10	82.8	12.0	69.0	10.0	13.8	2.0	100
9	103.5	15	124.2	18.0	103.5	15.0	20.7	3.0	100
10	138.0	20	165.6	24.0	138.0	20.0	27.6	4.0	100
11	20.7	3	45.5	6.6	41.4	6.0	4.1	0.6	100
12	41.4	6	91.1	13.2	82.8	12.0	8.3	1.2	100
13	69.0	10	151.8	22.0	138.0	20.0	13.8	2.0	100

14	103.5	15	227.7	33.0	207.0	30.0	20.7	3.0	100
15	138.0	20	303.6	44.0	276.0	40.0	27.6	4.0	100
16	20.7	3	66.2	9.6	62.1	9.0	4.1	0.6	100
17	41.4	6	132.5	19.2	124.2	18.0	8.3	1.2	100
18	69.0	10	220.8	32.0	207.0	30.0	13.8	2.0	100
19	103.5	15	331.2	48.0	310.5	45.0	20.7	3.0	100
20	138.0	20	441.6	64.0	414.0	60.0	27.6	4.0	100
21	20.7	3	207.6	15.6	103.5	15.0	4.1	0.6	100
22	41.4	6	215.3	31.2	207.0	30.0	8.3	1.2	100
23	69.0	10	358.8	52.0	345.0	50.0	13.8	2.0	100
24	103.5	15	538.2	78.0	517.5	75.0	20.7	3.0	100
25	138.0	20	717.6	104.0	690.0	100.0	27.6	4.0	100
26	20.7	3	149.0	21.6	144.9	21.0	4.1	0.6	100
27	41.4	6	298.1	43.2	289.8	42.0	8.3	1.2	100
28	69.0	10	496.8	72.0	483.0	70.0	13.8	2.0	100
29	103.5	15	745.2	108.0	724.5	105.0	20.7	3.0	100
30	138.0	20	993.6	144.0	966.0	140.0	27.6	4.0	100

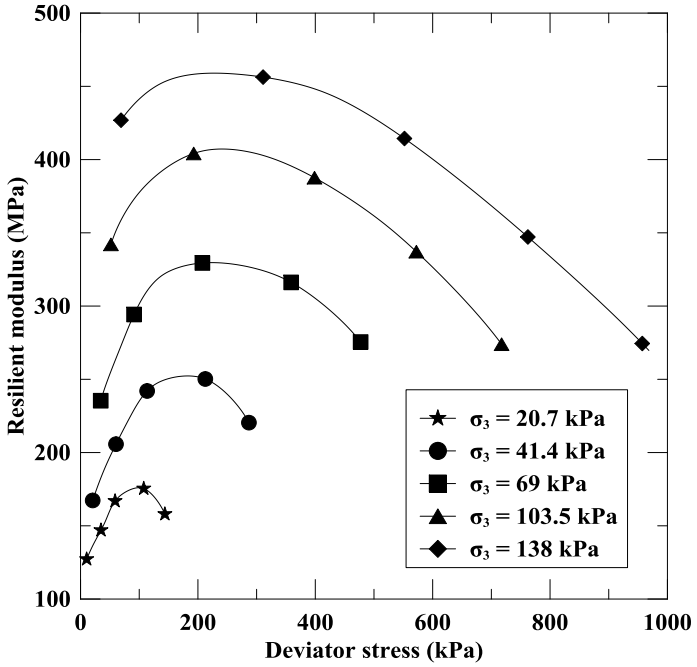

Figure 3.9 RLTT result of the RAP material

The consolidated data of material properties of the RAP with the standards adopted to perform the respective tests are listed in Table 3.5.

Table 3.5 RAP material properties with the corresponding standards

Material Properties	Values	Standard
Specific gravity	2.49	ASTM D 854 (2014)
Maximum dry density (kg/m^3)	1958	Tex-113 E (2011)
Optimum moisture content (%)	7.9	Tex-113 E (2011)
Resilient modulus (MPa)	159	NCHRP 01-28A (2004)
Permeability (m/day)	1.6	ASTM D-2434 (2000)
Cohesion (kPa)	98	ASTM D-7181 (2011)
Angle of internal fiction (°)	32	ASTM D-7181 (2011)
Unconfined compressive strength (kPa)	131	ASTM D-2166 (2016)

3.2.4 *Subgrade*

The locally available clay, obtained from a site in Alvarado, Texas (South-west of Dallas), was used as the subgrade material for this study. The soil obtained from the site was air dried and stored in buckets. Figure 3.10 show the clay stockpile from where the subgrade material was collected for the large-scale testing. The sieve analysis was carried out to determine the gradation of the clay subgrade. The grain size distribution curve of the subgrade material is shown in Figure 3.11. The clay was found to be low-plastic (CL) from Atterberg Limit tests (ASTM D4318 2010) and also based on the Unified soil classification system (USCS). The specific gravity of clay subgrade in accordance with ASTM D854 (2014) was observed to be 2.7.

Figure 3.10 Clay stockpile at Alverado, Texas

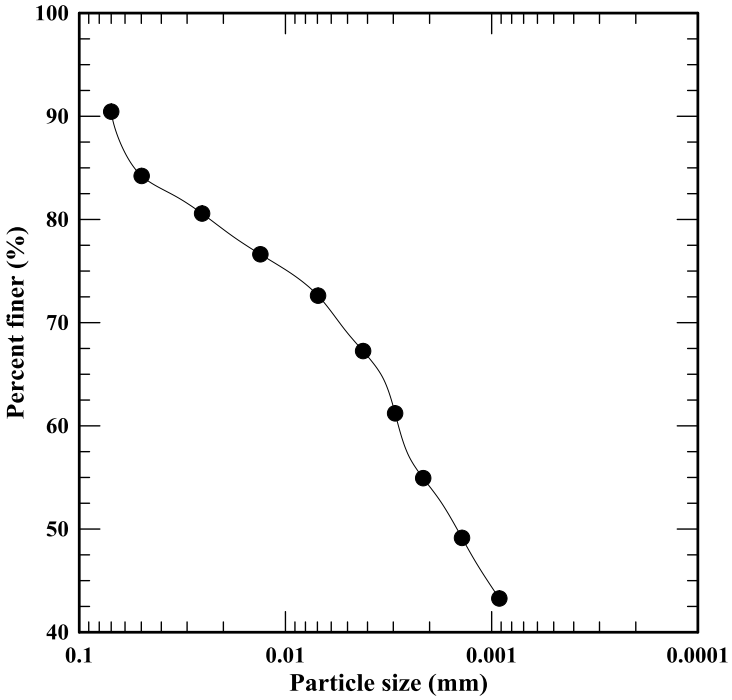

Figure 3.11 Gradation curve of clay subgrade

Standard Proctor tests were performed on clay subgrade in accordance with Tex-113 E (2011) procedure (shown in Figure 3.12), and the MDD of 1703 kg/m^3

was obtained at an OMC of 11.5 %. The M_r of 76 MPa for the clay subgrade was obtained by performing RLTTs corresponding to the last loading sequence of the AASHTO T307-99 (2003) standard which is recommended for cohesive subgrade soils. The specimens were prepared carefully as change in moisture content and compaction energy has a significant effect on the values of M_r and its strength (Banerjee 2017, Banerjee, Patil, *et al.* 2018, Patil, Banerjee, *et al.* 2018, Patil, Puppala, *et al.* 2018). The AASHTO testing sequence to determine M_r for subgrade soil is shown in Table 3.6. The variation of M_r with deviator stress for the subgrade material is shown in Figure 3.13. Since the overburden pressure was expected to be moderate during the testing, the M_r corresponding to the last loading sequence (confining pressure = 13.8 kPa and maximum deviator stress = 68.9 kPa) was adopted.

Table 3.6 AASHTO testing sequence to determine M_r for subgrade soil (AASHTO T307-99 2003)

Sl. #	Confining Pressure		Max. Axial Stress		Cyclic Stress		Contact Stress		No. of Load Cycles
	kPa	psi	kPa	psi	kPa	psi	kPa	psi	
0	41.4	6	27.6	4	24.8	3.6	2.8	0.4	500-1000
1	41.4	6	13.8	2	12.4	1.8	1.4	0.2	100
2	41.4	6	27.6	4	24.8	3.6	2.8	0.4	100
3	41.4	6	41.4	6	37.3	5.4	4.1	0.6	100
4	41.4	6	55.2	8	49.7	7.2	5.5	0.8	100
5	41.4	6	68.9	10	62.0	9	6.9	1	100
6	27.6	4	13.8	2	12.4	1.8	1.4	0.2	100
7	27.6	4	27.6	4	24.8	3.6	2.8	0.4	100
8	27.6	4	41.4	6	37.3	5.4	4.1	0.6	100

9	27.6	4	55.2	8	49.7	7.2	5.5	0.8	100
10	27.6	4	68.9	10	62.0	9	6.9	1	100
11	13.8	2	13.8	2	12.4	1.8	1.4	0.2	100
12	13.8	2	27.6	4	24.8	3.6	2.8	0.4	100
13	13.8	2	41.4	6	37.3	5.4	4.1	0.6	100
14	13.8	2	55.2	8	49.7	7.2	5.5	0.8	100
15	13.8	2	68.9	10	62.0	9	6.9	1	100

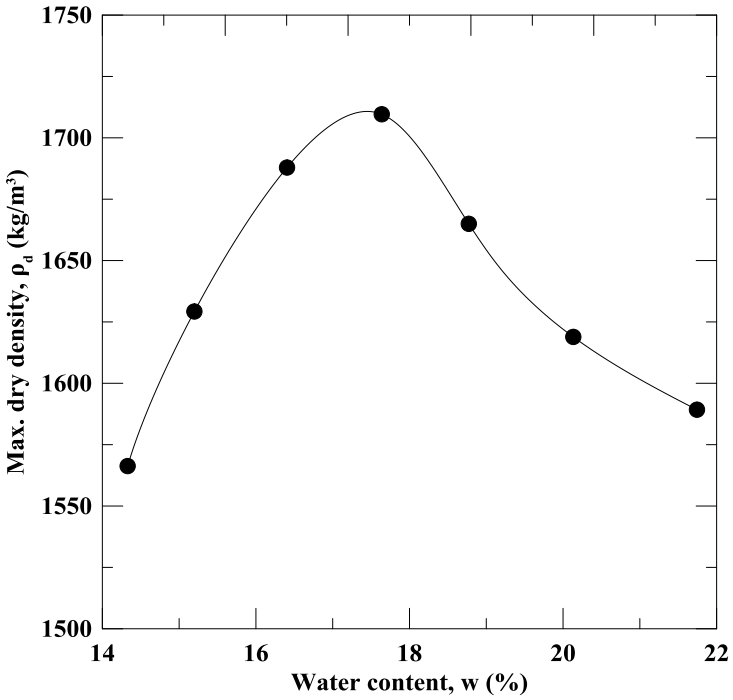

Figure 3.12 Compaction curves of the subgrade material

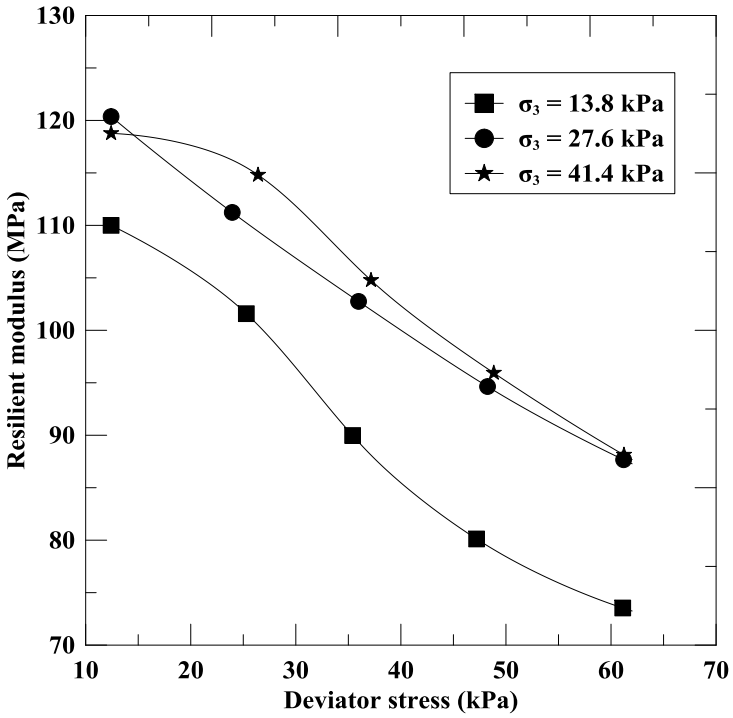

Figure 3.13 Variation of M_r with deviator stress for subgrade material

The physical and engineering properties of the clay subgrade are summarized in Table 3.7.

Table 3.7 Physical and engineering properties of clay subgrade used in the study

Material Properties	Values	Standards
Specific gravity	2.7	ASTM D 854 (2014)
Liquid limit (%)	42.1	ASTM D 4318 (2017)
Plastic limit (%)	25	ASTM D 4318 (2017)
Plasticity index (%)	17.1	ASTM D 4318 (2017)
Maximum dry density (kg/m^3)	1703	Tex-113 E (2011)
Optimum moisture content (%)	11.5	Tex-113 E (2011)
Unified soil classification	CL	ASTM D-2487 (2017)
Resilient modulus (MPa)	76	AASHTO T 307-99 (2003)

3.3 Equipment Setup and Instrumentation

A large-scale laboratory box test setup was designed and fabricated to facilitate repeated load tests to evaluate the performance of HDPE geocell-reinforced RAP bases. The test set-up consists of a large steel tank with dimensions 1.83 m × 1.83 m × 1.52 m with a loading frame, accumulator and hydraulic pump to control and regulate hydraulic fluid, cyclic load regulator for controlling the repeated load application, load cell to measure the applied load and linear variable displacement transducers (LVDTs) for measuring the vertical surface deformations, and data acquisition (DAQ) system to collect the data from LVDTs and load cell. A circular steel plate of 152.4 mm (6 in.) diameter and 12.7 mm (0.5 in.) thickness was used to simulate tire contact area. The schematic diagram for the entire test setup is shown in Figure 3.14. A detailed study on equipment design and setup is given in Saladhi (2017).

3.3.1 *Large Testing Box and Loading Frame*

The large-scale laboratory box consists of detachable steel plates of 0.76 m (30 in.) height stacked and bolted in two layers on all three sides of a 1.83 m × 1.83 m steel base plate, as shown in Figure 3.15. The front part of the box consists of three 0.5 m high detachable steel plates for the easy placement of pavement layers inside the test box. A reference beam was placed at the top of the tank to attach the LVDTs with the help of adjustable magnetic holders.

The loading frame accommodates a hydraulic actuator and a servo control unit. The load cell was connected to the hydraulic actuator with a loading arm. The experimental data measured by the load cell was then transferred to the data acquisition system. The repeated load cycles were applied on the loading plate by pumping the hydraulic fluid into a vertical actuator through a servo control unit.

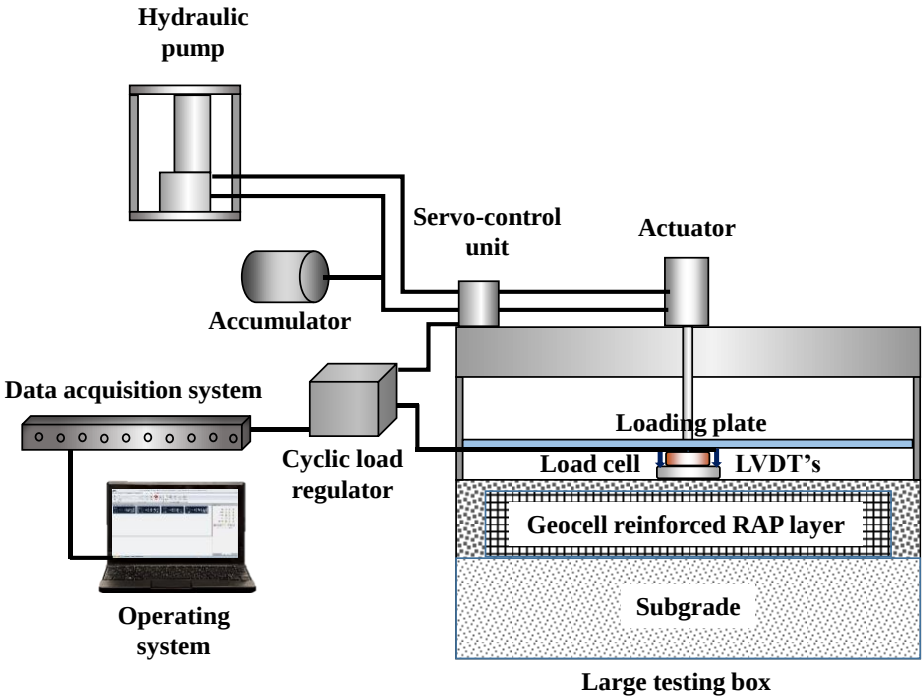

Figure 3.14 Schematic diagram of the laboratory box setup for repeated load tests

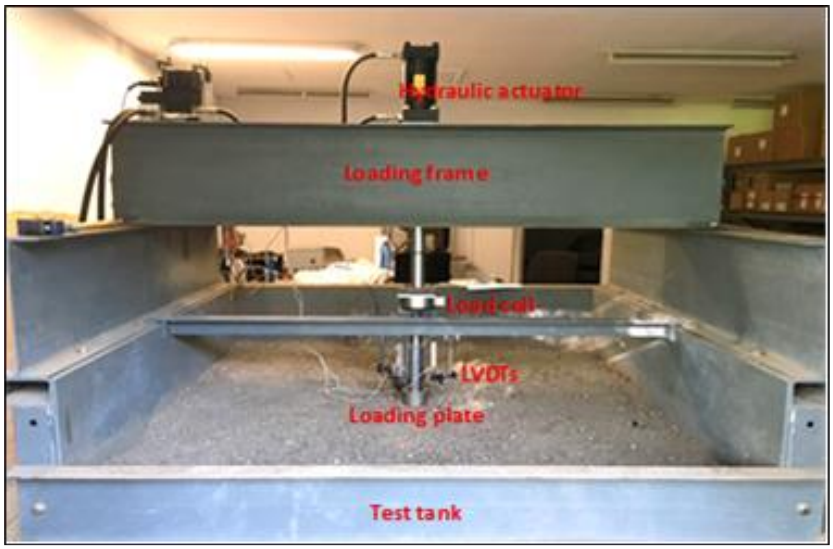

Figure 3.15 Laboratory test box for repeated load test

3.3.2 *Accumulator and Hydraulic Regulator*

The hydraulic fluid was controlled and regulated by the accumulator and hydraulic regulator. The pressure was regulated in the system by setting up an accumulator bottle. This accumulator bottle prevents the pressure drop. The hydraulic fluid was recirculated through a flow control system using an accumulator and hydraulic pump which was connected to the servo control unit. A constant high pressure of 18 MPa (2600 psi) was maintained in the accumulator throughout the test for carrying out the repeated load tests. The accumulator and the regulator used in this study is shown in Figure 3.16.

3.3.3 *Cyclic Load Regulator*

For controlling the repeated load application during the testing, a cyclic load regulator was connected to the servo control unit. It can aid the simultaneous

execution of multiple programs and was connected with a Return Motion Control (RMC) software to control the test using the motion controllers. The algorithm offered by the RMC software allows the user to regulate the speed of the actuator. It also permits the user to develop their own test methods for performing the repeated load tests at different frequencies.

Traffic load was simulated by applying a portion of equivalent single axle wheel load (ESAL) repeatedly on the loading plate with the help of a computer-controlled servo-hydraulic actuator. The frequency of the load application was kept constant at 0.2 Hz by applying a maximum load of 9.5 kN and a minimum load of 0.95 kN in 5 seconds to replicate the traffic loading pattern. The continuous haversine load wave used for applying axial load is shown in Figure 3.17.

Figure 3.16 Accumulator and hydraulic regulator (Saladhi 2017)

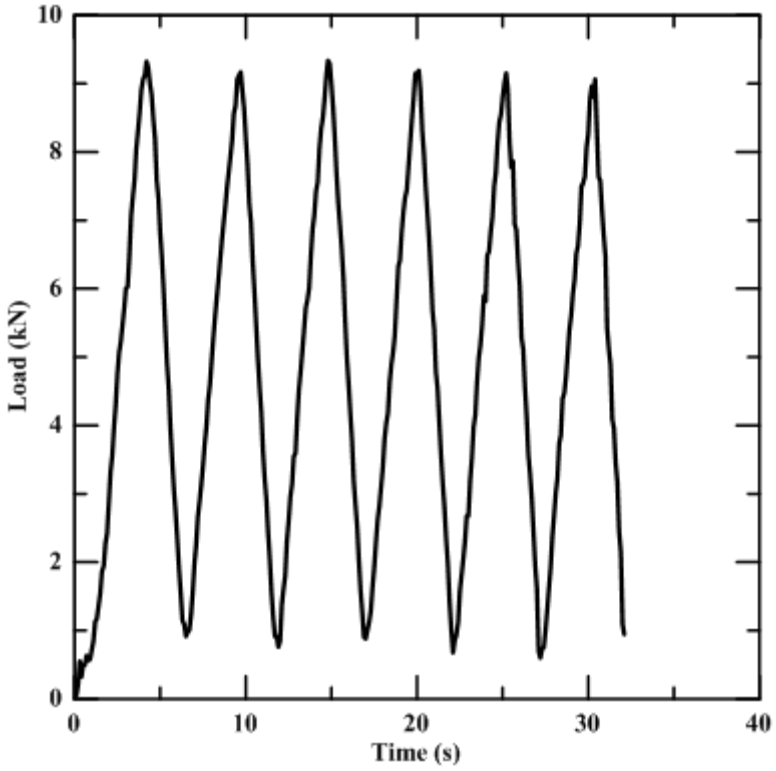

Figure 3.17 Load wave used for repeated load tests

3.3.4 *Instrumentation*

The axial load applied was measured using a load cell connected to the loading shaft and the corresponding displacement at the surface of the loading plate was measured using two LVDTs.

3.3.4.1 Load Cell

The axial load applied was measured using a pre-calibrated load cell connected to the loading shaft. A compression load cell which can measure a point load was used in this study. The load cell used in this study is shown in Figure 3.18.

3.3.4.2 Linear Variable Displacement Transducers

The vertical settlement of the GRRB under repeated load was measured using high-resolution LVDTs. The LVDTs had displacement ranges from 0 to 10 cm (0 to 4 in.). The two LVDTs were placed on both edges of the loading plate as shown in Figure 3.18. Both the LVDT's were linked to the StrainSmart DAQ system to monitor the vertical deformation from the repeated load tests.

Figure 3.18 Load cell and LVDTs

3.3.5 *Data Acquisition System*

The data collected from the repeated load tests using the load cell and LVDTs was collected by the System 8000 StrainSmart DAQ system. The DAQ system used in the repeated load box test is shown in Figure 3.19. The System 8000 StrainSmart software allows the user to configure, control, and acquire data from the large-scale box testing.

Figure 3.19 System 8000 StrainSmart data acquisition system (Saladhi 2017)

3.4 Test-section Preparation

3.4.1 *Subgrade*

The subgrade material from the site was transported and was allowed to air dry for a week. The physical and engineering tests were then performed on the subgrade material, as described in Section 3.2. Each test section included 0.3 m clay subgrade compacted at 95% MDD maintaining the water content at OMC. The clay subgrade was brought to the required moisture content of 13%, which was slightly higher than the OMC, by adding water. The mixing of subgrade material by adding the required moisture content is showed in Figure 3.20.

Figure 3.20 Mixing of subgrade material by adding the required moisture content

The subgrade was placed in four equal lifts of 0.076 m (3 in.) height and each lift was compacted to the required dry density using a vibratory compactor as shown in Figure 3.21. The required quantity of soil for each lift was estimated based on the required dry density and the volume in the tank for each lift thickness. The lower two layers of the subgrade were not replaced during the entire testing. The upper two layers were replaced and recompacted after each test. The moisture content of the subgrade was measured at various locations after the placement of the subgrade to ensure uniform moisture content throughout the soil. If the measured value was different from the required moisture content, then the subgrade moisture content was brought to the required amount by either adding more water or allowing the soil to dry. The compaction density and subgrade strength were ensured by performing the sand-cone test (ASTM D1556 2005) and dynamic cone penetrometer (ASTM D6951 2015), respectively.

Figure 3.21 Compacting subgrade material using vibratory compactor

3.4.2 *Base Layer*

The unreinforced or geocell-reinforced base layer was prepared over the clay subgrade by maintaining the density of RAP material at 95% maximum dry density. A non-woven geotextile was used between the base layer and subgrade as a separator for preventing the penetration of RAP into the subgrade during loading. The geocell mattress was placed on the geosynthetic membrane and was anchored to the subgrade as shown in Figure 3.22. The quantity of RAP material required for each lift was calculated based on the MDD of the RAP material and the volume of the tank to fill each lift.

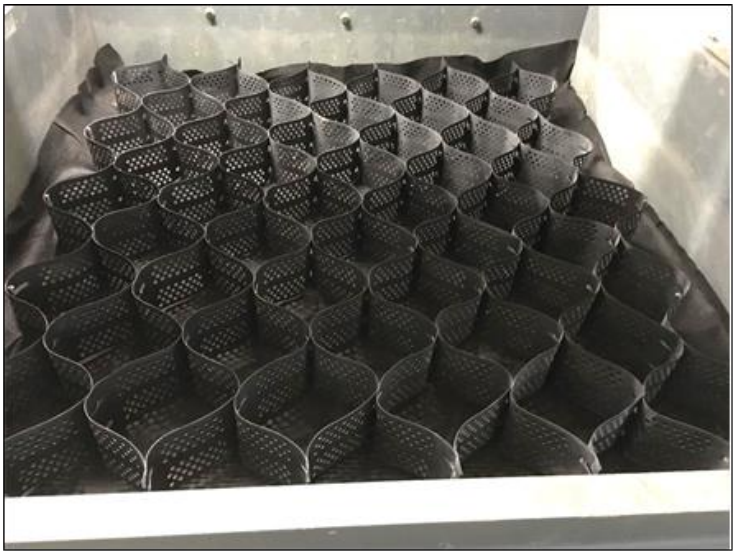

Figure 3.22 Geocell anchored over the geotextile membrane

The compaction of URB was done using the vibratory compactor in three equal lifts. For the geocell-reinforced case, the RAP material was placed in the geocell pockets and was compacted individually using hand vibratory compactor in two equal lifts as shown in Figure 3.23. A 0.025 m (1 in.) RAP cover was placed over the GRRB for the uniform load application on the geocell reinforcement. This also helps the uniform compaction of the RAP inside the geocell pockets. After preparing the test bed, a polyethylene sheet was used to cover the exposed RAP surface for a few hours for allowing uniform moisture distribution throughout the RAP layer.

Figure 3.23 Compacting RAP material inside geocell pockets using hand vibratory compactor

3.5 Performance Monitoring and Repeatability Check

3.5.1 *Performance Monitoring*

The RMC tool and StrainSmart 8000 software were used for controlling and monitoring the large-scale repeated load testing. The RMC helps the user to regulate the location and speed of the actuator, using an algorithm, as shown in Figure 3.24. It also permits the user to develop their own test methods to apply repeated loading at various frequencies and magnitudes. The StrainSmart 8000 window with the measurements from the load cell and LVDTs during the repeated load test is shown in Figure 3.25.

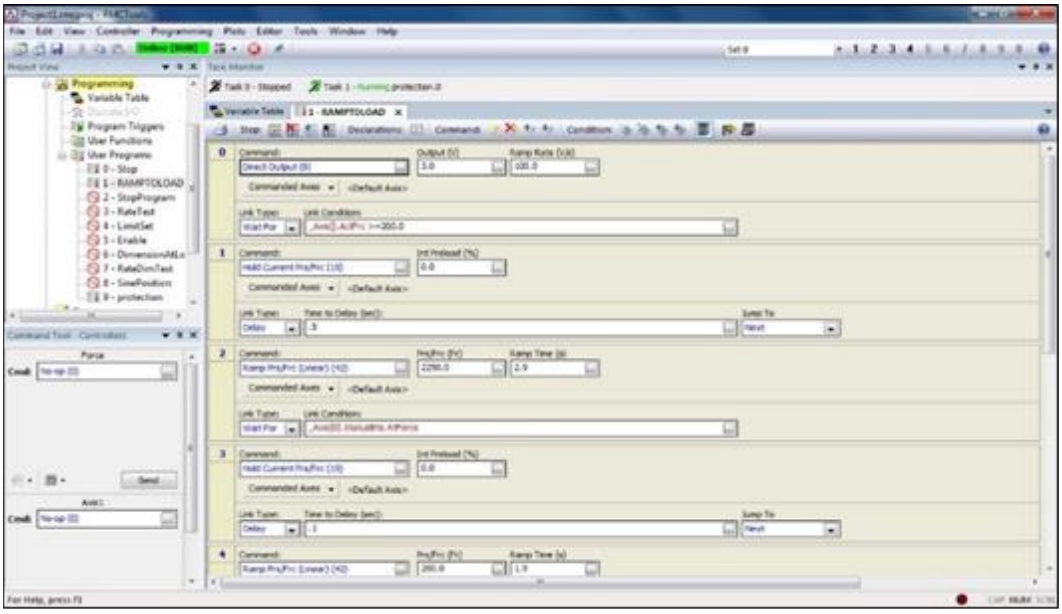

Figure 3.24 RMC tool window (Saladhi 2017)

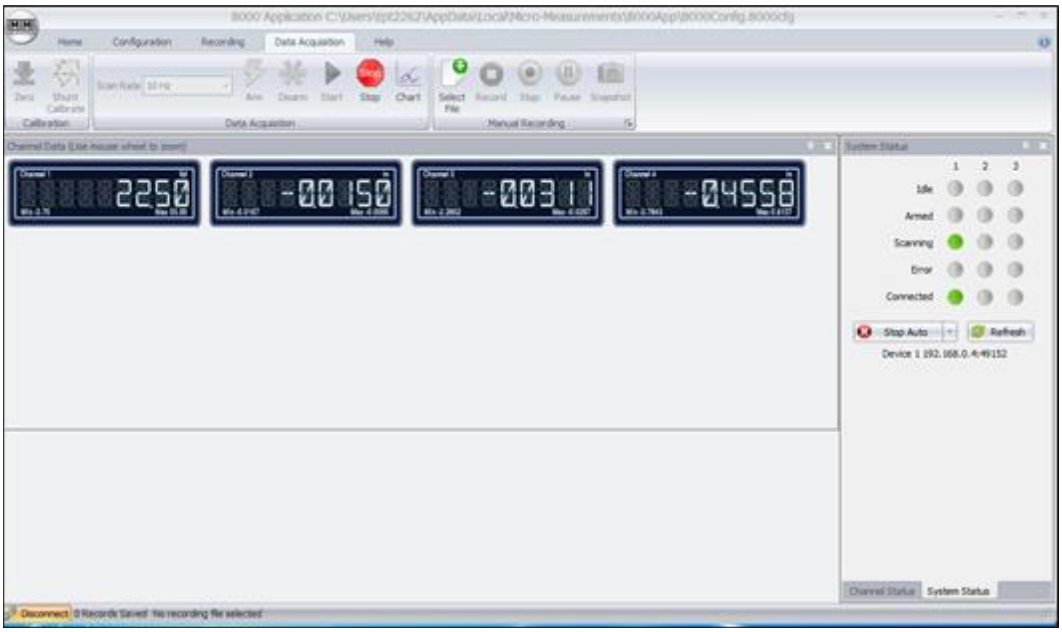

Figure 3.25 StrainSmart 8000 window showing the test data (Saladhi 2017)

3.5.2 *Check for Repeatability*

Repeatability check is necessary to evaluate the credibility of the laboratory test method. To perform the check for repeatability, four similar geocell-reinforced tests were carried out under same loading conditions. 10-cm geocell reinforcement was used for all these tests. It was observed that almost 95% of the results are matching with the repetition which indicates that the test beds prepared are well maintained and the testing equipment used is absolutely working fine. The coefficient of variance for unreinforced and 10-cm geocell-reinforced RAP laboratory tests was found to be 7% and 2%, respectively.

3.6 Static Load Box Tests

The static load box tests were carried out to evaluate the ultimate strength for unreinforced and reinforced test sections.

3.6.1 *Test Procedure*

A series of laboratory tests were conducted on a 0.6 m × 0.6 m × 0.6 m (2' × 2' × 2') steel tank with URB and GRRB sections as shown in the Figure 3.26. The strain-controlled method was selected for all the static load box tests. The load was applied by keeping the displacement rate constant at 0.02 mm/sec (0.05 inch/min) until failure. The response in terms of pressure and settlement is obtained to analyze the data further. A typical variation of pressure with settlement ratio due to static plate load test for a geocell-reinforced RAP bed is shown in Figure 3.27.

After filling the test bed, the loading plate was located carefully at the center of the hydraulic actuator mounted to the reaction frame to avoid eccentric loading. The actuator was then slowly advanced to the loading plate at a very slow rate such that the plate is in contact with the actuator. Each test according to the requirement was preloaded in the software and all the settings such as the acquisition rate, the load rate, and the loading pattern were established. The test command was then given to execute the test with the limits given in terms of displacement. The loading plate was allowed to settle for about 25% of the plate width to ascertain the failure. However, no distinct failure pattern was observed in the geocell-reinforced cases.

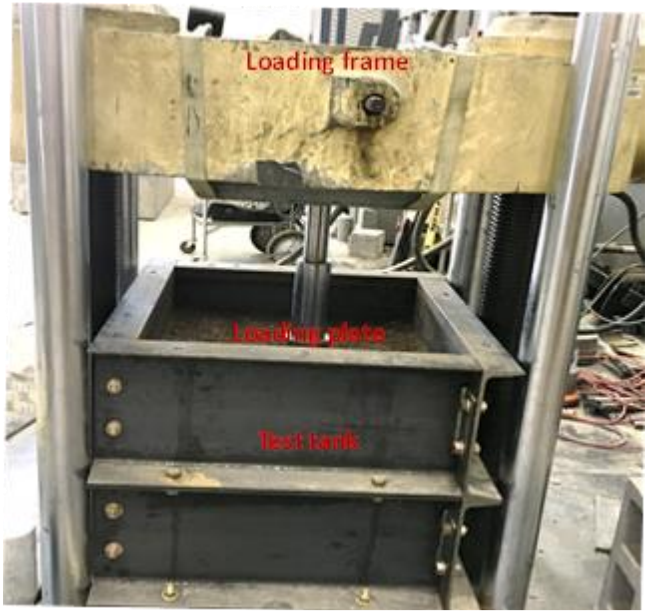

Figure 3.26 Large-scale laboratory testing facility for static load box test

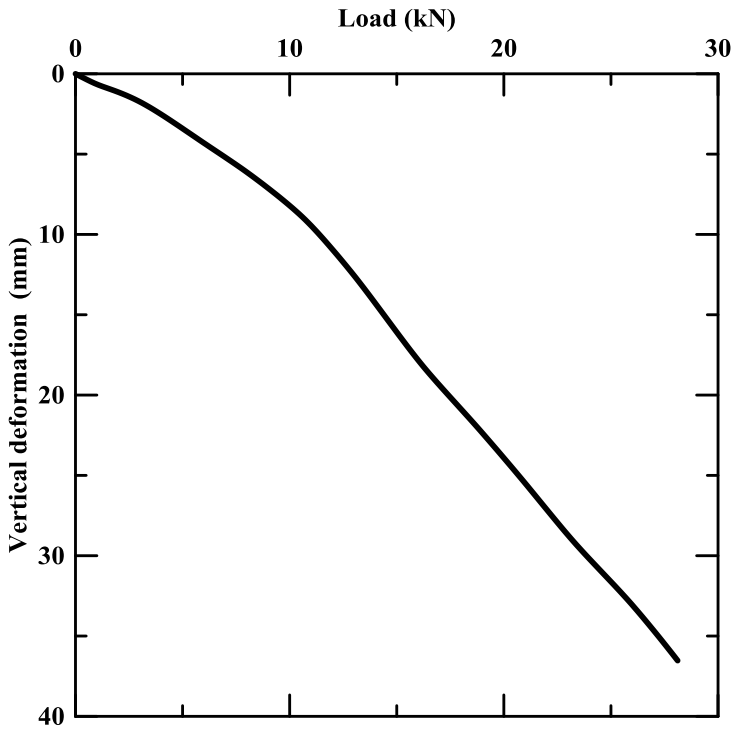

Figure 3.27 Typical load-deformation plot from the static load box test

3.7 Repeated Load Box Tests

The large-scale repeated load box tests were performed to assess the resilient behavior of the GRRB.

3.7.1 *Test Procedure*

A series of large-scale laboratory tests were conducted on steel tank of dimensions 1.83 m × 1.83 m × 1.52 m (6’ × 6’ × 2.5’) with unreinforced and geocell-reinforced RAP test sections. The same circular steel plate used for the static load test was used for the repeated load test to simulate the tire contact area. Repeated load tests were performed on the test bed by placing the circular steel

plate at the center of the actuator. Traffic load was simulated by applying a portion of ESAL repeatedly on the loading plate employing a computer-controlled servo-hydraulic actuator. The frequency of the load application was kept constant at 0.2 Hz by applying a maximum load of 9.5 kN and a minimum load of 0.95 kN in 5 seconds to replicate the traffic loading pattern. Tests were performed on both unreinforced and geocell-reinforced (10-cm and 15-cm geocell) RAP bases for 1000 load cycles.

Thousand load cycles of 9.5 kN magnitude were applied on the loading plate for both unreinforced and geocell-reinforced test sections and the performance of the geocell reinforcement on the RAP base layer was analyzed based on M_r and PD of the test bed. The total surface deformation and the applied axial load at the loading area were measured at an interval of 0.1 seconds using two LVDTs and a load cell, respectively. The total surface deformation of the loading plate was measured by averaging the deformation values obtained from the two LVDTs. A typical variation of axial strain with applying stress from the repeated loading testing of GRRB is shown in Figure 3.28.

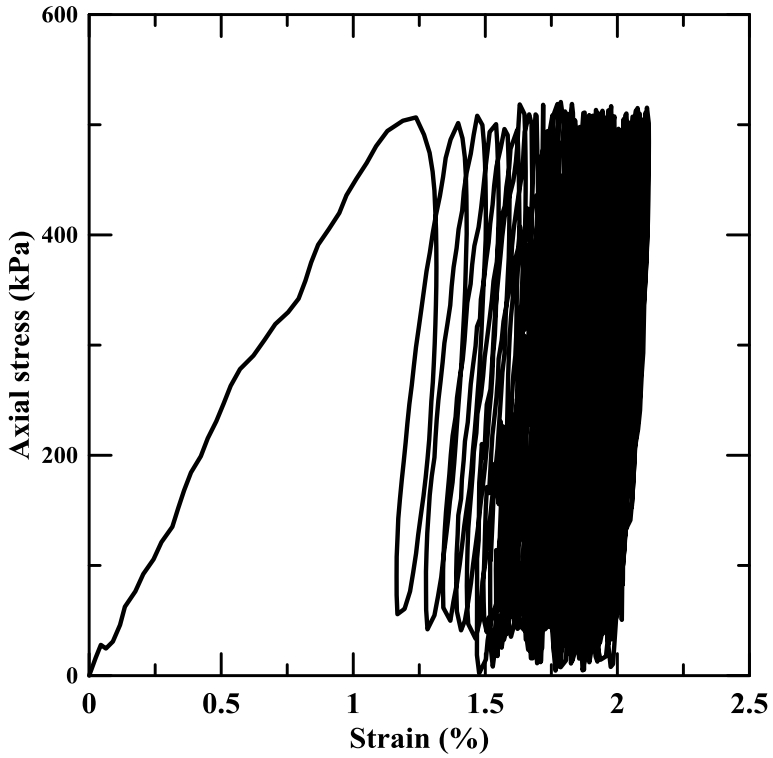

Figure 3.28 Typical load deformation plot from the repeated load test

3.8 Summary

In this chapter, a detailed characterization of each material used in this study was discussed. An elaborate discussion on the test setup and procedures followed to assess the behavior of GRRB is presented. The RMC tools and StrainSmart 8000 software used for controlling and monitoring the large-scale repeated load testing were briefly discussed along with the adopted loading pattern for performing the static and repeated load tests. The methods adopted to analyze the data are also presented. These results were later used for analyses and to study the improvement in performance of pavement section.

Chapter 4

PERFORMANCE ASSESSMENT OF GEOCELL-REINFORCED RAP BASES

4.1 Introduction

The performance assessment of geocell-reinforced RAP bases (GRRB) under static and repeated loading are discussed in this chapter. Several large-scale static and repeated load testing were performed on unreinforced RAP base (URB) and GRRB to assess the strength and deformation characteristics. The performance improvement of GRRB under static load tests was evaluated in terms of bearing capacity (q) and subgrade modulus (k_s). Non-dimensional performance indicators such as improvement factors (I_f) and percentage reduction in settlement (PRS) are also used to quantify the improvement using geocell reinforcement under static loading. For the repeated load testing that simulates the traffic loading, the improvement in the strength and deformation behavior due to geocell reinforcement is presented in terms of elastic deformations (ED), cumulative permanent deformations (PD), resilient modulus (M_r), traffic benefit ratio (TBR), and rut depth reduction (RDR). The performance indicators are discussed in detail in the following sections.

4.2 Static Load Box Tests

Static load box tests were carried out to evaluate the load-settlement behavior of GRRB subjected to monotonic loading. Commercially available cellular confinement system from 'Envirogrid' was used for this purpose. Low

plasticity clay and RAP material were used as the subgrade and base material, respectively for all the test cases. The results from URB and GRRB were compared to evaluate the performance of geocell reinforcement.

4.2.1 *Experimental Program*

A series of six static load box tests were carried out to evaluate the feasibility of the GRRB over clay subgrade. The static load tests were performed on URB and GRRB with 10-cm and 15-cm geocell reinforcement. The width of the geocell reinforcement (B_g) was maintained as four times the width of the footing (B). A cover thickness of one-inch RAP was provided above the geocell-reinforced base layer to facilitate proper compaction of infill material. Figure 4.1 shows the schematic of GRRB over clay subgrades. Tests were terminated at a loading plate settlement of about 25% the footing width.

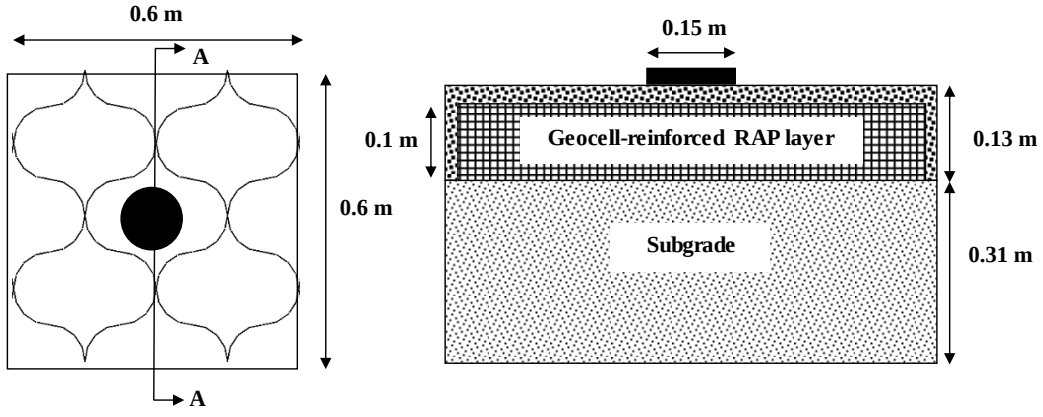

Figure 4.1 Schematic of geocell-reinforced RAP base over clay subgrades
(a) plan view (b) cross-section view of section A-A

4.2.2 *Test Results*

The results from the static load box tests on URB and GRRB were analyzed to evaluate the efficacy RAP base reinforced with geocell subjected to static loading. The performance improvement due to the introduction of geocell is quantified in terms of bearing capacity (q) and subgrade modulus (k_s) and by using non-dimensional performance indicators such as I_f and PRS.

4.2.2.1 Bearing Capacity

The pressure-settlement response from the static load tests on URB and GRRB over the clay subgrade is presented in Figure 4.2. The vertical settlement (s) of the loading plate due to static loading is typically expressed in terms of a non-dimensional parameter known settlement ratio (SR) which is given by,

$$SR = \frac{s}{B} \times 100 \tag{4.1}$$

where B is the diameter of the loading plate.

For the URB, the variation of bearing pressure with settlement ratio curve gradually reduces its gradient and becomes nearly perpendicular to the x-axis at about 25% settlement ratio, indicating that the base layer is approaching its ultimate bearing capacity and is incapable of resisting the extra pressure. The maximum bearing capacity of 1050 kPa was observed for URB layer over clay subgrade.

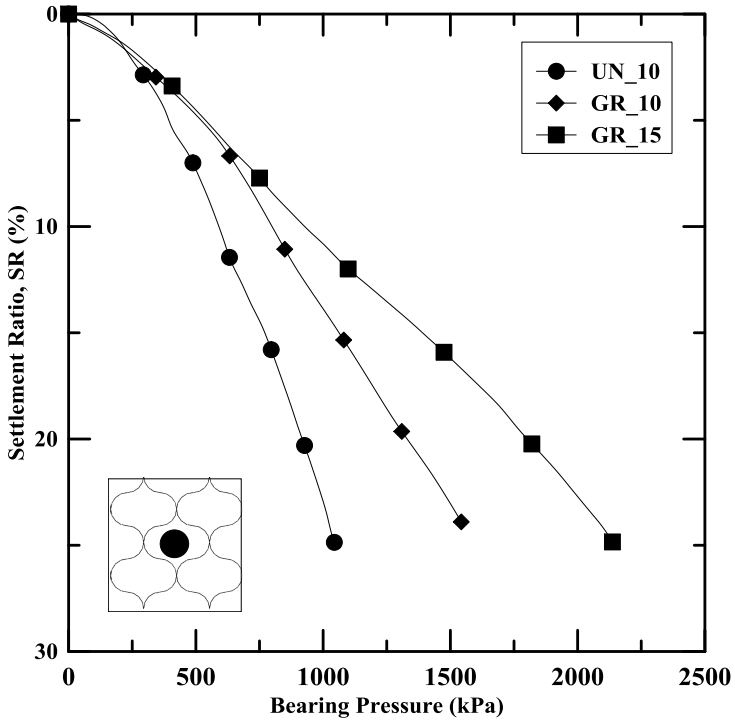

Figure 4.2 Variation of bearing pressure with settlement ratio for static load tests

For the reinforced case, where geocell reinforcement is used for confining the RAP material, a clear-cut failure was not noticed in the bearing pressure - settlement ratio plot. A change in the slope of bearing pressure - settlement ratio plot can be observed for geocell-reinforced cases at a settlement ratio between 3% and 5%. The change in slope might be attributed to the occurrence of a local failure of the RAP base and at that settlement, and thereafter the additional strength is mobilized due to lateral confinement offered by the geocell reinforcement. The bearing pressure at 25% settlement ratio was observed to be 1550 kPa and 2150 kPa, respectively, for 10-cm and 15-cm GRRB.

4.2.2.2 Modulus of Subgrade Reaction (k_r)

The stiffness of the clay subgrade can be quantified in terms of subgrade modulus or modulus of subgrade reaction (k_r). Conventionally, the subgrade modulus is defined as the secant modulus at a point on the curve, corresponding to a particular settlement (Dash *et al.* 2008). The subgrade modulus of the pressure settlement response, calculated at different footing settlements is shown in Figure 4.3. It can be noticed that the geocell reinforcement enhanced the stiffness of the clay subgrade thereby improving the subgrade modulus substantially.

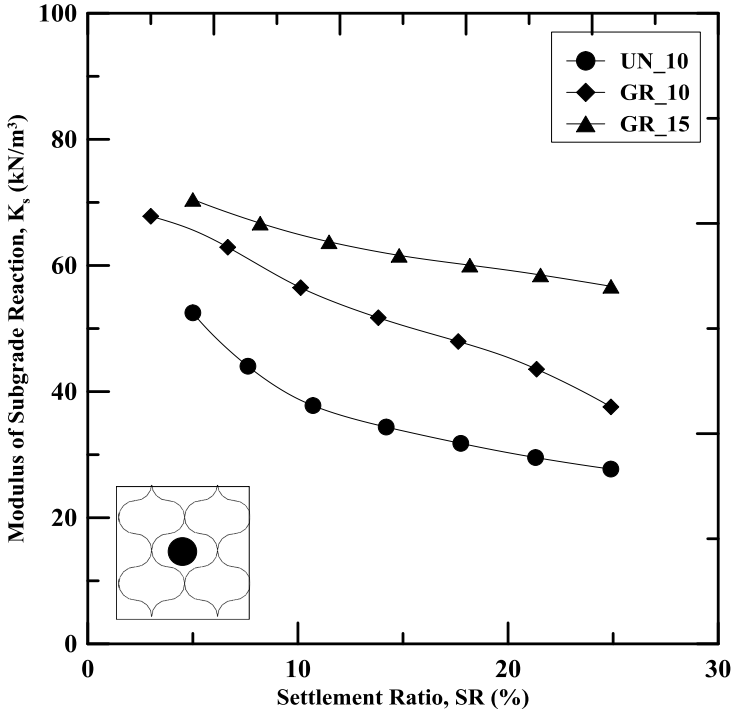

Figure 4.3 Variation of subgrade modulus with settlement ratio

4.2.2.3 Bearing Capacity Improvement Factor (I_f)

The increase in the bearing capacity due to geocell reinforcement can be quantified using a non-dimensional parameter called bearing capacity improvement factor (I_f) (Dash, Saride, *et al.* 2003, Saride, Rayabharapu, *et al.* 2015, Hegde and Sitharam 2017b), which is defined as,

$$I_f = \frac{q_r}{q_0} \tag{4.2}$$

where q_r and q_0 are the bearing capacities corresponding to a settlement ratio for the geocell-reinforced and unreinforced case, respectively. The bearing capacity improvement factors for 10-cm and 15-cm GRRB are compared in Figure 4.4. It was noticed that I_f increased with increase in settlement ratio for both the cases. This implies that geocell reinforcement effect is maximum at higher settlements and the improvement is higher with the increased height of geocell. At higher loads, the mobilization of the tensile strength takes place in the reinforcements, which contributes to the improvement in the performance of the GRRB. When the RAP base over clay subgrade was reinforced with 10-cm and 15-cm geocell reinforcement, a maximum I_f of 1.5 and 1.95, respectively was observed. The substantial increase in I_f with the height of geocell is attributed to the increase in the modulus of the geocell-RAP composite which further reduced the vertical load transmitted to the subgrade.

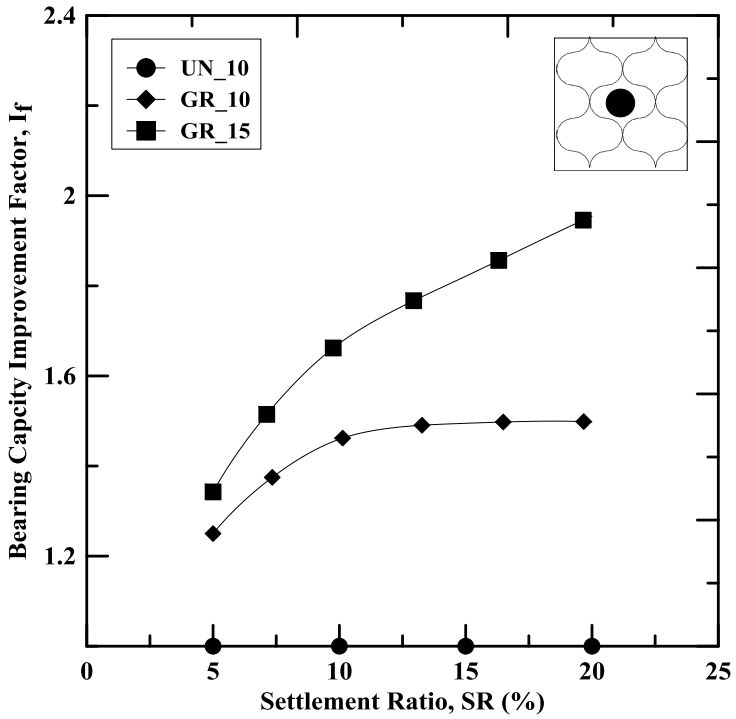

Figure 4.4 Variation of bearing capacity improvement factor with settlement ratio

4.2.2.4 Percentage Reduction in Settlement (*PRS*)

The performance improvement of GRRB can be measured in terms of the reduction in the settlement of the reinforced layer using a non-dimensional parameter called percentage reduction in settlement (*PRS*) (Hegde and Sitharam 2017b). *PRS* is defined as,

$$PRS = \frac{S_0 - S_r}{S_0} \times 100 \qquad (4.3)$$

where, S_o and S_r are the settlement of the URB and GRRB corresponding to its ultimate bearing capacity. The ultimate bearing capacity was estimated using Vesic's double tangent method (Vesic, 1973). In this study, the ultimate bearing

capacity was observed to be 20% of the footing width corresponding to settlement ratio of 20%. It was observed that the maximum *PRS* value for 10-cm and 15-cm GRRB are 30% and 75%, respectively. This clearly shows that the presence of geocell reinforcement not only improved the bearing capacity of RAP base but also reduced the vertical settlement of the RAP bases significantly. The reduction in the settlement is due to the additional lateral confinement offered by the geocell reinforcement that increased the stiffness of the geocell-RAP composite.

4.3 Repeated Load Box Tests

Repeated load box tests were performed to assess the resilient and permanent deformation behavior of GRRB under repeated loading condition. Low plasticity clay was used as the subgrade material for all the tests. Commercially available geocell reinforcement from 'Envirogrid' with apertures was used as the base reinforcement for RAP material. The results from URB and GRRB were compared to evaluate the performance of geocell-RAP composite under repeated loads.

4.3.1 *Experimental Program*

A series of repeated load box tests were carried out to demonstrate the effectiveness of the GRRB over clay subgrade (Table 4.1). The model tests include URB and GRRB sections. Repeated load tests were conducted as discussed earlier in section 3.7 of chapter three. Figure 4.5 shows the schematic of the GRRB over subgrades.

Table 4.1 Large-scale repeated load box tests performed on RAP base

Sl. #	Type of Test	# of Tests	Variable Parameter	Constant Parameter
1	Repeated load test	2	Unreinforced RAP	-
2	Repeated load test	4	Height of geocell reinforcement: 10-cm and 15-cm	Type of RAP: RAP 1 Location of applied load: at center
3	Repeated load test	4	Gradation of RAP: RAP1(coarse-grained without fines), and RAP2 (with fines)	Height of geocell: 10-cm Location of applied load: at center
4	Repeated load test	4	Location of applied load: Loading at center, and Loading at joint	Height of geocell: 10-cm Type of RAP: RAP 2

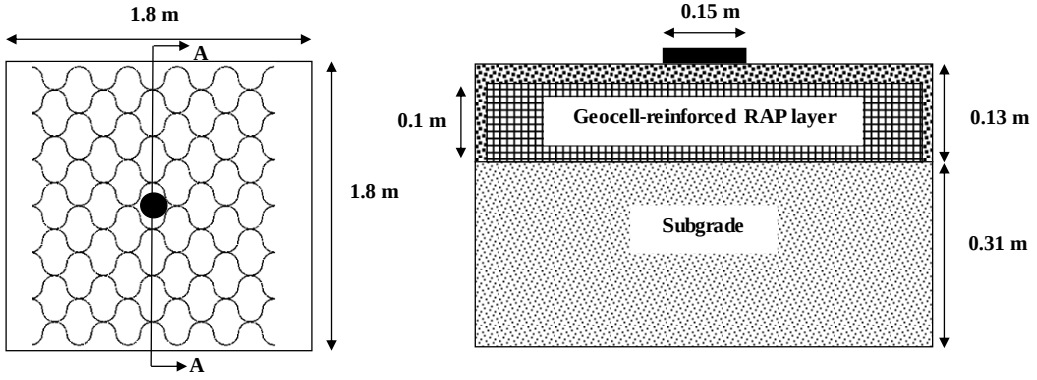

Figure 4.5 Schematic diagram of geocell-reinforced RAP base over clay subgrade (a) plan view (b) cross-section view of section A-A

The width of the geocell reinforcement, B_g (including all the geocell pockets) used for the repeated load tests were maintained as 12 times the width of the loading plate, *B*. A cover thickness of one-inch RAP was provided above the geocell-reinforced base layer to facilitate proper compaction of infill material. The equivalent diameter of geocell pockets, d_c was maintained at about twice the footing

width in all the tests. Tests were performed only up to 1000 load cycles as the resilient and permanent deformation was found to be constant after 500-700 load cycles.

Parametric studies were also performed to evaluate the influence of height of geocell, gradation of RAP, and location of loading on the resilient behavior of the GRRB. The load carrying capacity of geocell reinforcement is greatly affected by the seam strength, as it is the weakest zone in the geocell mattress (Saride *et al.* 2015). Therefore, a parametric study on the location of loading was performed, in which the repeated load is applied directly on the seam of geocell and on the cell pocket of the geocell reinforcement.

4.3.2 *Test Results*

The section presents the results of the large-scale repeated load box tests on URB and GRRB to evaluate the resilient behavior of GRRB under repeated loading. The performance improvement due to repeated loading is presented in terms of non-dimensional parameters such as ED, PD, M_r, *TBR*, and *RDR*. A detailed discussion on the performance indicators is provided in the following sections.

4.3.2.1 Elastic Deformation (ED)

Elastic deformation at the loading surface of the test bed under repeated loading was calculated from the rebound curve, during the unloading of each load cycle. The variation of resilient deformation developed at the center of the loading area with loading cycles for the unreinforced (UN_10) and geocell-reinforced

(GR_10 and GR_15) case is shown in Figure 4.6. UN_10 is the URB sections with 10-cm base thickness, GR_10 and GR_15 are the GRRB sections with 10-cm geocell and 15-cm geocell reinforcement, respectively. The magnitude of resilient deformation for all the three cases decreased gradually to a constant value after 500 load cycles. The 15-cm geocell-reinforced test bed exhibit 2.5 times less resilient deformation compared to the unreinforced test bed. This indicates that the lateral confinement offered by the geocell reinforcement is a major factor in improving the resilient behavior of the RAP base. This observation is in agreement with the results obtained by Acharya (2007).

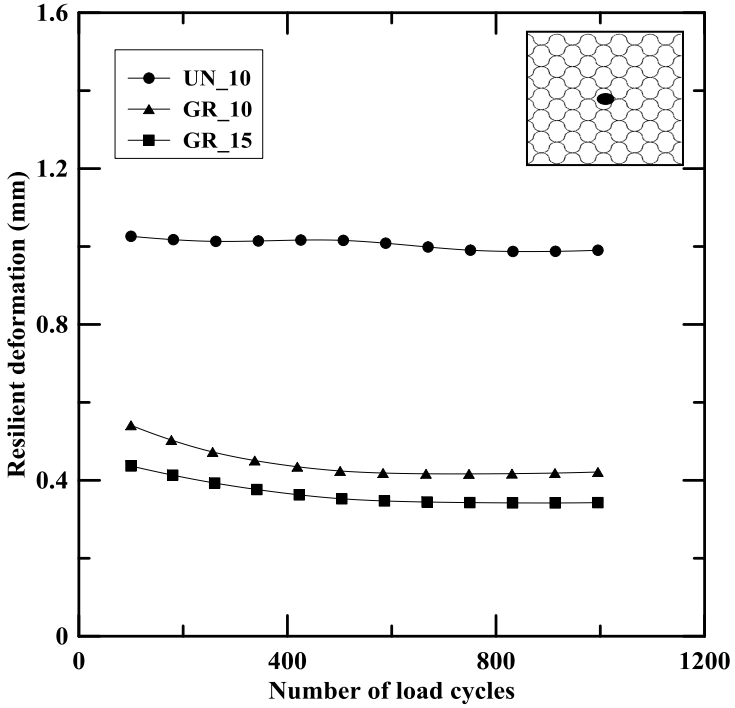

Figure 4.6 Variation of resilient deformation with number of load-cycles

4.3.2.1 Cumulative Permanent Deformation (PD)

Cumulative permanent deformation/permanent deformation is the plastic settlement accumulated at the center of the loading area during each load cycle (Sireesh et al. 2015). The variation of PD with the number of load cycles for the URB and GRRB sections are shown in Figure 4.7. The PD of both URB and GRRB sections increased with increase in load cycle, however, the rate of increase in PD of GRRB decreased with increase in load cycles.

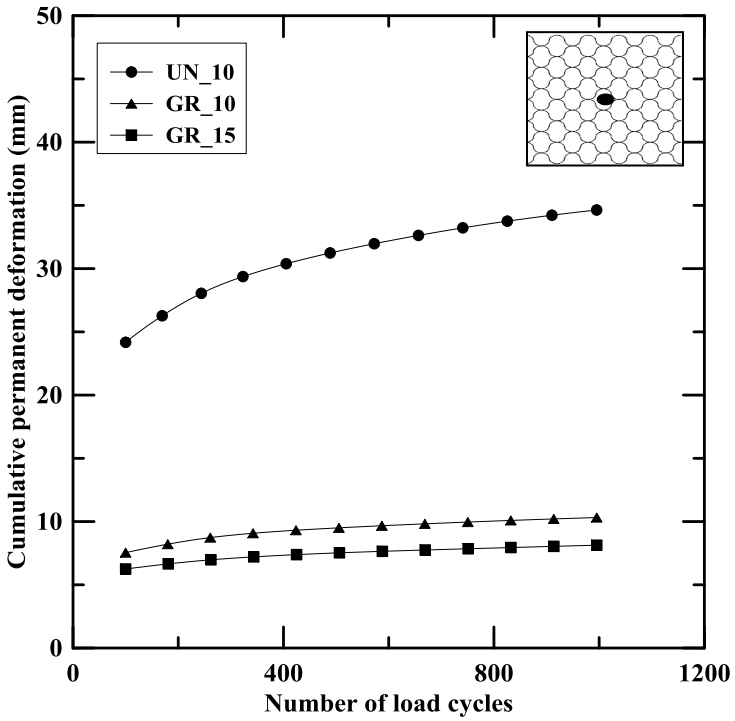

Figure 4.7 Variation of PD with number of load-cycles

The increase in PD is significant until 500 load cycles and after that, it remains relatively constant for GRRB sections. Geocell reinforcement substantially improved the PD behavior of RAP base by 70%-80% owing to the lateral

confinement offered by the geocell pockets on the infill RAP material. The improved performance may also be due to the tension membrane effect (Thakur et al. 2012) in which tensile forces are developed in geocell reinforcement under repeated loading. This resulted in the formation of a zone of tension at the lower section of the geocell-reinforced layer, which in turn increased the structural support offered by the geocell thereby reducing the vertical deformation of the subgrade. A similar trend in the variation of PD was also observed by Thakur et al. (2016) in which the PD of RAP base was improved by a factor of 1.6 by the use of 15-cm geocell reinforcement.

4.3.2.2 Resilient Modulus (M_r)

Resilient modulus is the ratio of cyclic stress applied to the recoverable strain. M_r was calculated for the last five cycles of 100, 250, 500, 750, and 1000 load cycles, respectively, and the average value was taken as the actual M_r of the test section. The resilient modulus of the entire test section is given by,

$$M_r = \frac{\sigma_d}{\varepsilon_a} \tag{4.4}$$

where σ_d is the deviatoric stress applied to the sample and ε_a is the axial elastic strain developed due to the applied σ_d. Typical stress-strain plot for a load cycle and the elastic and plastic strains are shown in Figure 4.8.

To evaluate the M_r of the GRRB layer, stresses developed at the mid-height of each layer was calculated. For conservative analysis, a stress dispersion angle of 26° was used based on conventional 2 Vertical to 1 Horizontal method for the URB

and 30° (Thakur et al. 2011) for GRRB as shown in Figure 4.9. Total elastic strain (ε_{tot}) developed in the test bed is the sum of elastic strains developed in the individual layers.

$$\varepsilon_{tot} = \varepsilon_{GR} + \varepsilon_s \tag{4.5}$$

where, ε_{GR} and ε_s are the elastic strains developed in the GRRB layer and subgrade, respectively. Equation (4.5) can also be expressed as:

$$\varepsilon_{tot} = \frac{\sigma_{1,\,GR}}{M_{r,\,GR}} + \frac{\sigma_{1,\,s}}{M_{r,\,s}} \tag{4.6}$$

where, M_{GR} and M_s are the resilient moduli of the GRRB layer and the subgrade, respectively; and $\sigma_{1,GR}$ and $\sigma_{1,s}$ are the vertical stress at mid-height of GRRB layer and the subgrade, respectively.

Therefore, the resilient modulus of the GRRB is given by,

$$M_{r,GR} = \frac{\sigma_{1,\,GR}}{\varepsilon_{tot} - (\sigma_{1,s}/M_{r,s})} \tag{4.7}$$

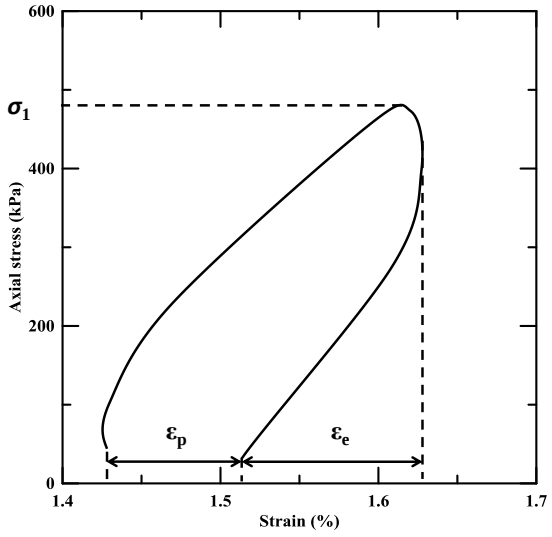

Figure 4.8 Typical stress-strain plot for a load-cycle

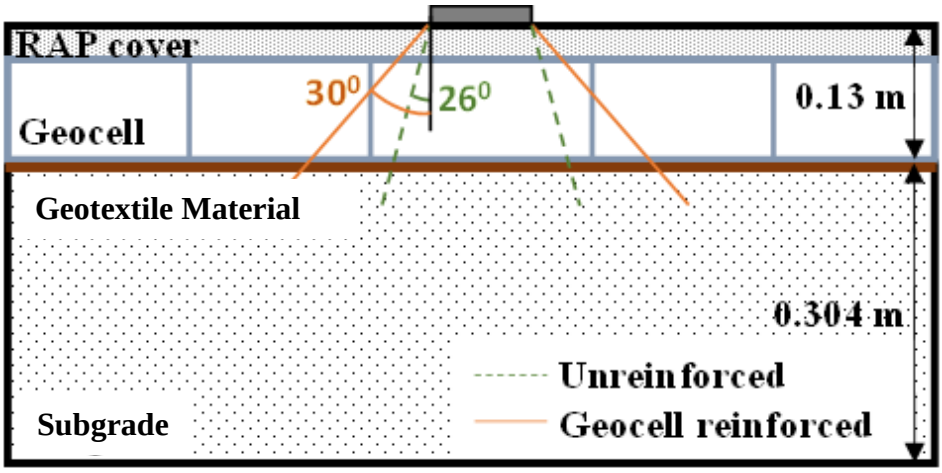

Figure 4.9 Load dispersion angle for URB and GRRB

The variation of M_r of URB and GRRB with number of load cycles is shown in Figure 4.10. M_r of GRRB is nearly three times higher than that of the URB at the end of 1000 load cycles. The rate of increase in M_r of 10-cm GRRB is significant till 750 cycles and then it reaches a constant value of 325 MPa. The sharp increase in the initial phase might be due to the rearrangement of particles under initial loading and the confinement offered by the cellular structure of geocell reinforcement, which resulted in a compact arrangement, thereby increasing the (particle) interlocking between RAP particles and stiffness of the geocell-reinforced RAP material. The initial increase in stiffness is equivalent to the pre-conditioning cycles applied to a traditional repeated-load triaxial test, where 500 to 1000 cycles are applied prior to initiating the actual loading sequences. Similar observations were made by Thakur (2010) for RAP reinforced with NPA geocell, where the M_r of GRRB was 1.6 times higher as compared to the URB.

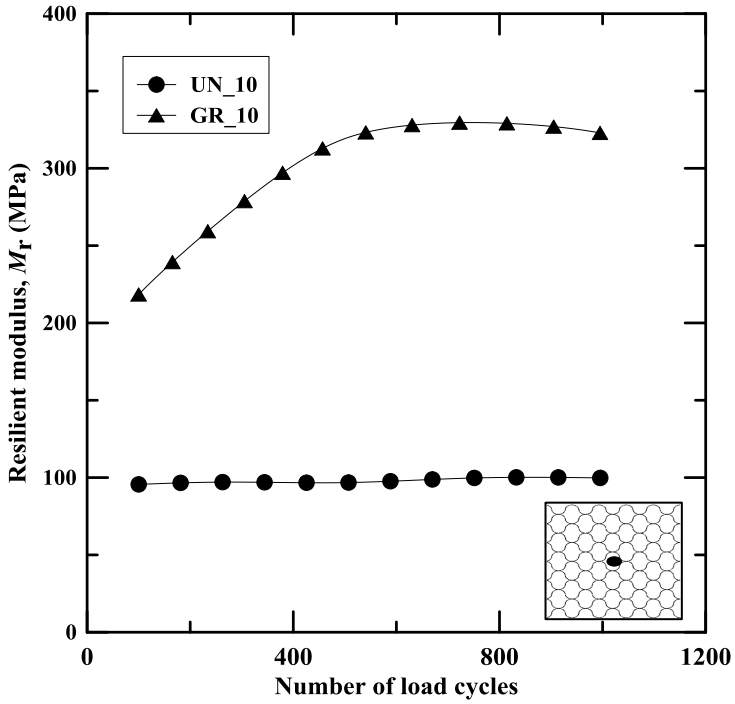

Figure 4.10 Variation of M_r with the number of load-cycles

4.3.2.3 Traffic Benefit Ratio (*TBR*)

The extension of pavement life is typically expressed in terms of a dimensionless index, Traffic Benefit Ratio (*TBR*). It is the ratio of the number of load cycles required to reach a given amount of rutting in the reinforced section to the number of cycles required in the unreinforced section to reach the same amount of rutting. *TBR* shows the additional traffic loads that can be applied to the pavement when a geocell reinforcement is added, with all the other pavement materials and geometry being equal. The *TBR* is also denoted to as the traffic improvement factor and is given by,

$$TBR = \frac{N_r}{N_u} \tag{4.8}$$

where N_r is the number of load cycles on the geocell-reinforced test section and N_u is the number of load cycles on the unreinforced test section. Figure 4.11 shows the variation of *TBR* with number of load cycles. At the end of 1000 load cycles, *TBR* value of 15-cm geocell-reinforced base is 60% more than that of the 10-cm GRRB.

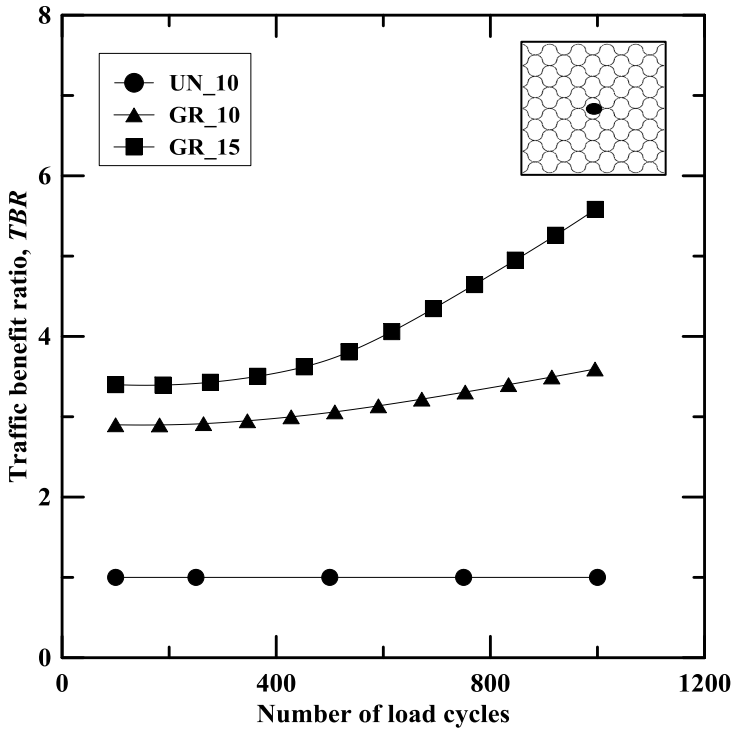

Figure 4.11 Variation of TBR with the number of load-cycles

4.3.2.4 Rut Depth Reduction (*RDR*)

The rutting behavior of GRRB is quantified in terms of a parameter called rut depth reduction (*RDR*). It is the ratio of the difference between PD of the unreinforced test section (D_u) and the geocell-reinforced test section (D_r) to that of

the unreinforced test section at a specific number of load cycle (Saride et al. 2015). Hence, *RDR* at a particular load cycle can be expressed as:

$$RDR = \left(1 - \frac{D_r}{D_u}\right) \times 100\ \% \tag{4.9}$$

Figure 4.12 shows the comparison of *RDR* of 10-cm and 15-cm geocell-reinforced test bed. *RDR* initially increases and then attains an approximately constant value of 70% for 10-cm and 76% for the 15-cm geocell-reinforced test bed, respectively. This indicates that the geocell height has a substantial effect on the rutting behavior of GRRB. When the height of geocell is less than the width of the loading plate, a membrane effect is developed under the application of wheel load and as the geocell height increases to more than the width of the loading plate, a beam bending effect is developed in the GRRB (Thakur et al. 2012) which reduce the rutting of the pavement layers.

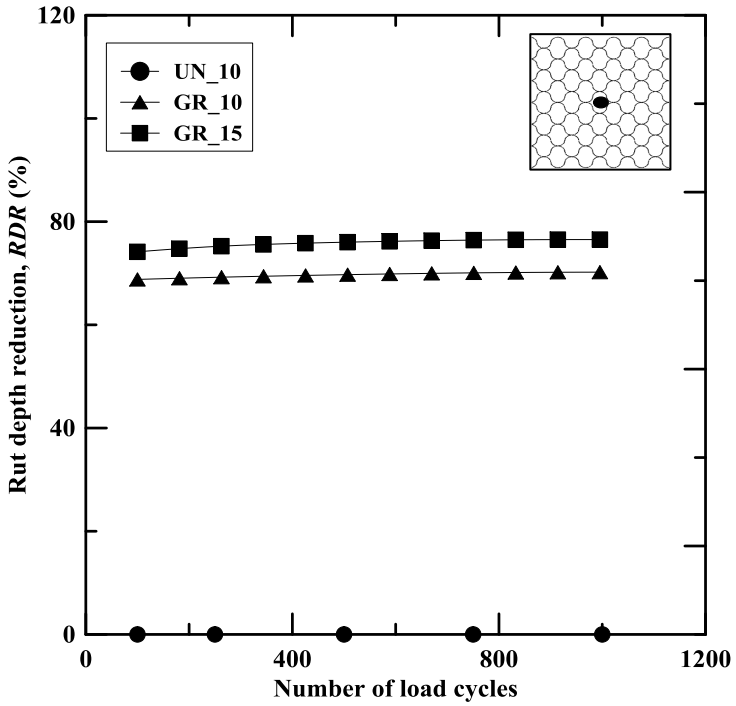

Figure 4.12 Variation of RDR with number of load-cycles

4.3.3 *Parametric Studies*

Parametric studies were performed on the GRRB layer under repeated loading by varying the height, gradation of RAP, and location of loading (George *et al.* 2019b). The performance of the geocell-RAP system was evaluated based on the improvement in the M_r of the geocell-reinforced RAP sections.

4.3.3.1 Geocell Height

Geocell reinforcement with two different heights, 10-cm, and 15-cm, were used for the study. The M_r variation with number of load cycles for the unreinforced and geocell-reinforced case is shown in Figure 4.13. It can be noticed that the M_r of reinforced RAP increased with an increase in the height of geocell reinforcement.

The rate of increase in M_r of GRRB is significant till 750 cycles and then it reaches a constant value of 325 MPa and 450 MPa for 10-cm and 15-cm height geocell, respectively. With the increase in height of geocell, the additional lateral confinement in the RAP base increases and the applied load is transferred to a larger area resulting in the improvement in overall performance of the RAP layer. A similar observation was also made by Thakur et al. (2012).

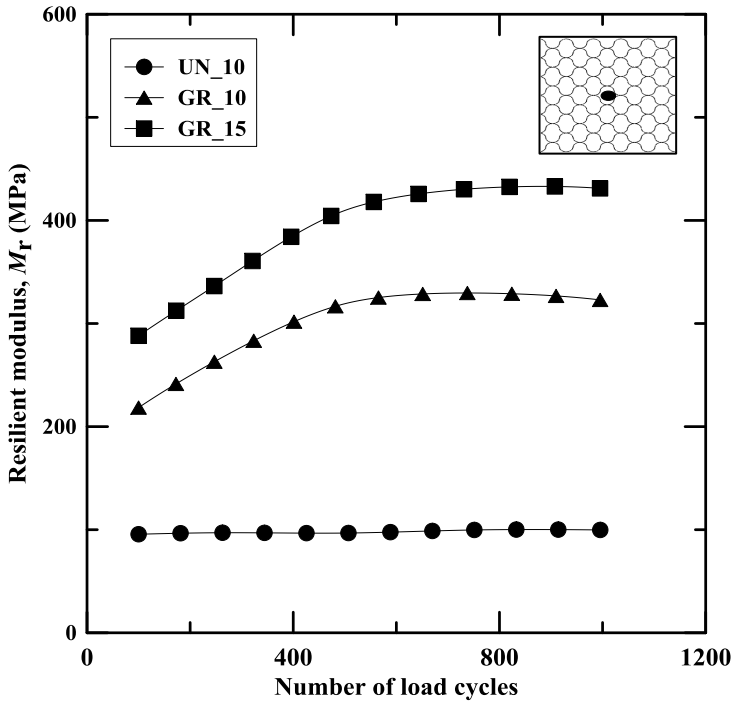

Figure 4.13 Variation of M_r with height of geocell

4.3.3.2 Gradation of RAP

To analyze the effect of gradation on the strength and stiffness behavior of the test bed, repeated load tests were carried out on two different RAP materials, R1 and R2 from different locations in Texas. R1, which is coarse-grained with

fewer fines, was used for all the static and repeated laboratory testing. R2 contained more amount of fine particles than R1. The test results are shown in Figure 4.14. It can be noticed that the gradation of the RAP layer has a significant effect on the M_r of the GRRB. GR10_R1 (GR10 is the 10-cm geocell-reinforced and R1 is the coarse RAP with fewer fines) with the coarser RAP particles showed substantial improvement compared to GR10_R2 (GR10 is the 10-cm geocell-reinforced and R2 is the RAP with more fines). This may be due to the development of particle interlocking through the apertures of the geocell reinforcement which will tend to reduce with increase in fineness of the material.

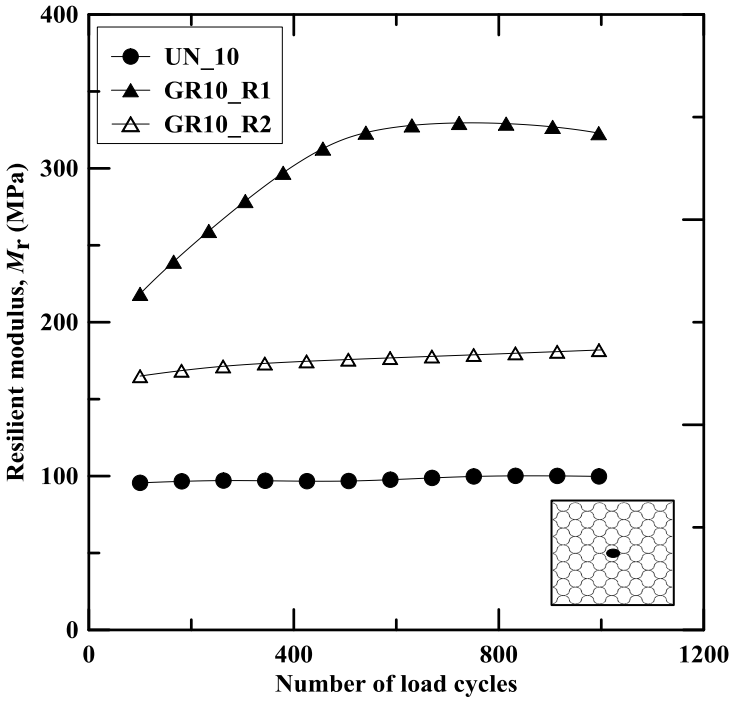

Figure 4.14 Variation of M_r with gradation of RAP

4.3.3.3 Location of Loading

The location of the loading can influence the behavior of the geocell-reinforced RAP base. The load can be applied by placing a loading plate either on the center of geocell ('a' in Figure 6) or on the joint of geocell ('b' in Figure 6). Laboratory testing was performed on both the cases and the results are plotted in Figure 4.15. It can be noticed that the test bed with loading on joint performed better than the loading on the center case. The slight improvement of about 7% in M_r was due to the presence of weld on the joint which enabled the reinforced test bed to sustain the higher load.

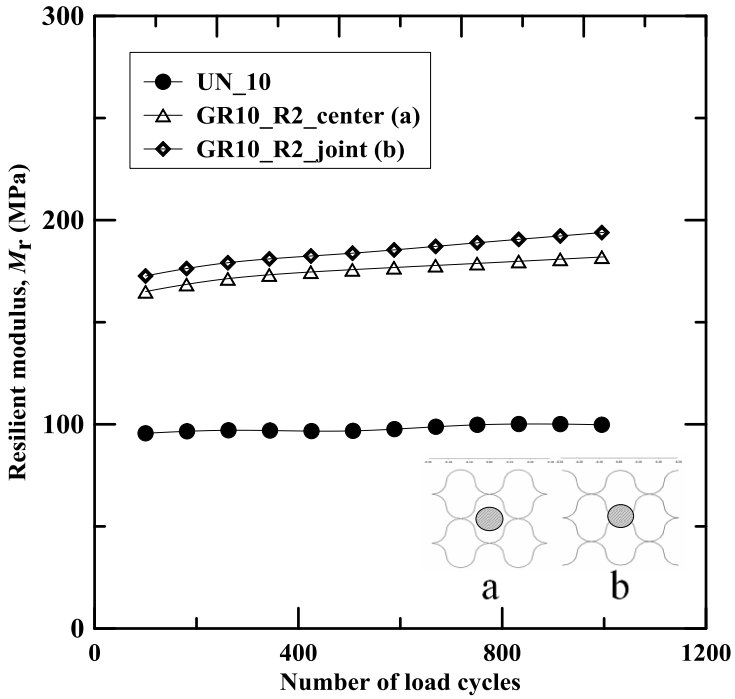

Figure 4.15 Variation of M_r with location of loading

4.4 Design of Geocell-reinforced Flexible Pavements

A modified AASHTO 1993 method based on *TBR* by Holtz et al. (2008) was used for designing the geocell-reinforced pavement sections. Mechanistic-Empirical Pavement Design (MEPD) method was not used in this study as it requires information regarding several complex and intricate variables which are generally not available to practitioners. Additionally, the option for accommodating geocell reinforcement in the flexible pavement design is not currently available in the AASHTO MEPDG manual of practice (AASHTO 2008). For unreinforced sections, the traditional AASHTO 1993 method was adopted.

According to the AASHTO 1993 method, the pavement is considered as a multi-layer elastic system with an overall structural number (SN) which indicates the total pavement thickness and its resiliency to repeated traffic loading. According to AASHTO 1993, the number of cumulative 18-kip ESAL over the design life of the pavement is given by,

$$\log W_{18} = Z_R \times S_0 + 9.36 \times \log(SN+1) - 0.2 + \frac{\log\left(\frac{\Delta PSI}{2.7}\right)}{0.4 + \left[\frac{1094}{(SN+1)^{5.19}}\right]} + 2.32 \times \log(M_{rs}) - 8.07 \quad (4.10)$$

where Z_R is the standard normal deviate for reliability level, S_0 is the combined standard error of the traffic prediction and performance prediction, SN is the structural number of the pavement layer, ΔPSI is the allowable loss in serviceability, and M_{rs} is the resilient modulus of the subgrade. The structural

number of the pavement is calculated using the nomograph of equation (4.10) corresponding to the desired design life and allowable loss in serviceability (W_{18} = *1,000,000* ESALs, reliability = 95%, standard deviation = 0.45, ΔPSI = 1.7, and subgrade modulus = 76 MPa are adopted for this study). Once the required overall *SN* has been estimated, the base layer thickness for the unreinforced pavement ($h_{2,u}$) can be designed using the following equation:

$$h_{2,\,u} = \frac{SN - (a_1 \times h_1)}{(a_2 \times m_2)} \tag{4.11}$$

where, a_1 and a_2 are the layer coefficient of surface and base courses, respectively, h_1 is the thickness of the surface course, and m_2 is the drainage coefficient (m_2 = 1.2*)* for the base layer. The surface and base layer coefficients are usually computed from the resilient or elastic modulus of the respective layers. The structural coefficient of the surface layer a_1 (corresponding to $M_{r,s}$ = 2900 MPa) and the URB a_2 are determined using the AASHTO equation:

$$a_1 = 0.398 \times \log M_{r,s} - 0.953 \tag{4.12}$$

$$a_2 = 0.249 \times \log M_{r,b} - 0.977 \tag{4.13}$$

where $M_{r,s}$ and $M_{r,b}$ is the resilient moduli of surface and base courses, respectively.

For the geocell-reinforced case, a modified form of AASHTO procedure based on TBR proposed by Holtz et al. (2008) was used to calculate the reinforced base thickness. The extended pavement life, W_{18r} with geocell reinforcement,

expressed in terms of *TBR* and the design life without reinforcement, W_{18u} is given by:

$$W_{18r} = TBR \times W_{18u} \quad (4.14)$$

The modified structural number, SN_r corresponding to the extended pavement life can be calculated from equation (4.10). The increase of structural number, ΔSN, which quantifies the benefit of geocell reinforcement is given by the equation (4.15). The increase in structural number with geocell reinforcement is shown in Figure 4.16. The structural number increased from 3.4 to 4.2 and 4.5 for 10-cm and 15-cm geocell-reinforced pavement, respectively.

$$\Delta SN = SN_r - SN_u \quad (4.15)$$

The reduced thickness of the reinforced base layer can be calculated from,

$$h_{2,r} = \frac{(SN_u - \Delta SN) - a_1 h_1}{a_2 \times m_2} \quad (4.16)$$

Figure 4.17 shows the reduction in thickness of the base layer with the geocell reinforcement. The reduction in base thickness is about 30% to 50% when geocell is used to reinforce the RAP material. This results from the improved strength and stiffness characteristic of the RAP material due to lateral confinement offered by geocell walls on the encapsulated material.

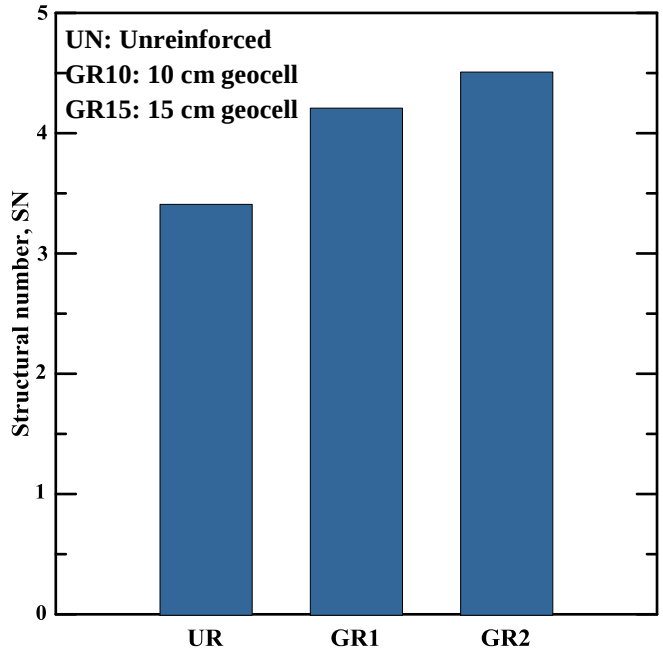

Figure 4.16 Increase in structural number with geocell reinforcement

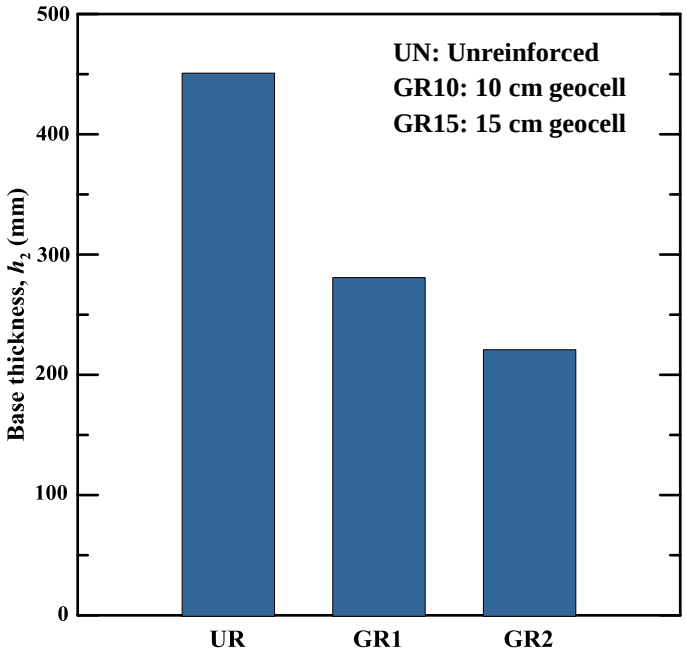

Figure 4.17 Reduction in base thickness with geocell reinforcement

4.5 Analysis of Geocell-Reinforced Flexible Pavements

To evaluate the effect of geocell reinforcement on the fatigue and rutting behavior of pavement, a 10-cm and 15-cm geocell-reinforced pavement sections and the corresponding unreinforced pavement sections with same thickness were adopted and a layered elastic analysis was performed by applying traffic loading. A typical steer axle load of 32 kN (7200 lbs) was applied at a radius of 11 cm (4.37 in.) to simulate a tire pressure of 827 kPa (120 psi) as shown in Figure 4.18. A 3 cm RAP cover was used for both 10-cm and 15-cm GRRB in the analysis. Strains developed at the two-critical location of the pavement were considered for the analysis: The horizontal tensile strain (ε_t) developed at the bottom of the HMA layer and the vertical compressive strain (ε_v) at the top of the subgrade.

The fatigue life (N_f) was computed from ε_t and the rutting life (N_r) from ε_v using fatigue (Timm et al. 1999) and rutting (Asphalt Institute, 1982) models, respectively and are tabulated in Table 4.2.

$$N_f = k_1 \times 10^{-6} \left(\frac{1}{\varepsilon_t}\right)^{k_2} \tag{4.17}$$

$$N_r = k_3 \times \left(\frac{10^{-6}}{\varepsilon_v}\right)^{k_4} \tag{4.18}$$

where, k_1 = 2.830, k_2 = 3.148, k_3 = 1.077 x 10^{18} and k_4 = 4.484.

The analysis result shows that the geocell reinforcement increased the fatigue and rutting life by approximately three to eight times and 8 to 30 times, respectively.

The rutting life showed significant upsurge due to the increase in M_r of the base layer that resulted from the presence of additional lateral confinement offered by the geocell reinforcement.

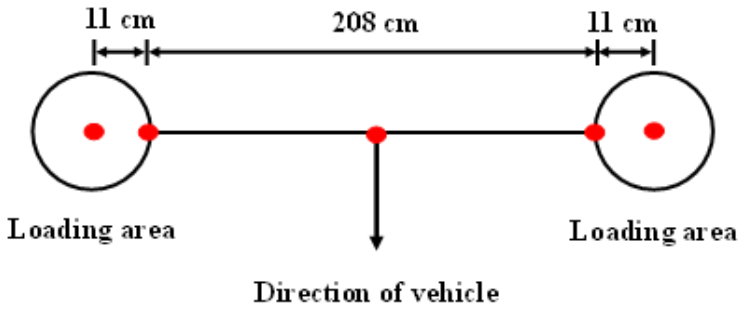

Figure 4.18 Sigle axle wheel load used to simulate tire pressure

Table 4.2 Fatigue and rutting life of the pavement section for same base thickness

Pavement type	Thickness (mm)	ε_t ($\times 10^{-6}$)	ε_v ($\times 10^{-6}$)	N_f (cycles)	N_r (cycles)
Unreinforced	130	802	885	15756	65650
10-cm geocell-reinforced	130	542	552	54095	545178
Unreinforced	180	782	868	16788	71616
15-cm geocell-reinforced	180	397	396	139665	2417526

Note:
ε_t is the horizontal tensile strain,
ε_v is the vertical compressive strain, and
N_f and N_r are the fatigue and rutting life of the pavement, respectively.

4.6 Summary

This chapter demonstrates the results from large-scale experimental studies performed to quantify the benefits of using HDPE geocell-reinforced RAP material as the pavement base layer. For static loading case, the performance improvement

of geocell reinforcement was quantified in terms of bearing capacity (q) and subgrade modulus (k_s). The bearing pressure at 25% settlement ratio was observed to be 1550 kPa and 2150 kPa, respectively for 10-cm and 15-cm GRRB. Test results showed that the maximum PRS value for 10-cm and 15-cm GRRB are 30% and 75%, respectively. This clearly shows that the presence of geocell reinforcement not only increased the bearing capacity but also reduced the vertical settlement of the RAP bases significantly.

The HDPE geocell increased the M_r of the base layer by approximately 3 to 4 times and reduced the PD of RAP base by 70% to 80% for 10-cm and 15-cm GRRB, respectively. The improvement in performance may primarily be due to the increase in stress distribution angle caused by the lateral distribution of stresses through the interconnected geocell pockets. The repeated loading on geocell-reinforced bases resulted in a confining mechanism within the geocell pockets, that resulted in the lateral distribution of stresses developed under loading. This lowered the vertical stresses and PD on the pavement subgrade. The magnitude of elastic deformation for all the three cases decreased gradually to a constant value after 500 load cycles. Additionally, the M_r and PD values were observed to gradually reach a constant after 500 load cycles. Hence, a minimum number of 500 load cycles is recommended as pre-conditioning cycles for large-scale repeated load box tests.

The test results were used to perform pavement design to quantify the reduction in base thickness with geocell reinforcement. It was observed that the

geocell reinforcement significantly reduced the thickness of the RAP base layer. This is due to the increase in stiffness of the geocell-RAP composite due to the lateral confinement and tension membrane effect offered by the geocell reinforcement. The increase in base stiffness reduced the vertical stress transmitted to the subgrade thereby improving the performance of the entire pavement section. A linear elastic analysis was also performed on the unreinforced and geocell-reinforced pavement section with the same base thickness to analyze the influence of geocell reinforcement in the rutting and fatigue life of the pavement. The analysis showed that the geocell reinforcement increased the fatigue and rutting life by approximately 8 and 30 times, respectively. Cost savings of these layers will be high as this system promotes the use of RAP types of recycled base aggregates while reducing landfilling and air pollution emissions.

Chapter 5

NUMERICAL ANALYSIS OF GEOCELL-REINFORCED RAP BASES USING FINITE-DIFFERENCE APPROACH

5.1 General

Numerical analysis was performed to analyze the load carrying mechanism of geocell-reinforced RAP bases (GGRB). A finite-difference (FD) based approach was adopted for performing this study. In this chapter, the model development and validation of large-scale static and repeated load tests and the load transfer mechanism of geocell reinforcement under static and repeated loading cases are discussed. Additionally, parametric studies were performed to study the effect of various factors such as height, modulus, size of geocell on the behavior of geocell.

5.2 Finite-Difference Approach

The FD method is the oldest numerical method used for solving differential equations with initial and boundary value problems. In this method, All the derivatives in the set of governing equation are substituted by an algebraic equation in terms of stresses and displacements at discrete points in space (Itasca 2013). In this study, an FD based *FLAC*^{3D} software is used for performing the numerical analysis. This approach uses explicit, time marching method to solve these algebraic expressions.

5.2.1 *FLAC^{3D} Software*

The Fast Lagrangian Analysis of Continua in three Dimensions (*FLAC^{3D}*) developed by Itasca Consulting Group, Inc. is a widely used FD commercial code in the field of geotechnical engineering. This software has been successfully used to numerically simulate various geotechnical problems in civil engineering. It offers many built-in constitutive material models and also provides a user interface to develop new constitutive material models. Hence, in this study, *FLAC^{3D}* is adopted for implementing the state dependent soil and geocell material model.

The explicit finite-difference solution scheme used in this approach has several advantages over finite elements, including the possibility of analyzing unstable systems (Itasca 2013). The explicit dynamic solution (EDS) scheme allows the implementation of strongly nonlinear constitutive models because the general calculation sequence allows the field quantities (velocities/displacements and forces/stresses) at each element in the model to be physically isolated from one another during one calculation step. The calculation sequence for one-time step in the EDS scheme is shown in Figure 5.1.

The calculation using EDS scheme involves solving two sets of equations including the equilibrium of motion and constitutive relationships. The new velocities and displacements for each tetrahedron element are derived from stresses and forces at each mass point. The new velocities are used to calculate the strain

rated of each tetrahedron element by using the Gauss divergence theorem. Then, the constitutive equations are used to calculate new stress from strain rates.

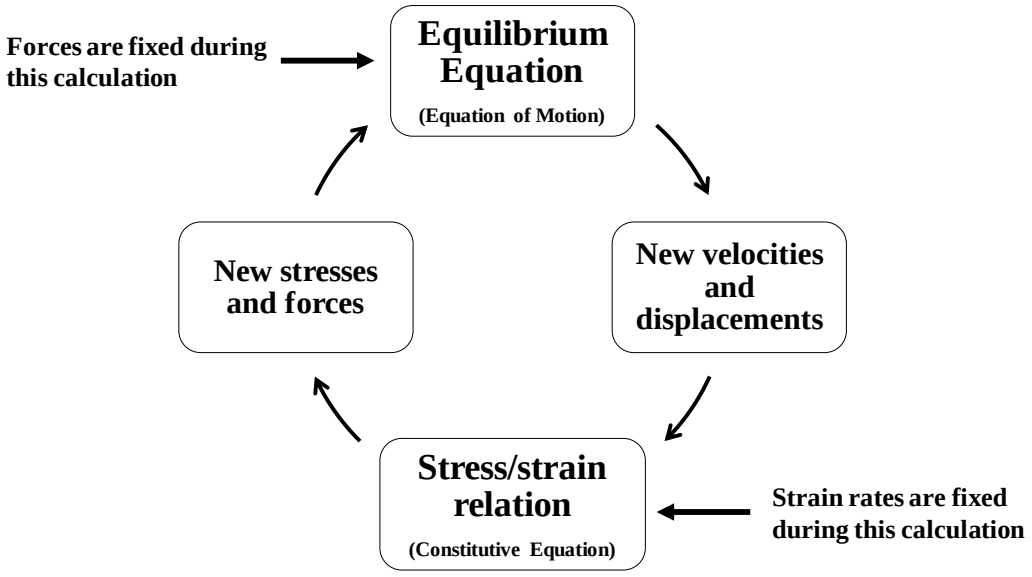

Figure 5.1 General calculation sequence for the EDS scheme (Itasca 2013)

5.2.2 *Material Models*

A constitutive model and the associated material properties are assigned to each material to simulate its actual behavior under static and repeated loading cases. This section briefly summarizes the material models used in this study.

5.2.2.1 Soil/RAP Model

The primitive radial cylinder mesh, which is basically radially graded mesh around a cylindrical loading area, was used to simulate the test bed model as shown in Figure 5.2. It has twelve reference points with four size entries and four dimension entries. The elastic-perfectly plastic Mohr-Coulomb model with tension cutoff as the failure criterion was used for RAP material and subgrade in this study.

The location of a stress point on this envelope is restrained by a non-associated flow rule for shear failure and an associated rule for tension failure(Itasca 2013). The Mohr-Coulomb criterion is articulated in terms of the principal stresses σ_1, σ_2 and σ_3 which are the three components of the generalized stress vector for this model (n = 3) as shown in Figure 5.3(Itasca 2013).

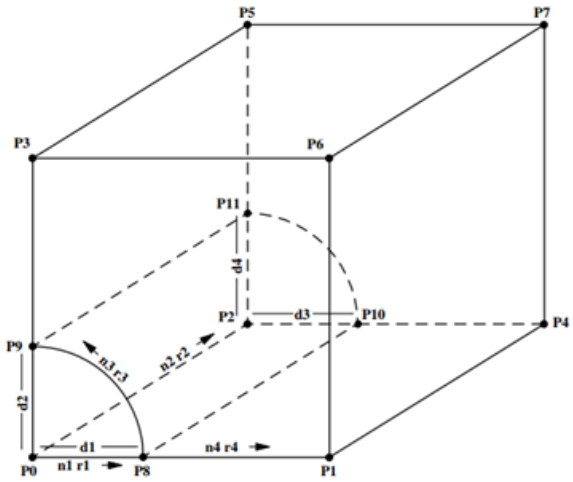

Figure 5.2 Radially graded mesh around cylindrical loading area (Itasca 2013)

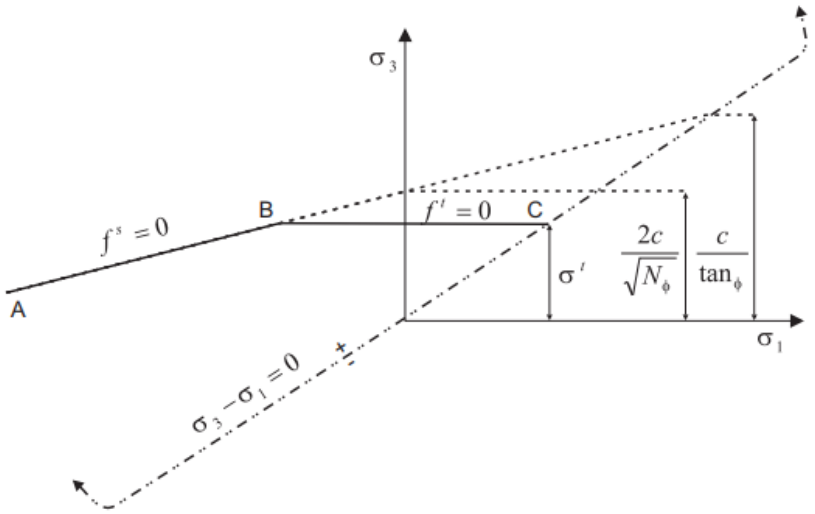

Figure 5.3 Mohr-Coulomb failure criterion used in the study (Itasca 2013)

5.2.2.2 Geocell Model

Geocell reinforcement was modeled using three-node flat geogrid structural elements as shown in Figure 5.4, which can resist membrane loading but have no resistance in bending. These elements will behave as an isotropic, linearly elastic material without failure limit. To simulate the three-dimensional honeycomb shape of geocell-reinforcement, zones with cylindrical mesh were used. The curved shape of the geocell was modeled using the cylindrical mesh zone of radius 0.075 m and the corners are modeled using cylindrical mesh zone of radius 0.075 m in the x-direction and 0.15 m in the y-direction. 224 geogrid elements were used to model a single geocell. The geocell mesh size was decided in such a way that the geocell nodes coincide with the nodes in the RAP zone to ensure proper transfer of stresses

between RAP and geocell. The honeycomb-shaped geocell model is shown in Figure 5.5.

The elastic modulus of the geocell material was calculated from the tensile stress-strain response provided by the geocell manufacturer. The secant modulus of geocell reinforcement was calculated with respect to 2% axial strain. The interface properties of the geocell and the RAP were incorporated in this model by providing interface shear modulus and interface friction angle as two third of the cohesion and friction angle of the infill material.

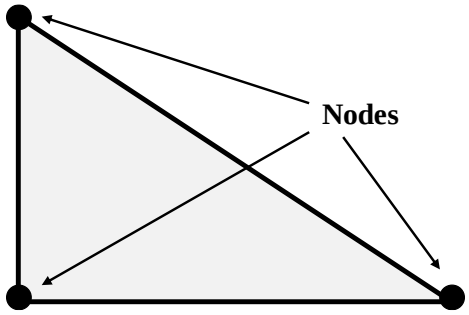

Figure 5.4 Three node flat geogrid element used in this study

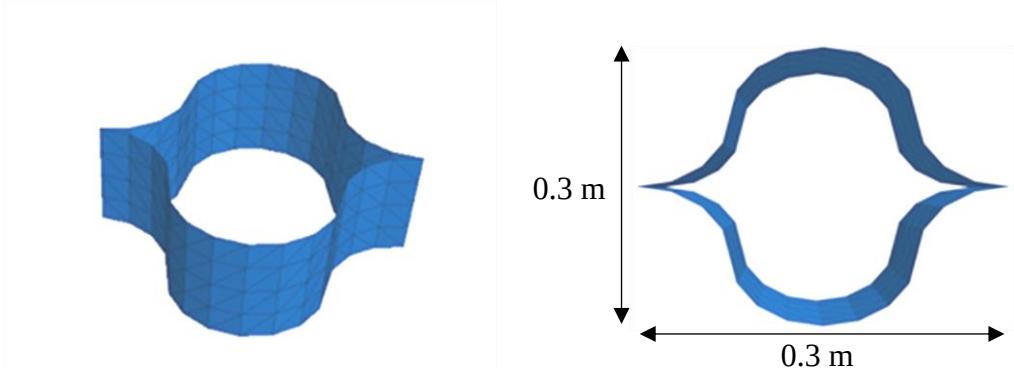

Figure 5.5 Honeycomb shaped geocell model

To simulate the realistic interaction between geocell and the infill material, additional interface properties were used such as interface friction angle, interface cohesion, and interface stiffness per unit area. The interface and shear behavior of the geocell-RAP composite was represented by providing a rigid attachment in the normal direction of each geocell node (Figure 5.6) and a cohesive and frictional behavior in the tangent plane to the geocell surface (Figure 5.7) (Itasca 2013). Based on previous literature (Yang *et al.* 2010, Hegde and Sitharam 2015a), the geocell-RAP interface friction angle and cohesion are adopted as:

$$\text{Interface fiction angle} = \arctan(0.8 \tan(\phi)) \quad (5.1)$$

$$\text{Interface cohesion} = 0.8 \times c \quad (5.2)$$

where ϕ and c are the friction angle and cohesion strength of infill material, respectively.

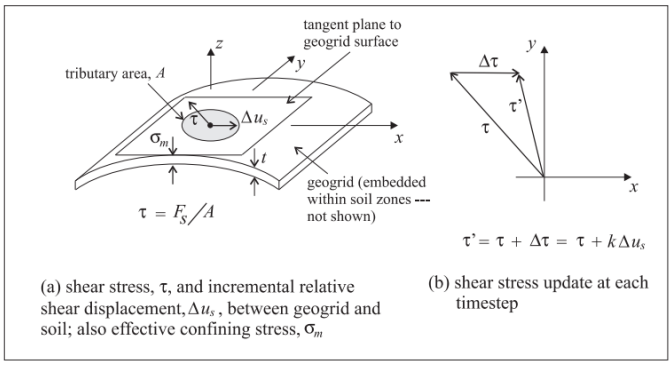

Figure 5.6 Interface behavior of geocell node used in this study (Itasca 2013)

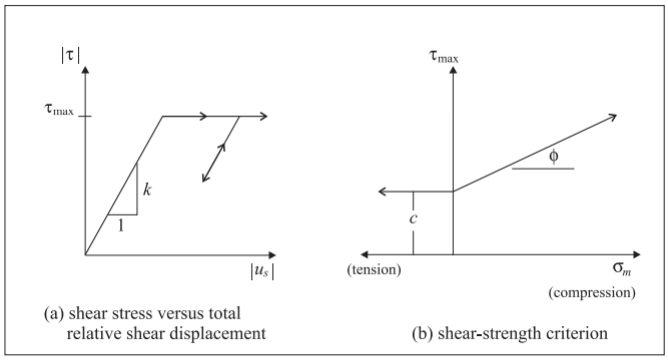

Figure 5.7 Shear-directional Interface behavior of geocell reinforcement (Itasca 2013)

5.3 Three-Dimensional Numerical Modeling of Static Load Box Tests

In this section, the model development, validation, and the confining mechanism of GRRB under static loading condition are discussed in detail. The fundamental components for modeling a problem are: defining the geometry of the problem by specifying a finite-difference grid, assigning a constitutive material behavior and the associated material properties and defining the initial state of the model by applying boundary and initial conditions. Once the model is developed, it was brought to an initial equilibrium state and then the actual analysis is performed by applying a static load on the surface of the model.

Two models were developed – one for the URB and the second model was for the GRRB where the geocell reinforcement was explicitly included. To perform a realistic study of geocell-reinforced RAP base and to avoid composite method errors, the geocell reinforcement was modeled separately and was added to the

unreinforced model. The modeling of honeycomb-shaped geocell reinforcement was discussed in section 5.2.2.2.

5.3.1 *Model Development*

The numerical model of the URB is a three-dimensional model based on the FD approach to matching the conditions for the test section discussed in section 5.2.2.1. Figure 5.8 illustrates the geometry and boundary conditions used for the model. The entire test section with a dimension of 0.6 m × 0.6 m × 0.44 m was modeled, and a uniform displacement was applied on the circular loading area of 0.15 m diameter to simulate rigid footing condition.

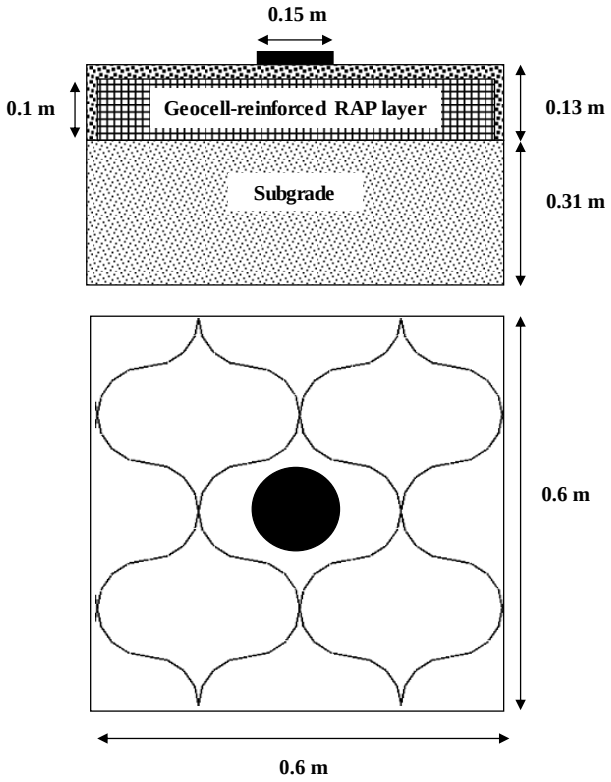

Figure 5.8 Geometry for the model under static loading

The built-in primitive radial cylinder shape which is radially graded mesh around cylindrical-shaped footing was used to expedite mesh generation for the experimental test box model. The use of radial cylinder mesh type also ensured the compatibility between the circular loading area and the RAP base. The finer mesh was adopted near the loading area to ensure proper stress transfer between the zones. The RAP base layer consisted of 1760 zones and subgrade consisted of 2112 zones.

Displacement along vertical direction was fixed at the bottom boundary of the model, and displacement along horizontal direction was fixed at all four sides of the test bed. Vertical displacement at a rate of 10^{-6} m/cycle was applied to the loading area and model was solved for 15000 iteration steps until the settlement at the surface of the RAP reached 15 mm. The FD model of the unreinforced case used for the analysis is shown in Figure 5.9. In geocell-reinforced case, geocell was placed by providing a cover thickness of 0.025 m from the surface. The FD model of GRRB is shown in Figure 5.10.

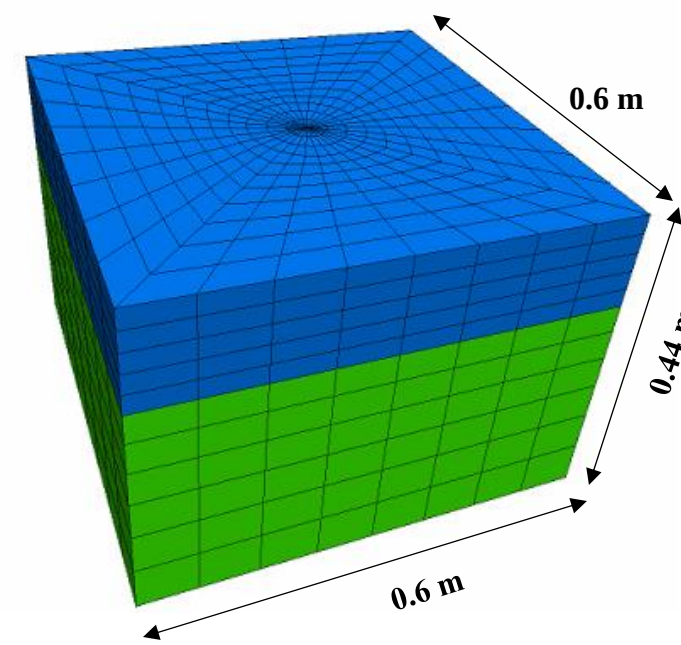

Figure 5.9 Finite-difference model for the unreinforced static load box test setup

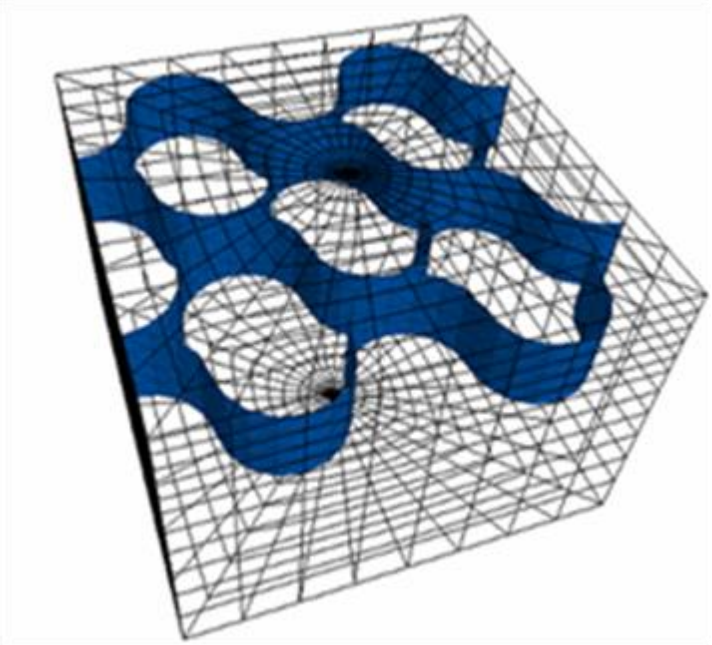

Figure 5.10 Finite-difference model with geocell reinforcement

5.3.2 *Material Models and Parameters*

Once the model development is complete, a constitutive model and the associated material properties were allocated to the model. Based on the extensive literature review, the elastic-perfectly plastic Mohr-Coulomb failure criterion was adopted for stiff clay subgrade and the RAP base layer in the numerical model (Sireesh *et al.* 2009, Hegde and Sitharam 2015a, Saride, George, V, *et al.* 2017a). The Mohr-Coulomb material model is discussed in detail in section 5.2.2.1.

The material properties assigned to RAP base and clay subgrade are listed in Table 5.1. Drained shear strength parameters (c' and ϕ') of the RAP material was obtained from the CD tests. The modulus of elasticity of the RAP material was determined from the large-scale tank tests (from load-settlement data). The modulus of elasticity of the RAP material was found using Burmister elastic layer theory as the confining stresses maintained in triaxial tests are much higher than the prevailed confining pressures in the large model test tank (Burmister 1943).

The geogrid structural element was used to model geocell reinforcement, that are three-node flat elements that resist membrane but does not resist bending loading. These elements will behave as an isotropic, linearly elastic material without failure limit. The elastic modulus of the geocell reinforcement was obtained from the tensile stress-strain response of the geocell material. The interface shear strength parameters (c_i and ϕ_i) for geocell reinforcement were calculated as two third of the cohesion and friction angle of the RAP material. The diameter of the

geocell pocket is approximately 30 cm. The parameters used for modeling geocell reinforcement are given in Table 5.2. The procedure adopted for modeling geocell is explained in section 5.2.2.2.

Table 5.1 Material parameters for RAP and clay subgrade

Properties	**RAP Base**	**Subgrade**
Material Model	Mohr-Coulomb	Mohr-Coulomb
Shear modulus (MPa)	14.6	2.8
Bulk modulus (MPa)	31.7	6.2
Cohesion (kPa)	98	130
Friction angle (°)	32	9
Density (kg/m^3)	1958	1703

Table 5.2 Material parameters used for geocell reinforcement layer

Properties	**Geocell**
Elastic Modulus (MPa)	400
Poisson's Ratio	0.45
Interface Cohesion (kPa)	78
Interface Friction Angle (degrees)	27
Thickness (mm)	1.46

5.3.3 *Validation of the Model*

Preliminary analysis carried out on the developed numerical model showed that simulation results are not affected by the boundary distance as the stresses and deformations developed under the static loading were contained within the boundaries. A suitable mesh density was adopted for the study based on the sensitivity analysis performed to evaluate the effect of time of simulation and mesh size on the accuracy of the test results. Initially, the unreinforced model was

developed and validated. Then the geocell-reinforced model was developed and validated by placing geocell reinforcement in the base layer. Uniform vertical displacement was applied on the circular loading area and the corresponding bearing pressure vs settlement ratio curve was plotted and was compared with the experimental results as shown in Figure 5.11. A good match was obtained between the measured and calculated results.

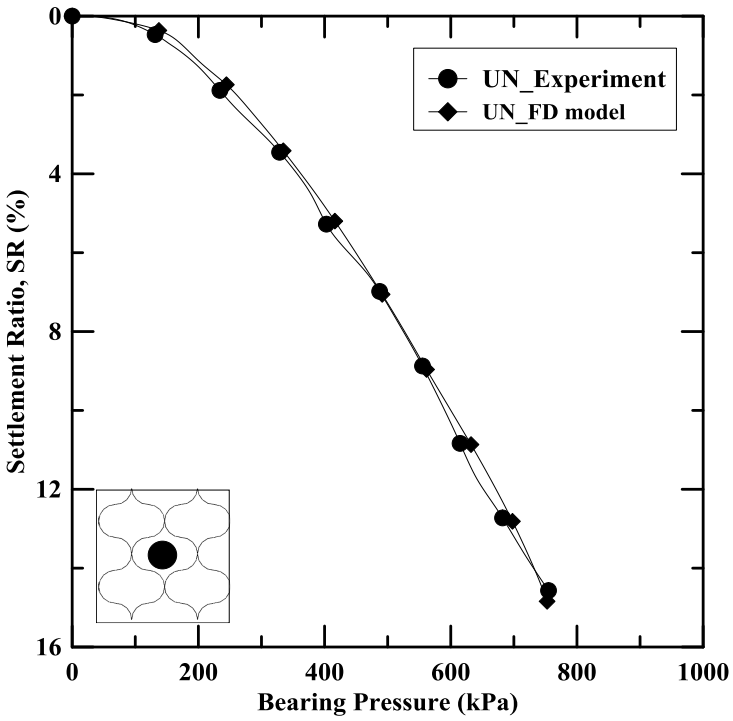

Figure 5.11 Validation of the unreinforced FD model - static load test

As a next step, the geocell-reinforced model was validated in the same way by plotting variation of bearing pressure with settlement ratio and by comparing it with the experimental result. The comparison of the laboratory and numerical results for the geocell-reinforced case is plotted and shown in Figure 5.12. Overall,

the FD model well simulated the behavior of GRRB under static loading condition. A slight deviation in the initial slopes can be observed in the comparison plots of the geocell-reinforced case. This might be due to compaction of RAP material inside the geocell reinforcement under the application of static loading.

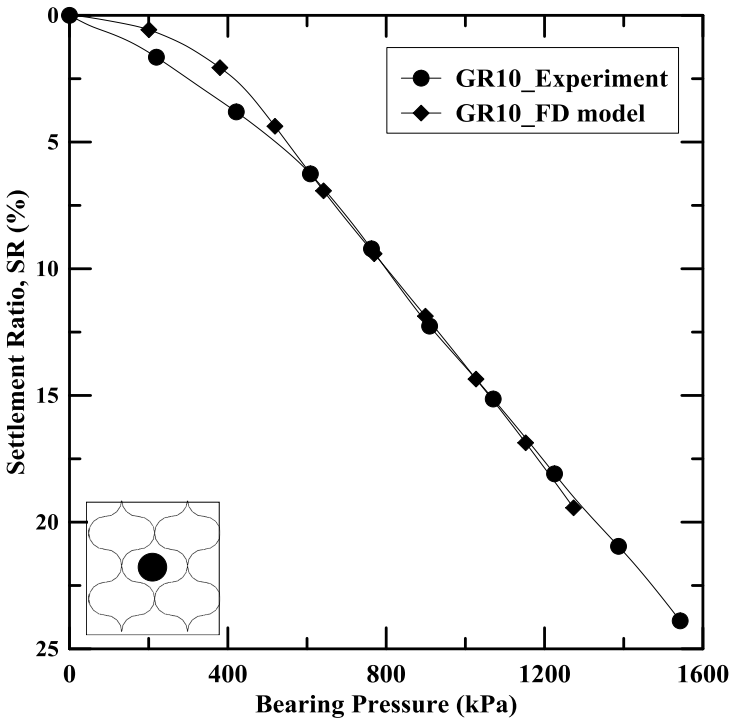

Figure 5.12 Validation of the geocell-reinforced FD model – static load test

5.3.4 *Results and Discussions*

The variation of bearing pressure with settlement ratio plots from both experimental and numerical analysis are compared and illustrated in Figure 5.13. The test section with 10-cm GRRB layer showed higher bearing capacity compared to the unreinforced case. It can also be observed that the geocell reinforcement

improved the performance of the RAP base layer by 45%, 43%, 35%, 34%, 59% at settlement ratios of 1%, 3%, 5%, 10%, and 20%, respectively.

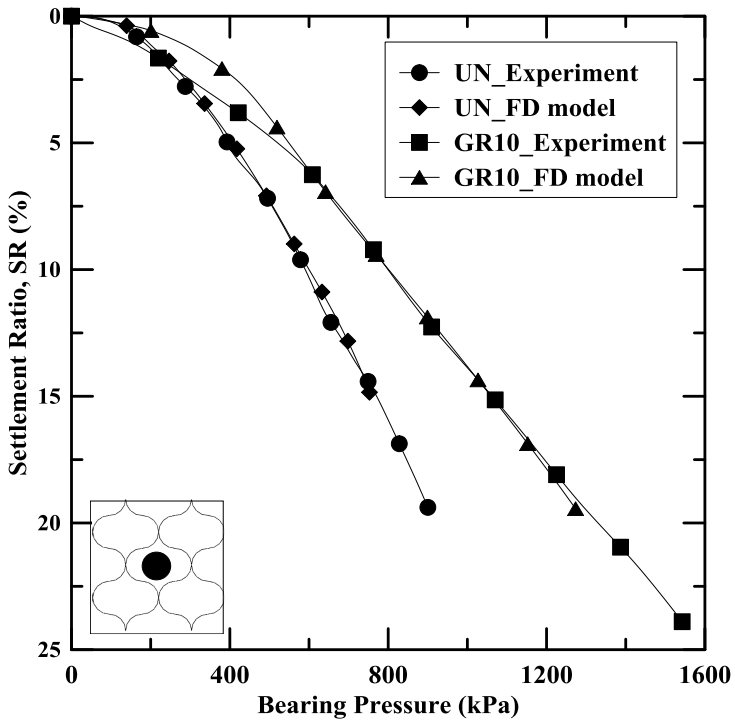

Figure 5.13 Comparison of the experimental and numerical results of unreinforced and geocell-reinforced sections

Figure 5.14 and Figure 5.15 show the contour profile of horizontal stress (vertical section) developed on the URB and GRRB, respectively. The lateral distribution of stresses under static loading is much more evident from the cross-section view of the contour profile of horizontal stress shown in Figure 5.16. These stress profiles are corresponding to a uniform settlement of 30 mm at the loading surface. From the figures, it can be observed that the stresses are distributed laterally to the wider areas in the geocell-reinforced RAP base layer. This is due to

the widening of stress distribution angle due to the presence of geocell reinforcement that causes the stress to spread laterally to the other geocell pockets. Similar observations were also made by Saride et al. (2009, 2017).

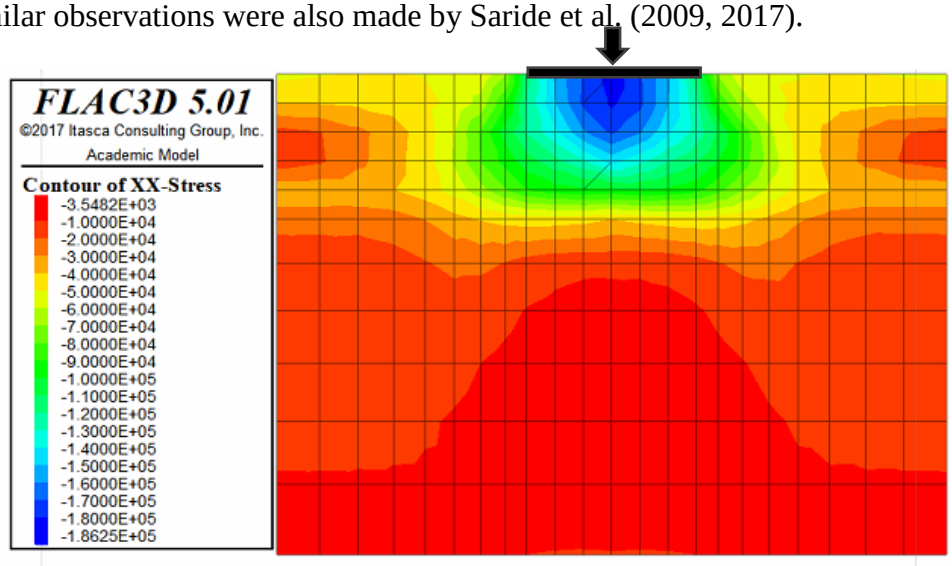

Figure 5.14 Contour profile of horizontal stress (vertical section) on the unreinforced model

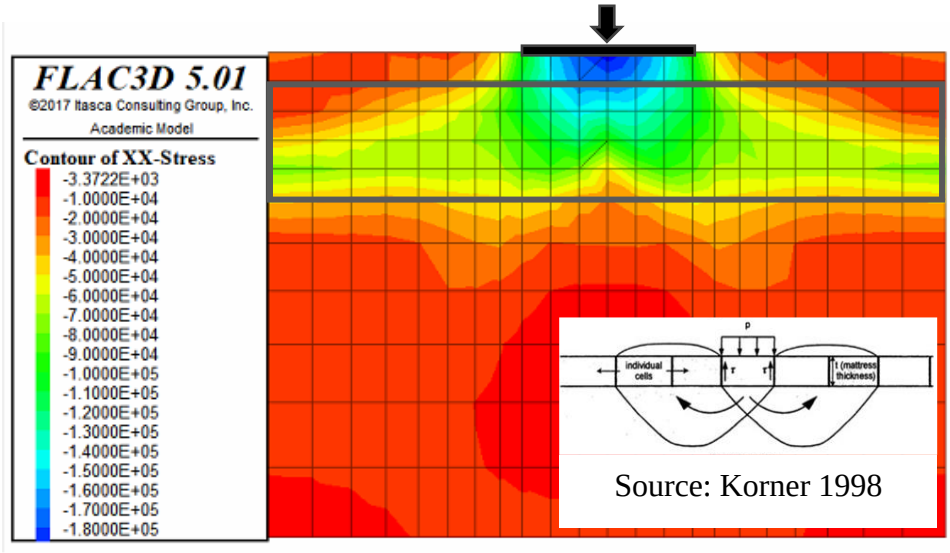

Figure 5.15 Contour profile of horizontal stress (vertical section) on the geocell-reinforced model

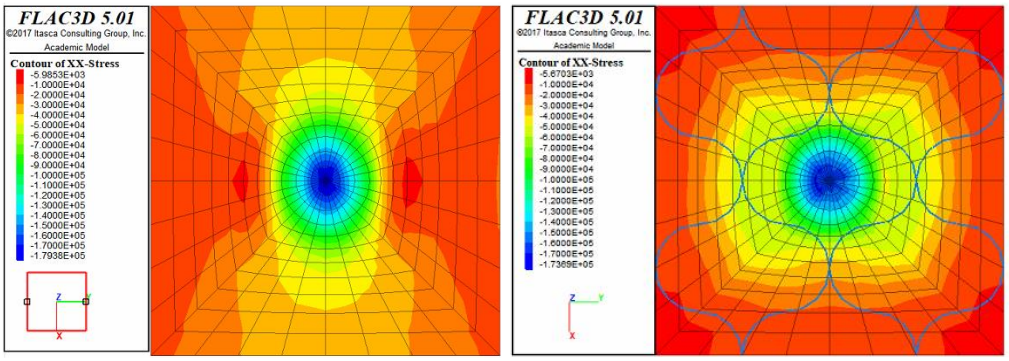

Figure 5.16 Contour profile of horizontal stress (horizontal cross-section) on the unreinforced and geocell-reinforced model

The vertical stress contour profile of the URB and GRRB sections corresponding to a uniform settlement of 30 mm at the loading area is illustrated in Figure 5.17 and Figure 5.18, respectively. Uniform distribution of stress to a larger depth can be observed in the case of test section with unreinforced RAP base (URB). For the GRRB section, the vertical stresses are observed to be accumulated in the geocell-reinforced region, resulted in a reduction in stress intensity at the subgrade. Similar observations were also made by Hegde and Sitharam (2015).

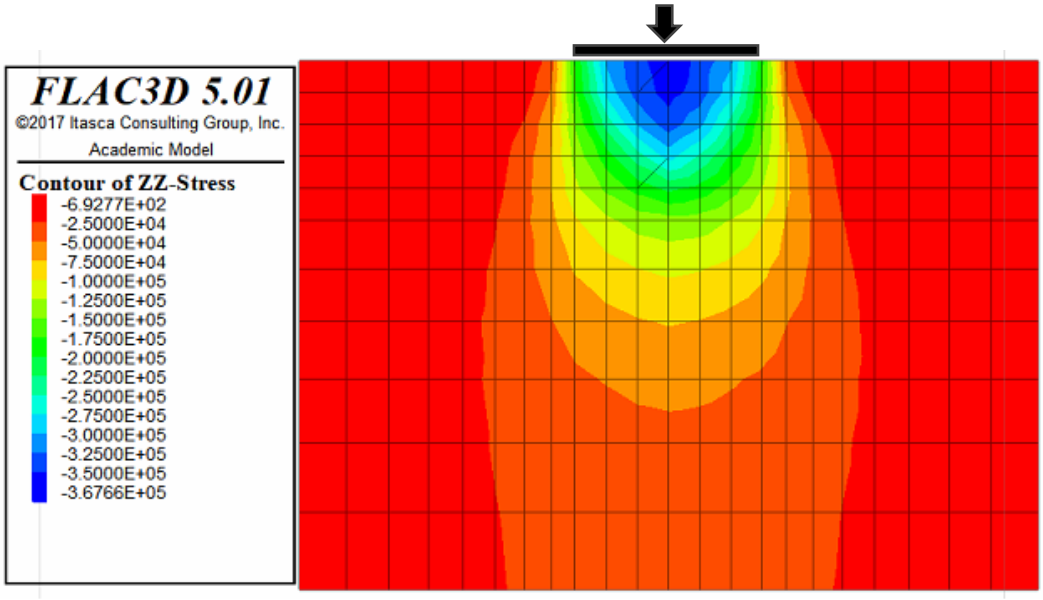

Figure 5.17 Vertical stress contour profile from the unreinforced model

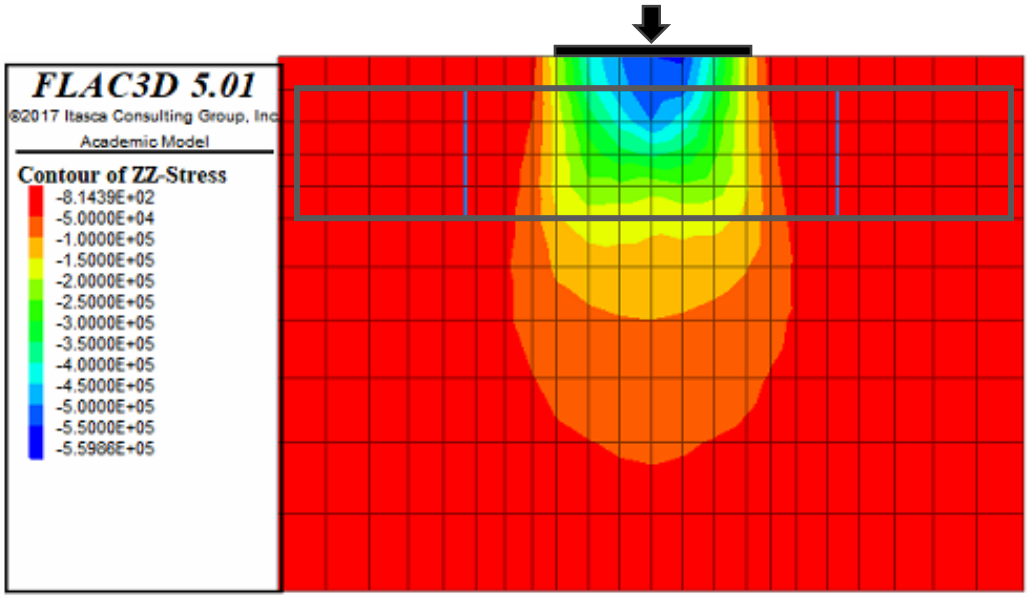

Figure 5.18 Vertical stress contour profile from the geocell-reinforced model

Figure 5.19 and Figure 5.20 show the vertical displacement contour profile of the URB and GRRB sections, respectively after the application of 30 mm

settlement at the loading surface. The heaving of the RAP material can be observed around the loading surface in the case of URB. It can also be observed that the vertical settlement at the surface of the subgrade is observed to be slightly higher for the GRRB than URB. This is due to the larger size of geocell compared to the diameter of the loading area. Previous researchers also identified the similar observation in their experimental investigation and concluded that the bearing capacity increases with an increase in pocket diameter at the cost of higher settlement (Mandal and Gupta 1994).

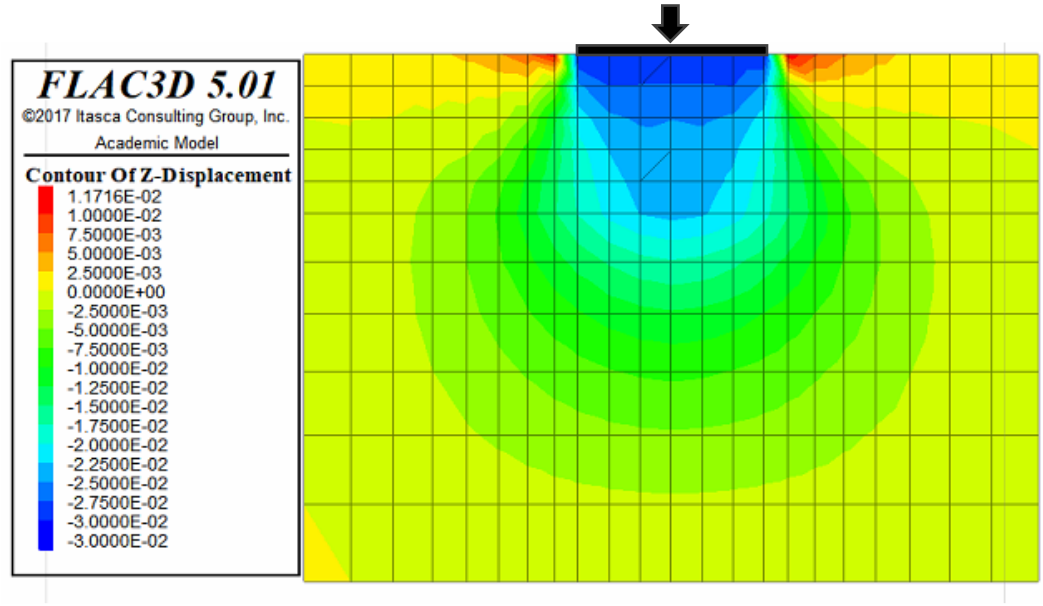

Figure 5.19 Vertical displacement profile of unreinforced model

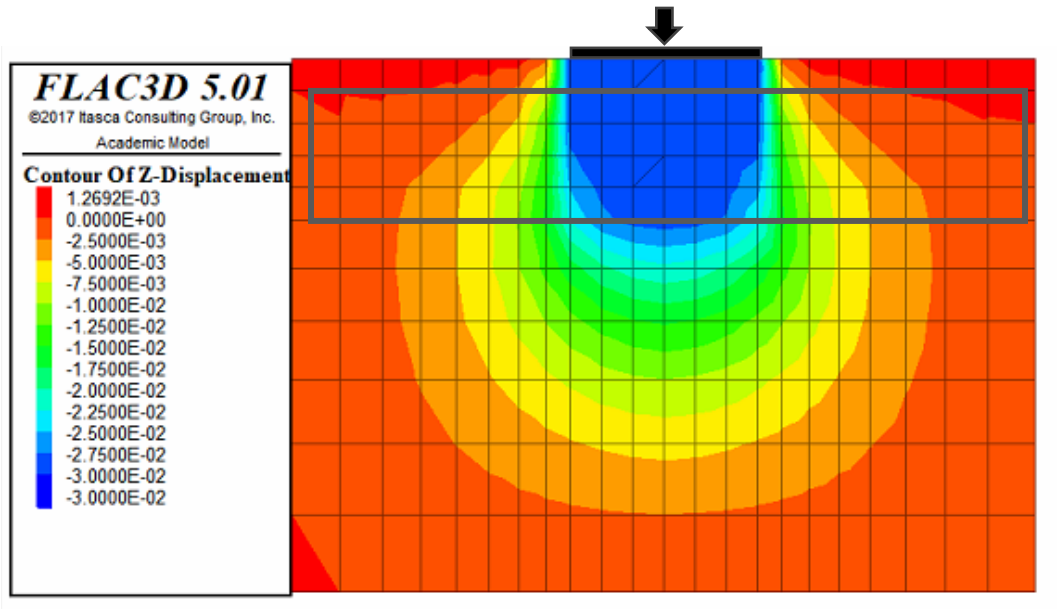

Figure 5.20 Vertical displacement profile of the geocell-reinforced model

The vertical displacement vector profile of geocell-reinforcement is shown in Figure 5.21. The red arrows indicate the displacement vectors of the geocell nodes and the length of each arrow show the corresponding nodal displacement. The beam bending effect of geocell reinforcement can be visibly observed in Figure 5.21. The geocell nodes at the top portion of the geocell-reinforcement are moving towards the loading area and the nodes at the bottom portion moving radially outward under the influence of static load. The displacement vector plot of geocell pocket on which the load was applied directly, is shown in Figure 5.22. The inward and outward movement of geocell nodes can be clearly observed in this figure.

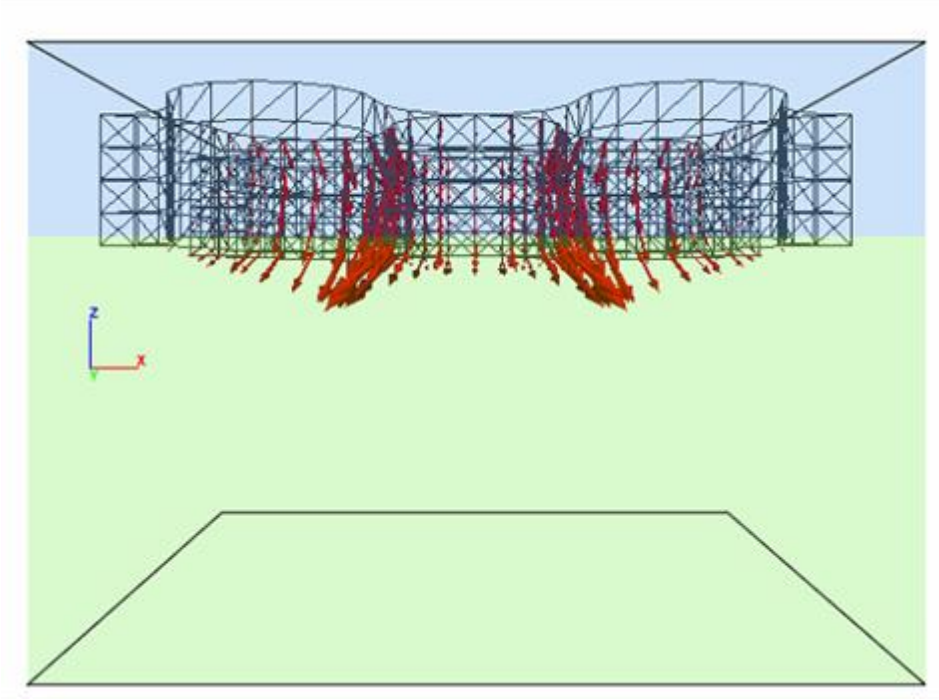

Figure 5.21 Vertical displacement vector profile of geocell reinforcement

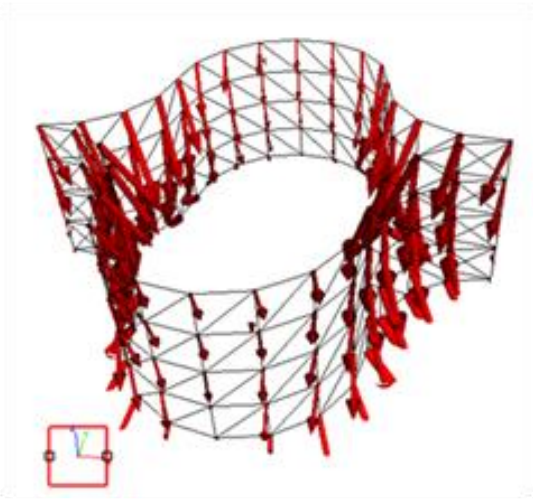

Figure 5.22 Vertical displacement vector profile of geocell pocket directly below the loading area

The shear stress developed on the geocell element due to loading is termed as coupling stress. The contour profile of coupling stress developed on geocell-reinforcement after the application of 30 mm settlement is shown in Figure 5.23. The variation of coupling stress developed at the top and the bottom portion of geocell reinforcement at different locations are plotted in Figure 5.24 and Figure 5.25. It can be observed that the coupling stress is significantly higher near the joint region (Location 2) which is closer to the loading area. This might be due to the highest radial movement of RAP material under static loading in that direction. The variation of coupling stress with applied stress at various location along the depth of geocell reinforcement at the maximum coupling stress location (Location 2) is shown in Figure 5.26.

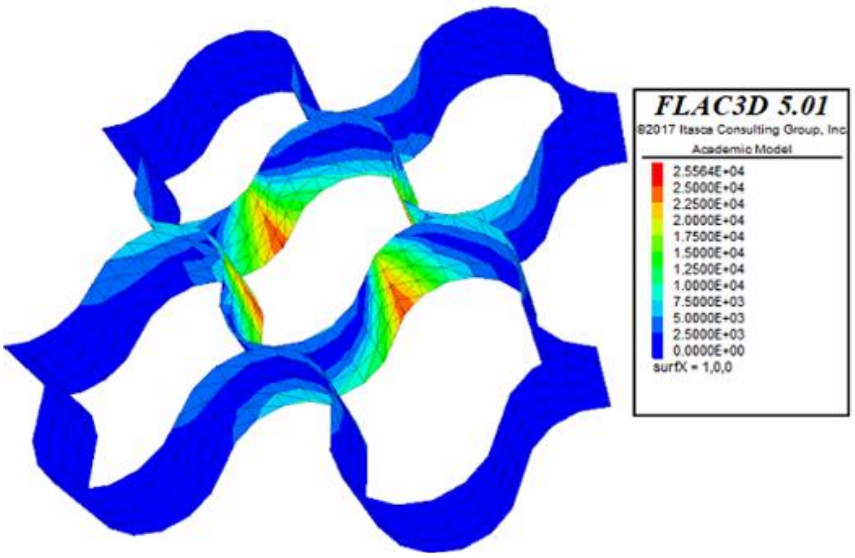

Figure 5.23 Coupling stress profile of geocell reinforcement

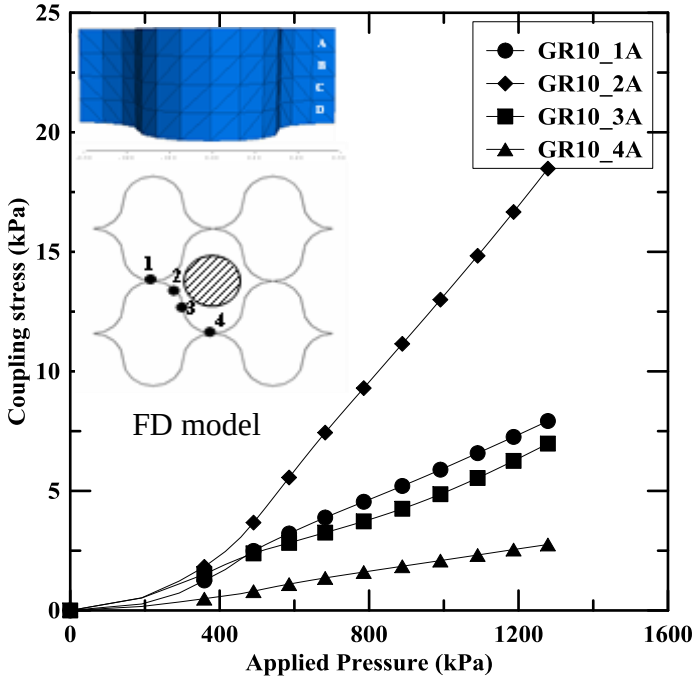

Figure 5.24 Variation of coupling stress developed at the top of geocell

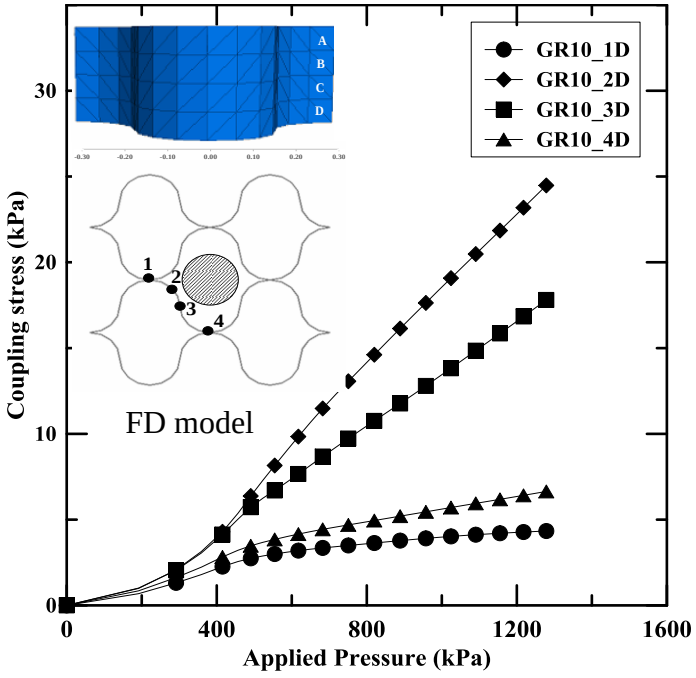

Figure 5.25 Variation of coupling stress developed at the bottom of geocell

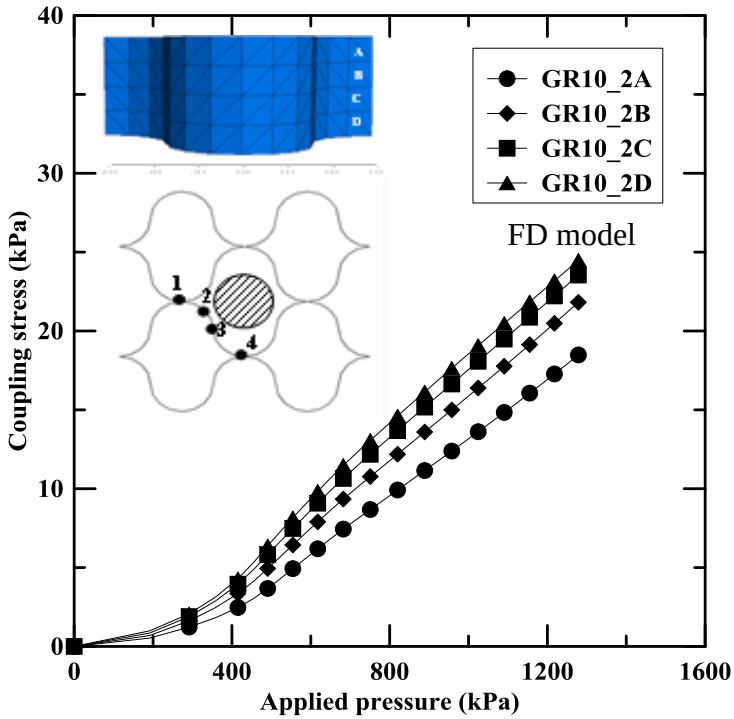

Figure 5.26 Variation of coupling stress throughout the depth of geocell at Location 2

5.3.5 *Parametric Studies*

5.3.5.1 Effect of Location of loading

The location of the geocell mattress on which the load applied plays a vital role in the behavior of geocell-reinforced bases. The load can be applied either directly on the geocell pocket (location *a*) or on the cell joint (location *b*). The possibility of joint failure is high when the loading plate rests directly on the joint of geocell reinforcement at very high loads. Figure 5.27 illustrates the comparison of both the cases. It can be observed that the test bed with loading plate on the weld

performed better than the one on which the load was applied on the geocell pocket due to the higher strength of the joint.

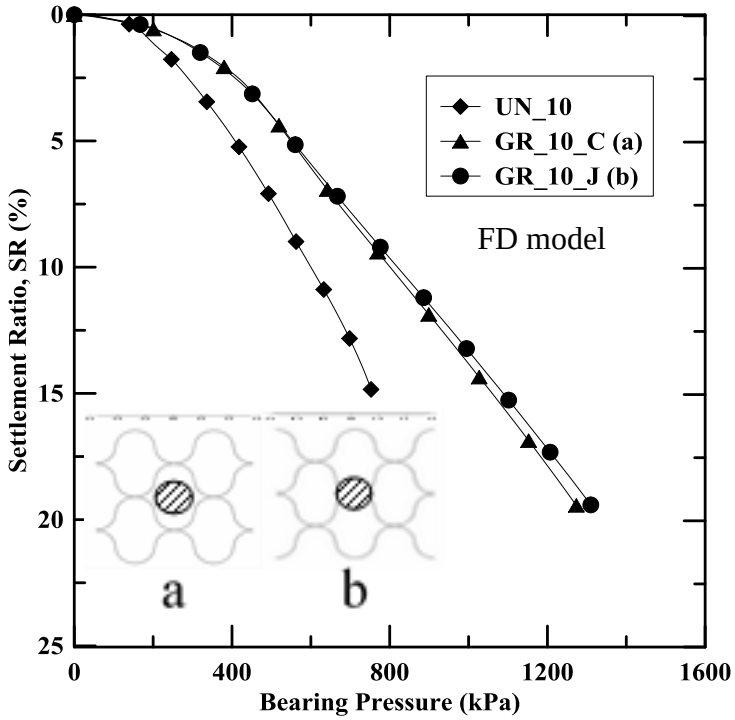

Figure 5.27 Effect of location of loading on bearing pressure

5.3.5.2 Effect of Height of Geocell

Three heights of geocell reinforcement including 10 cm, 15 cm, and 20 cm were compared in this study, to match the height of the commercially available geocells. The pressure-settlement behaviors of the three cases are shown in Figure 5.28. An increase in bearing capacity was observed with the increase in height of geocell reinforcement.

Dash et al. (2001) and (Hegde and Sitharam 2015c) were also made a similar type of observation for geocell-reinforced test beds under static loading.

With the increase in height of geocell reinforcement, the applied load will be dispersed laterally to a larger area. This results in the reduction of pressure transmitted to the subgrade which will improve the overall performance of the test section under static loading.

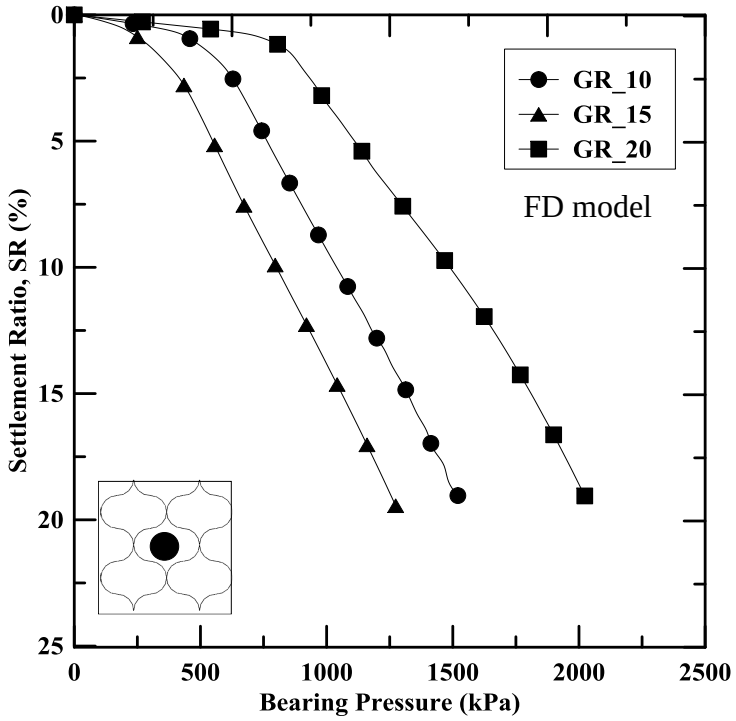

Figure 5.28 Effect of height of geocell on bearing pressure

5.3.5.3 Effect of Type of Infill Material

To evaluate the effect of different infill material on the performance of geocell-reinforced base layer over clay subgrade, a series of numerical simulations were performed. Three infill materials such as RAP, sand, and aggregates were considered for the study as shown in the plot Figure 5.29. The results clearly showed that geocell-reinforced aggregate material gives the highest improvement

in terms of bearing pressure followed by RAP material and sand. Aggregate infill due to its virtue of angularity provides higher elastic modulus and angle of internal friction which resulted in the improvement of the geocell-reinforced aggregate layer.

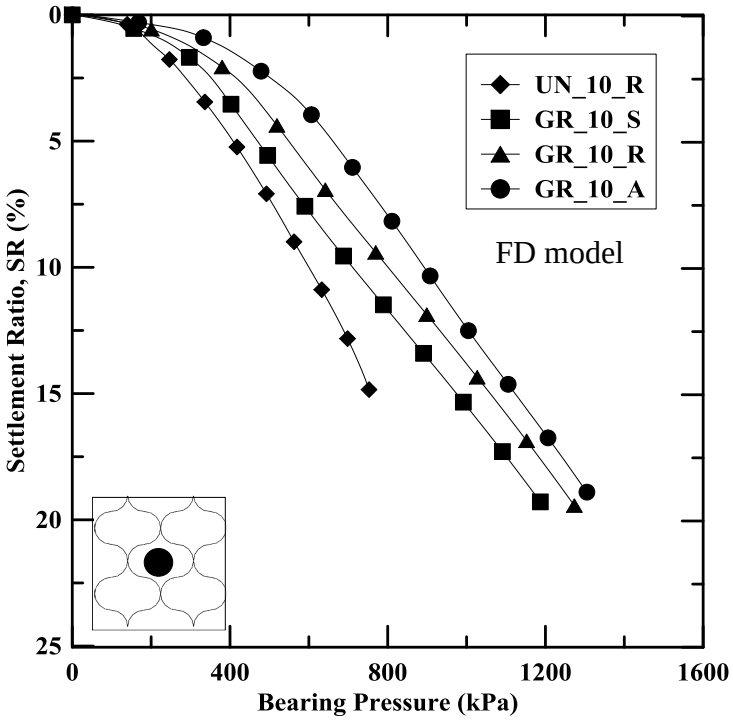

Figure 5.29 Effect of infill material on bearing pressure

5.3.5.4 Effect of Size of Geocell Pocket

To evaluate the influence of geocell pocket size on the performance of geocell-reinforced test bed, three geocell pocket width were considered in the analysis such as 0.2 m, 0.25 m and 0.3 m. The geocell pocket width was selected to match the commercial available geocell pocket sizes. Figure 5.30 shows the variation of bearing pressure with settlement ratio of RAP bases reinforced with

geocell reinforcement of different pocket sizes. The bearing pressure of GRRB increased with a decrease in the pocket size of the geocell reinforcement. The decrease in geocell pocket size resulted in an increase in lateral confinement of the infilled RAP material which in turn increased the load carrying capacity of the RAP base layer.

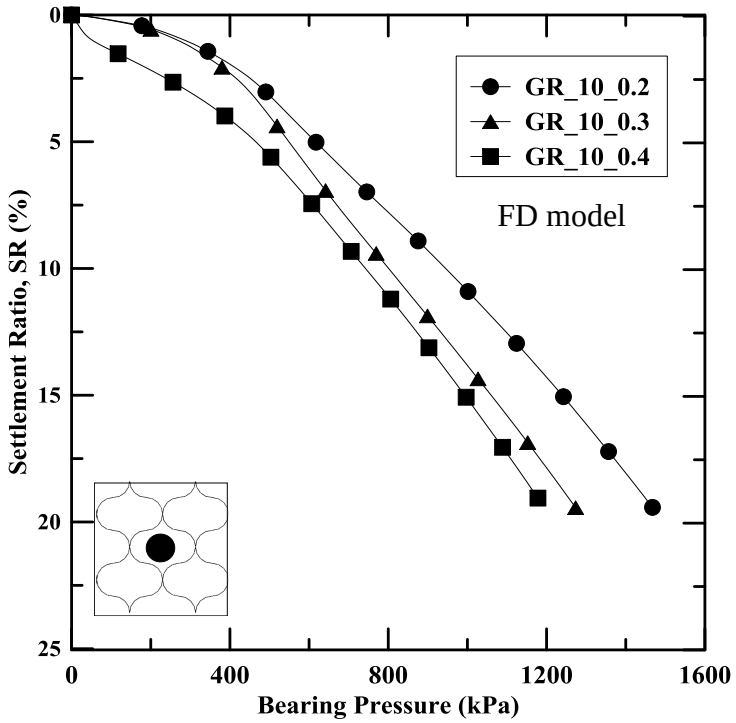

Figure 5.30 Effect of geocell pocket size on bearing pressure

5.4 Three-Dimensional Numerical Modeling of Repeated Load Box Tests

Numerical analysis was performed to investigate the load carrying mechanism of GRRB under repeated loading. A finite-difference based commercially available *FLAC*^{3D} software was used to model the large-scale laboratory box testing as shown in Figure 5.31. The fully nonlinear analysis method

is used by this approach to realistically predict the PD behavior of the model. In this section, the model development and validation with the large-scale repeated load laboratory test results, and the confining mechanism of geocell reinforcement under repeated loading are discussed.

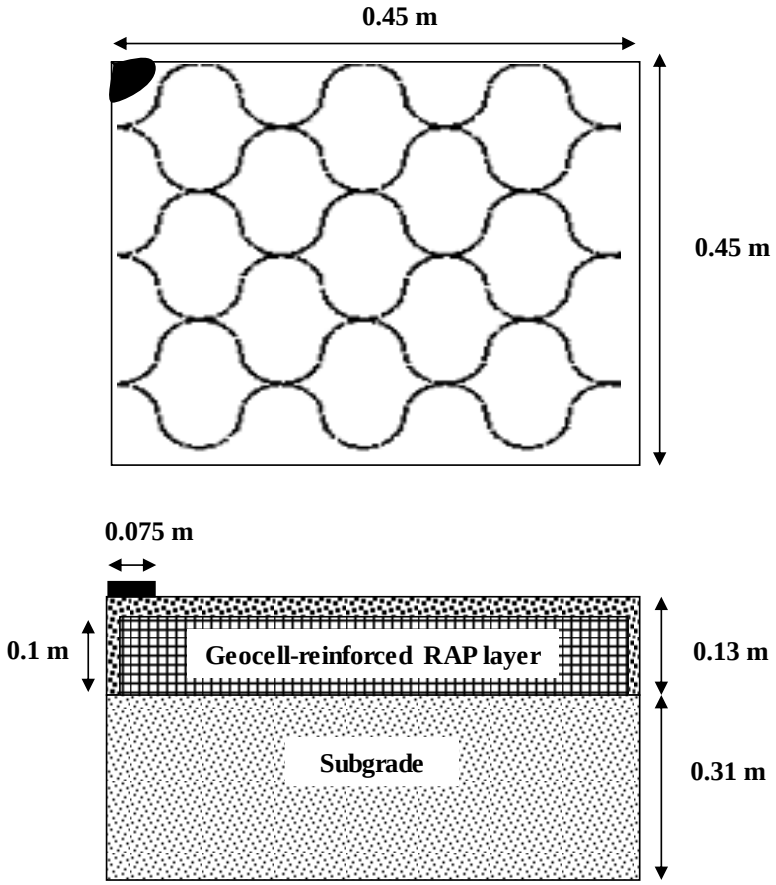

Figure 5.31 Large-scale repeated load laboratory test setup with boundary conditions

5.4.1 *Model Development*

A three-dimensional quarter symmetry model of the large-scale laboratory test set up with dimensions 0.45 m × 0.45 m × 0.435 m was modeled using primitive

mesh shape radial cylinder, which is radially graded mesh around cylindrical-shaped loading area. The use of radial cylinder mesh type was for ensuring the compatibility between the loading area and the RAP material. The numerical model of the unreinforced case used for the analysis is shown in Figure 5.32. The RAP base layer consists of 585 zones and the clay subgrade consist of 936 zones. The geocell reinforcement was modeled using 2304 linear elastic geogrid elements.

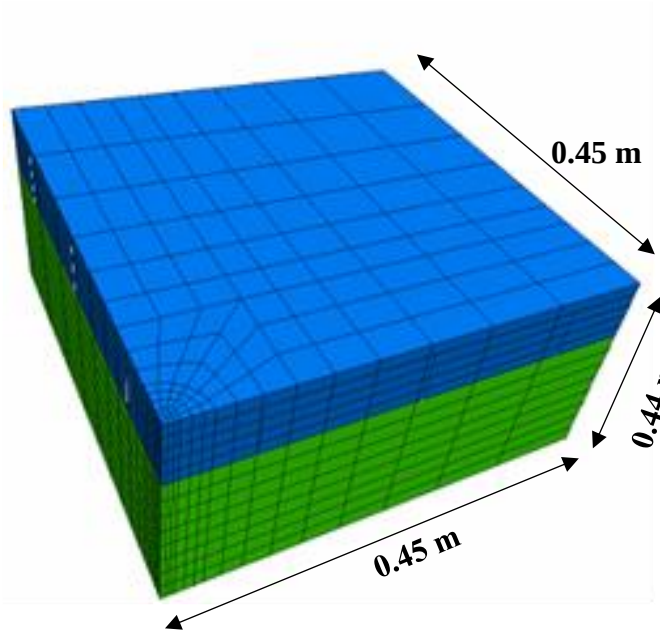

Figure 5.32 Unreinforced model for repeated load box test used in this study

Vertical displacement was fixed at the bottom boundary of the FD model and lateral displacement was fixed in the direction perpendicular to the tank wall at all the sides of the tank to simulate the actual test boundaries. Gravity load was applied to the model to bring it to the static equilibrium condition. Quiet or absorbent boundaries were applied on the model to avoid the reflection of outward

propagating waves back to the FD model. The quiet boundary, based on the viscous boundary developed by Lysmer and Kuhlemeyer (1969), is used in this study (Itasca 2013). The model was solved for 500 repeated load cycles by applying a stress history of 550 kPa magnitude using a haversine wave to evaluate the behavior URB and GRRB under traffic loading. In geocell-reinforced bed case, geocell was placed at a depth of 0.02 m from the surface to simulate actual test condition. The FD model of GRRB for performing repeated load test is shown in Figure 5.33.

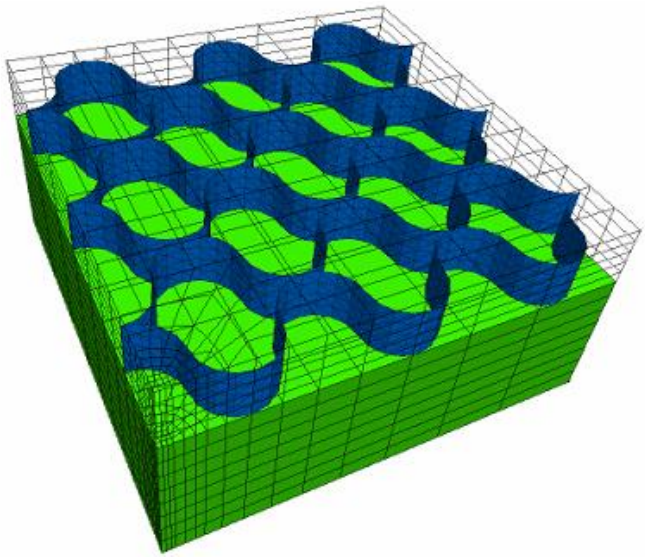

Figure 5.33 Geocell-reinforced model for repeated load box test

5.4.2 *Material Models and Parameters*

The same soil and geocell material models and parameters used for static load tests, given in Table 5.1 and Table 5.2, were used for the repeated load test. Additional damping parameters were used for the repeated load modeling case to impart damping to the loading wave inside the RAP medium. In this study Rayleigh

damping was used which consist of a mass proportional damping component (*M*) and stiffness proportional damping component (*K*).

The damping matrix, *C*, is given by

$$C = \alpha M + \beta K \tag{5.3}$$

where α is the mass proportional damping constant and β is the stiffness proportional damping constant. The mass-proportional and stiffness-proportional terms are analogous to a dashpot connecting every grid points to the ground and a dashpot connected across each zone, respectively. In this study, a damping ratio of 2% and center frequency of 11 Hertz was adopted as given by Itasca 2013.

5.4.3 *Validation of the Model*

Preliminary analysis was performed to check the influence of the boundary effect on the load-deformation behavior of the test section. Mesh convergence test was performed to decide the optimum mesh density that can produce reasonably accurate results. In this FD approach, dynamic analysis is considered as a loading condition on the numerical model. Therefore, a static equilibrium calculation should always precede a dynamic analysis (Itasca 2013).

Before performing the static and dynamic analysis, an additional check was performed to ensure that the model satisfies the requirements for accurate wave transmission (Kuhlemeyer and Lysmer 1973) by adjusting the zone sizes. This is to avoid the distortion of the propagating wave due to modeling conditions. The model was then brought to static equilibrium condition by applying gravity loading. Then

the dynamic module was turned on and the appropriate mechanical damping and the dynamic boundary conditions were applied to minimize the disturbance from the reflected waves at the boundary of the model. To validate the model, an input wave with a maximum vertical stress of 550 kPa as shown in Figure 5.34 was applied repeatedly on the loading area to simulate the large-scale laboratory testing. The axial stress vs axial strain plot for the first 100 load cycles from the FD model is shown in Figure 5.35.

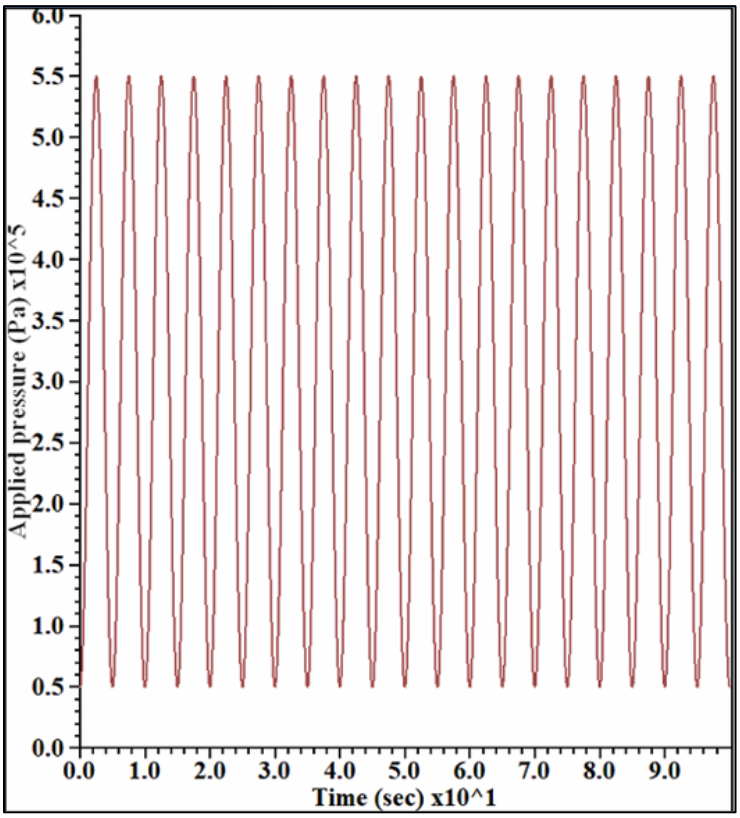

Figure 5.34 Input wave used in this model

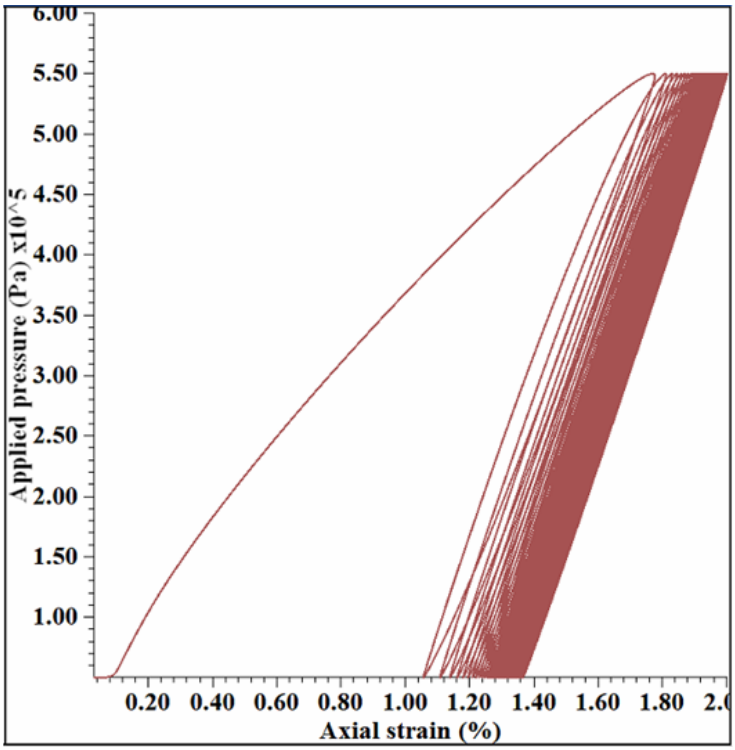

Figure 5.35 Output stress-strain plot for 100 cycles

The variation of PD with number of load cycles is plotted and is compared with the experimental result for validation of the model. The comparison of the laboratory and numerical results for the URB and GRRB are shown in Figure 5.36. Overall, the numerical model well simulated the PD behavior of the URB and GRRB.

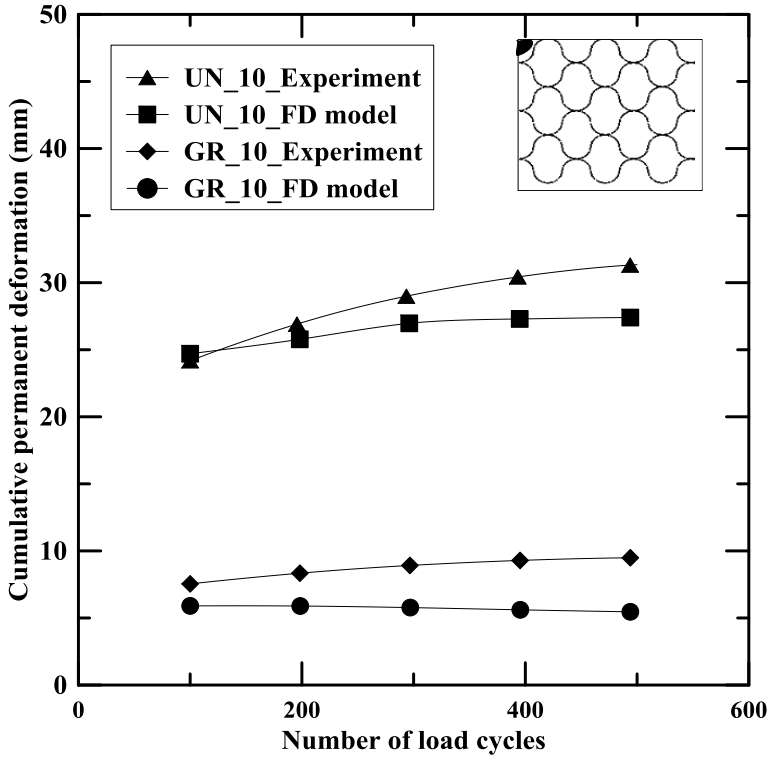

Figure 5.36 Validation of unreinforced and geocell-reinforced models

5.4.4 *Results and Discussions*

The variation of vertical deformation along the radial direction from the center of the loading area at the interface of base and subgrade for different load cycles is shown in Figure 5.37. It can be noticed that the vertical deformation on the subgrade is reduced substantially with the presence of geocell reinforcement. The confining effect of geocell reinforcement increases the stiffness of the geocell-RAP composite that in turn decreased the stresses transmitted to the subgrade. The vertical displacement is less for the first cycle and it gradually increases with the number load cycles.

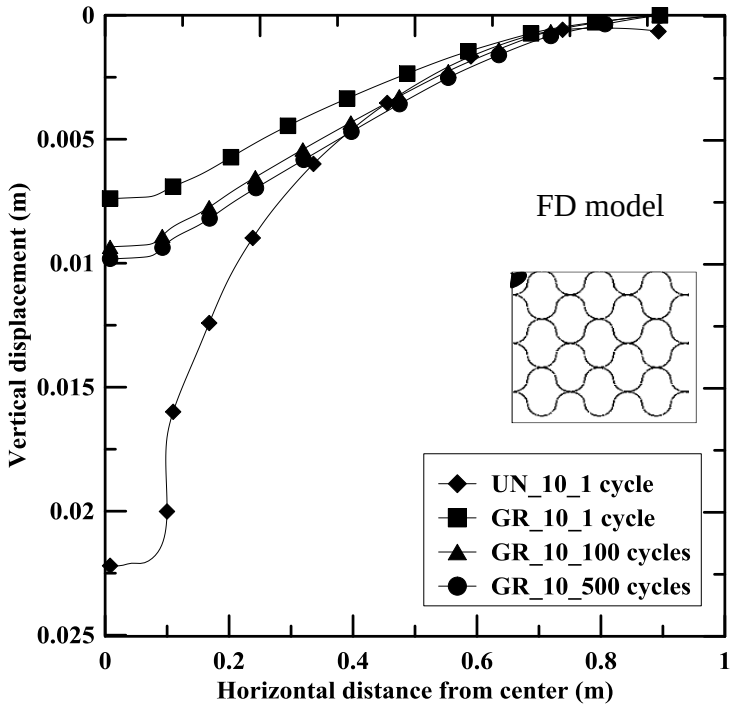

Figure 5.37 Variation of vertical deformation at the surface of subgrade

Figure 5.42 show the variation of horizontal stress at the surface of subgrade for different load cycles. A reduction in horizontal stress at the center and an increase in stress towards the edges of the model can be observed in the reinforced case as compared to the URB. This might be due to the load transfer mechanism of geocell reinforcement that transferred the stresses laterally to the adjacent cells thereby reducing the stress transmitted to the subgrade substantially. The contour profile of horizontal stress distribution in the test section after the application of 500 load cycles for URB and GRRB is shown in Figure 5.39 and Figure 5.40, respectively. It can be observed that horizontal stresses at the subgrade of the GRRB are trivial as compared to the URB.

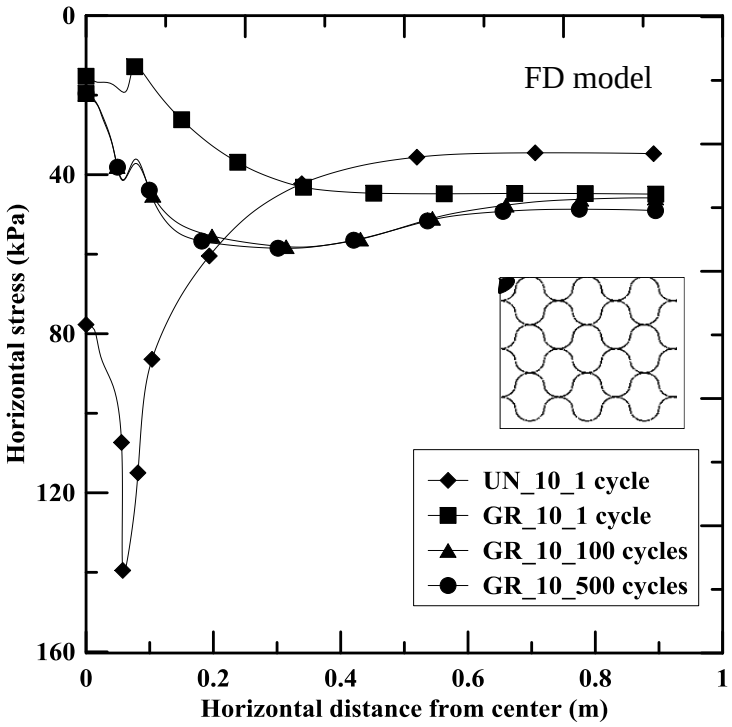

Figure 5.38 Variation of horizontal stress at the surface of subgrade

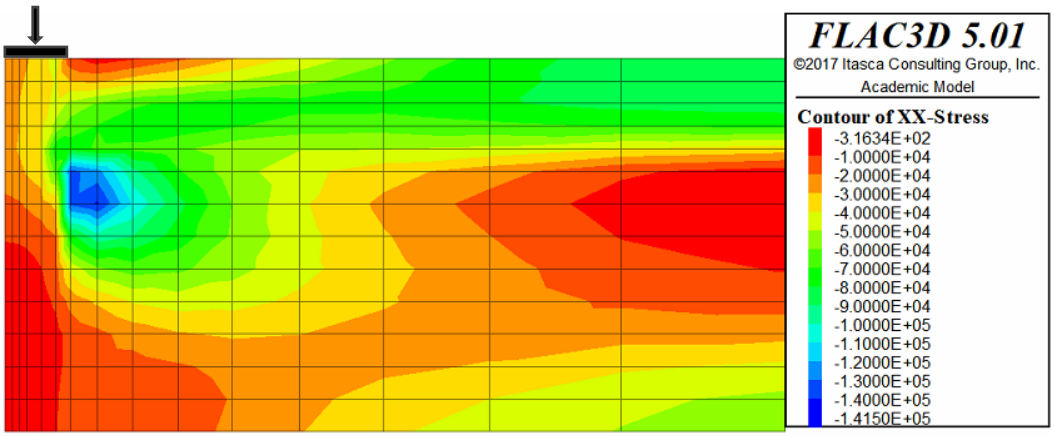

Figure 5.39 Horizontal stress contour profile for unreinforced case

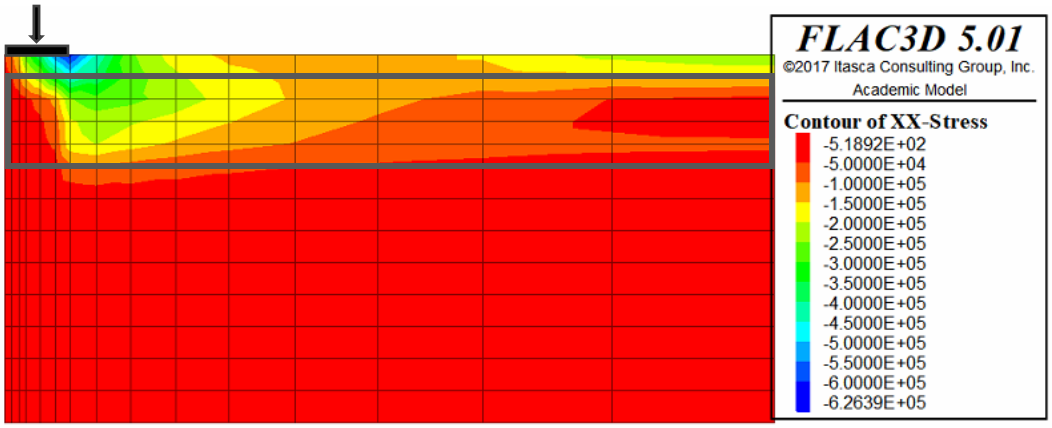

Figure 5.40 Horizontal stress contour profile for geocell-reinforced case

Variation of vertical stress with the depth after the application of 500 load cycles for unreinforced and geocell-reinforced models are shown in Figure 5.41 and Figure 5.42, respectively. A significant reduction of vertical stress on to the subgrade can be observed in the reinforced case. This is due to the lateral load transfer mechanism of geocell reinforcement that spreads the load to the adjoining cells thereby reducing the stress transmitted to the subgrade. Variation of vertical stress along the horizontal direction at the interface of base and subgrade is shown in Figure 5.43. The vertical stress on the subgrade is maximum at the loading area and it gradually reduced towards the edge of the model. A slight hike in the vertical stress near to the edge of the loading plate can be observed in the plot. This might be due to the presence of geocell wall at that region which restricts the movement of the RAP material.

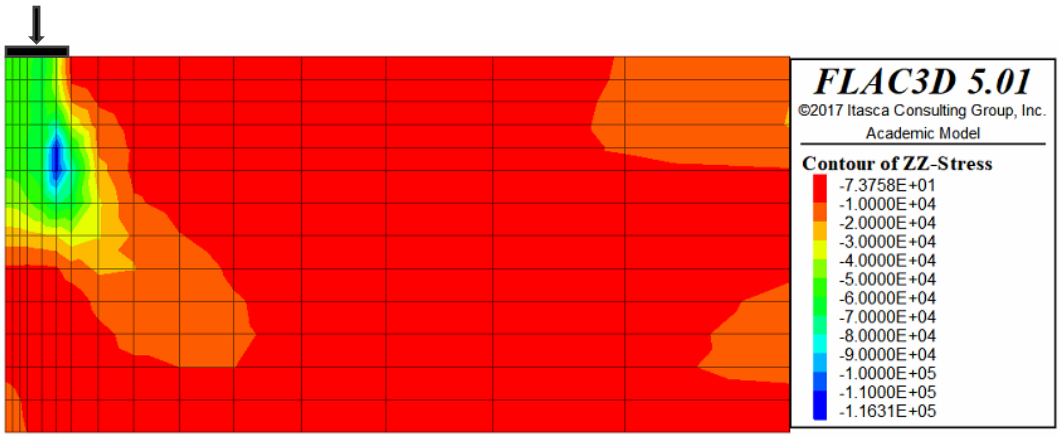

Figure 5.41 Vertical stress contour profile for unreinforced case

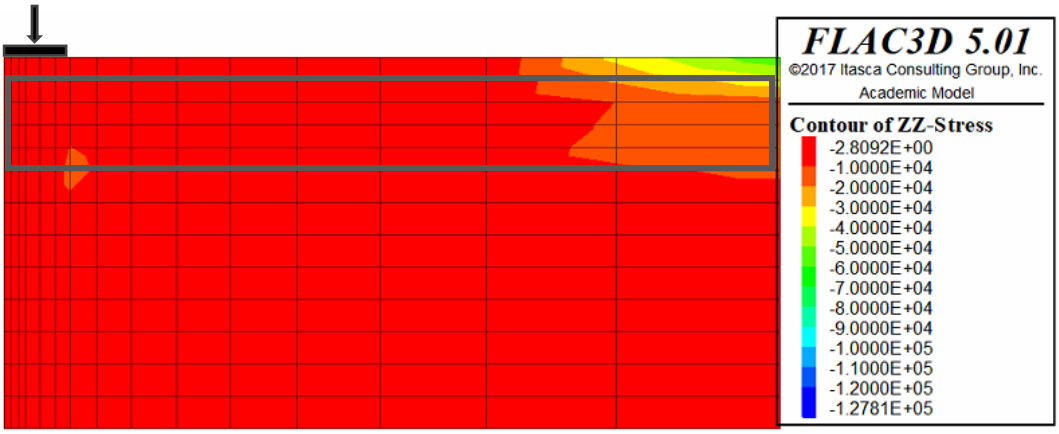

Figure 5.42 Vertical stress contour profile for geocell-reinforced case

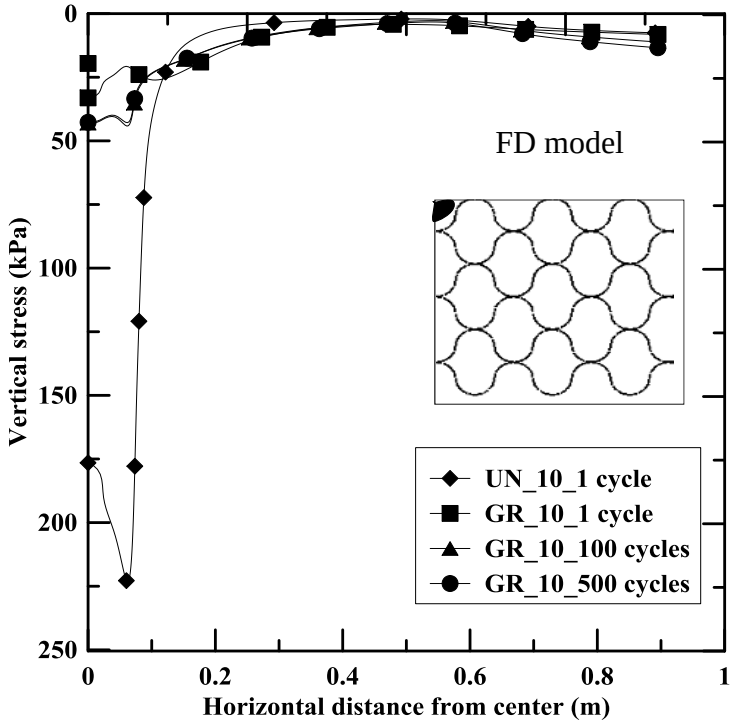

Figure 5.43 Variation of vertical stress at the surface of subgrade

The variation of geocell displacement with the number of load cycles is shown in Figure 5.44. It can be noticed that the geocell deformation increased with increase in number of load cycles and the rate of increase is noticeable during the initial cycles and the rate gradually reduced after 150 load cycles. The vertical deformation of geocell reinforcement after 500 load cycles is shown in Figure 5.45. A maximum displacement of 6.2 mm can be observed directly below the loading area and it nearly zero in the geocell pockets away from the loading area. It can also be observed that the deformation due to the repeated load cycles are significant only on the cells adjacent to the loading area and have no visible effects on the cells that are on the edges of the section.

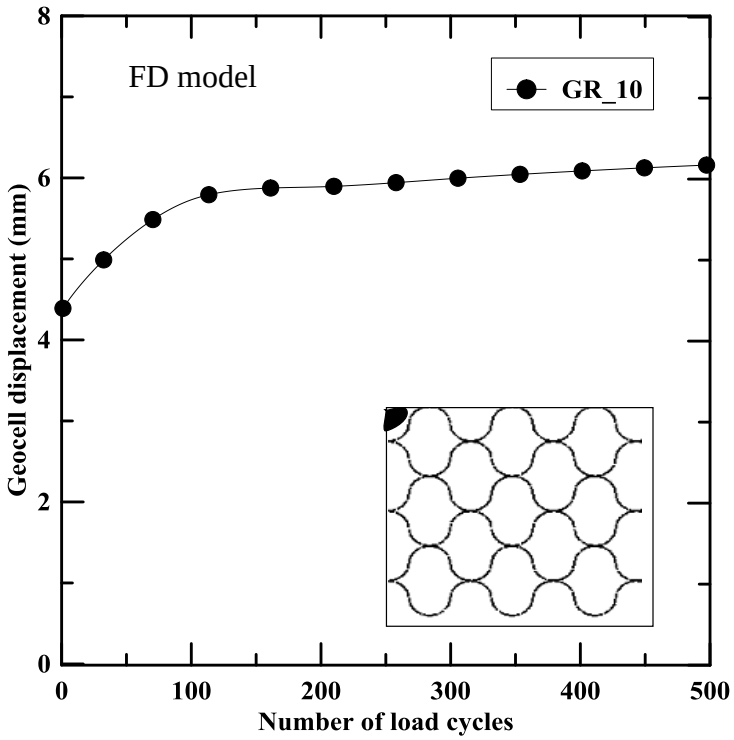

Figure 5.44 Variation of geocell displacement with load cycles

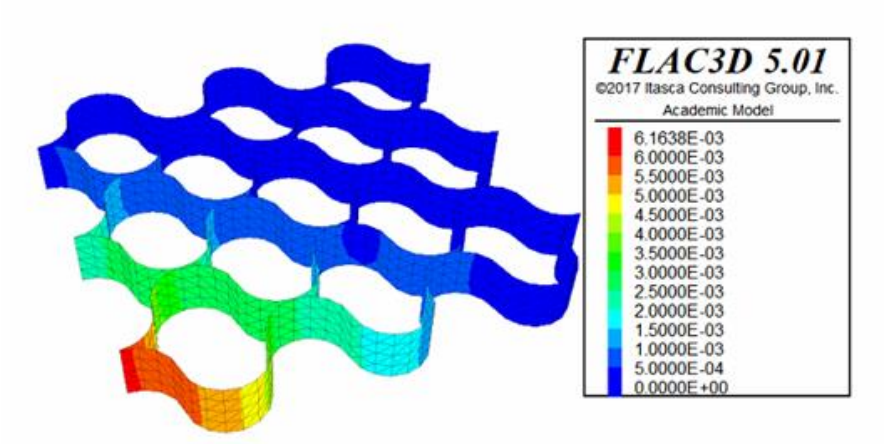

Figure 5.45 Geocell displacement contour profile after 500 load cycles

The variation of vertical strain with the depth along the loading plate for the geocell-reinforced case is shown in Figure 5.46. The negative sign corresponds to

compression. The effect of constraining lateral movement of the RAP material can be clearly observed up to the bottom of the RAP base layer and then to the subgrade. Similar observations were also made by Perkins and Edens (2002).

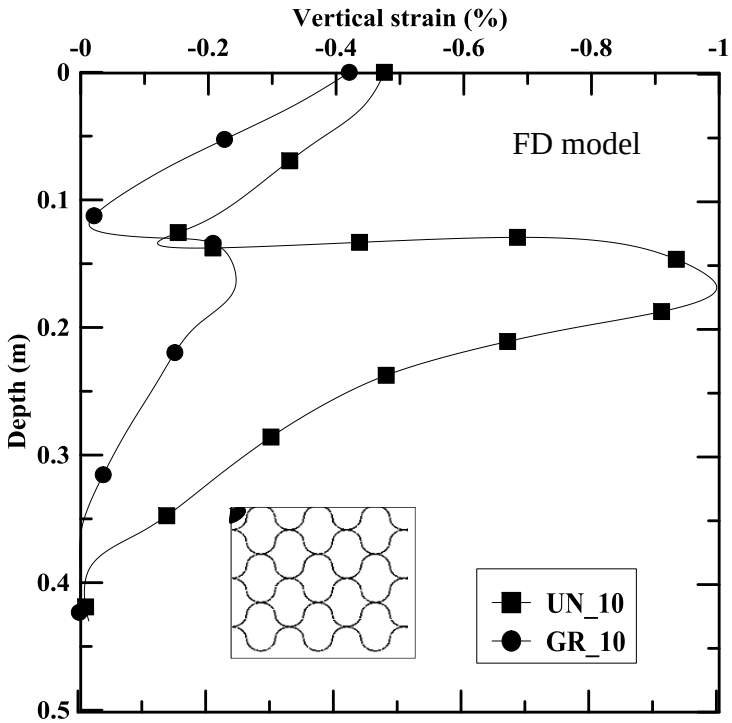

Figure 5.46 Variation of vertical strain with depth for geocell-reinforced case

5.5 Summary

This chapter presented a realistic approach to model GRRB using FD method. A commercial FD software *FLAC*^{3D} was used for the study. The study was performed for two different loading conditions - static and repeated loading. Two models were developed for each loading conditions - one for URB section and the second one for GRRB section.

The three-dimensional honeycomb shaped geocell reinforcement was modeled separately and integrated into the second model to eliminate composite method errors. Mohr-Coulomb material model was used to model both the RAP base material and the clay subgrade. Numerical simulations were carried out on both the models to evaluate the load transfer mechanism of geocell reinforcement under both static and repeated load conditions. The modeling results were compared and validated using the experimental results for both the cases.

The numerical analysis clearly demonstrated the load transfer mechanism of geocell reinforcement. The model could successfully capture the beam bending mechanism and the lateral distribution of stresses towards the adjacent cells. In addition, the shear stresses developed on the geocell reinforcement due to the static loading was also quantified. Parametric studies were also performed to evaluate factors affecting the improvement in the performance of GRRB in terms of bearing pressure when the test section is subjected to static loading.

In a similar way, numerical simulations were carried out on the unreinforced and geocell-reinforced models under repeated loading conditions by applying 500 load cycles. The variation of PD was plotted for both URB and GRRB and was validated with the experimental results. Significant reduction in the vertical and horizontal stresses was observed on the subgrade surface due to the presence of geocell reinforcement. Overall, the numerical models were able to simulate the reinforcement mechanisms of the geocell-reinforced pavement bases.

Chapter 6

SUSTAINABILITY ASSESSMENT OF GEOCELL-REINFORCED RAP BASES USING AN INTEGRATED LCA-LCCA FRAMEWORK

6.1 Introduction

Sustainability of the pavement infrastructure plays a significant role in the decision making process of pavement (base material) selection (Puppala *et al.* 2018). The utilization of recycled materials in the pavement base can substantially reduce the natural resource consumption and enhance the energy efficiency of the pavement. Currently, a number of metrics, tools, and rating systems exist to evaluate the sustainability of an infrastructure (Das *et al.* 2016, 2018a, 2018b). However, the studies reported so far were solely based on either the resource usage or the emissions during the life-cycle of the infrastructure. Only limited studies have addressed the influence of social, economic, and environmental impacts on the decision-making of a sustainable pavement selection.

This chapter attempts to present an integrated Life-Cycle Assessment and Life-Cycle Cost Analysis (LCA-LCCA) framework to assess overall long-term sustainability between competing alternatives in terms of economic efficiency (George, Banerjee, Anand J, *et al.* 2019). To illustrate this, a low volume farm-to-market (FM) road in North Texas with three alternate base materials is used as a test platform. The emissions during the entire life-cycle of the pavement were estimated by performing LCA and was converted to the equivalent dollars to

calculate the health and environmental impact costs. The agency and user cost of the pavement during its service life was estimated separately using LCCA and was integrated with the LCA results to determine the overall present value of the pavement. Finally, a sustainability factor was introduced to assess the sustainability metrics of each alternative to aid the decision-making process.

6.2 Model and Methodology

Pavement life-cycle comprises of raw material production, construction, usage, maintenance/ rehabilitation, and end of life. The health impact cost, environmental impact cost, agency cost, and user cost during each phase were estimated separately to assess the sustainability of the pavement design. The conceptual framework of the proposed model is shown in Figure 6.1.

The analysis was performed by considering three main scenarios:

i. Unbounded crushed limestone as the base material (CLS),
ii. 10-cm geocell-reinforced RAP as the base material (GR1), and
iii. 15-cm geocell-reinforced RAP as the base material (GR2).

A low-volume farm-to-market road with one lane in each traffic direction at Venus, Texas was considered for the analysis. Three pavement section alternatives were considered by keeping the subgrade and the surface layer same and by varying the base material. The 10-cm (4-in.) and 15-cm (6-in.) high-density polyethylene (HDPE) geocell was used in GR1 and GR2 scenarios to impart confinement to the RAP material.

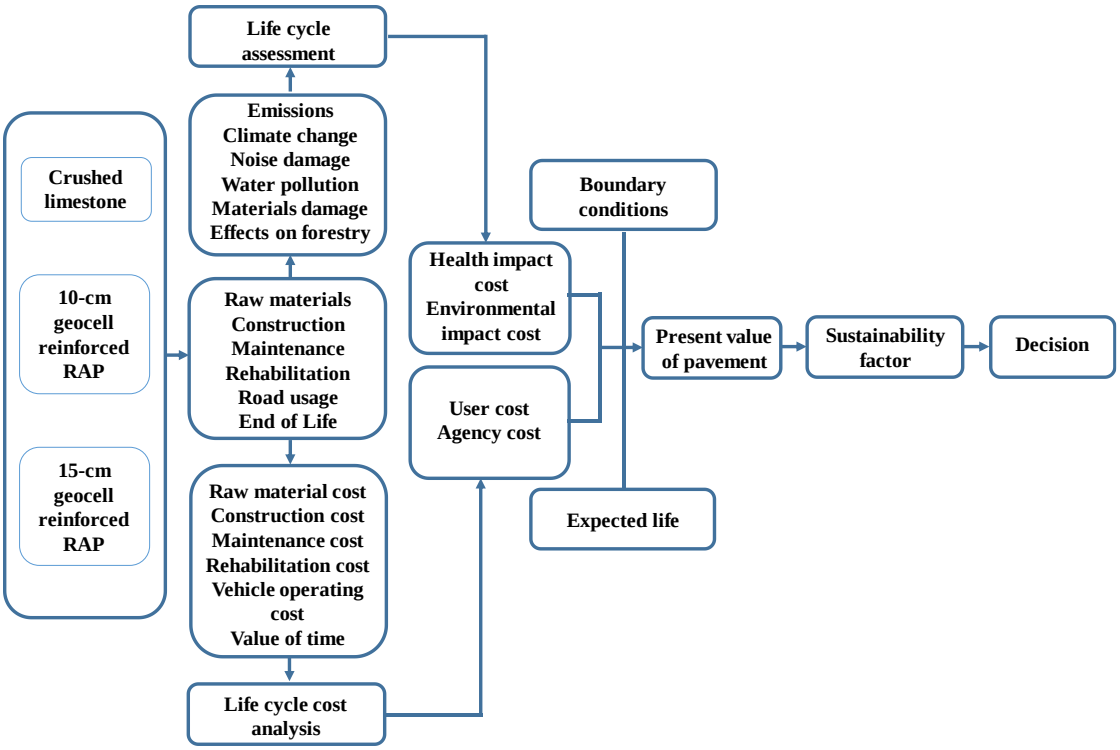

Figure 6.1 Conceptual framework of the proposed model

6.3 Model Development

The sustainability assessment model was developed in three stages. Firstly, the LCA was performed to estimate the emissions and impacts of each pavement phase and the corresponding damage cost was calculated in terms of health and environmental impact costs. Then, the LCCA was performed using LCCA framework developed by Praticò *et al.* (2011) for the low volume road to obtain the agency and user cost of the pavement alternatives. total life-cycle cost of the pavement system. Finally, both the LCA and LCCA analysis results were integrated

to an LCA-LCCA framework to estimate the present value of the pavement and the sustainability factor.

6.3.1 *Life-Cycle Assessment*

The Life-Cycle Assessment (LCA) offers a comprehensive approach that quantifies the resource use and environmental impacts throughout the life-cycle of an entity from raw material collection to the end of service life of the pavement. It can also be used as a tool to assess the overall long-term economic efficiency between competing alternatives (Walls III and Smith 1998). The life-cycle assessment of a pavement comprises of five phases: raw material acquisition, construction, usage, maintenance, and end of life. Understanding the relative significance of each component would provide valuable insight into best-practice methods that satisfy sustainability performance objectives (FHWA 2002).

Environmental conditions, type of traffic loading, maintenance and rehabilitation strategies, pavement material type, and reusing of in-situ materials will factor into the volume of emissions released over the service life of the pavement. The emissions from automobiles and construction equipment cause severe health issues in human, deterioration of materials, reduces visibility, and damages agriculture and forests. Traffic congestion due to the construction and maintenance activities and the resulting delay is the major contributing factor of GHGs emissions. Stop-and-go driving patterns that usually occurs in the congested work zones can drastically increase the emissions. In this study, the impact of

emissions in the society was considered under two sections: (a) health impact costs which include the effects of emissions on human health and (b) environmental impact costs which covers all the impacts on the environment such as materials, agriculture, and forestry.

6.3.1.1 Health Impact Costs

Long-term exposure to emissions from construction, maintenance, and rehabilitation activities can cause adverse health effects which includes asthma, bronchitis, emphysema, and possible cancer. The unit health impact cost (HIC) of emissions is highly dependent on the source-related factors such as population density and the work zone location (Mallela and Sadasivam 2011). The emission from the automobiles such as greenhouse gases (GHGs) and 'criteria air pollutants' specified by Environmental Protection Agency (EPA) accounts for the majority contribution to the atmospheric emissions which affect the human health. The criteria air pollutants include particulate matter, carbon monoxide (CO), lead, Sulphur dioxide (SO_2), Nitrogen oxides (NO_x), and volatile organic compounds (VOCs) (EPA 2015). The GHGs comprises carbon dioxide (CO_2), nitrous oxide (N_2O), and methane (CH_4).

The vehicle emission model *MOVES* developed by EPA was used to estimate vehicle fuel consumption and emission of key pollutants in accordance with the emission factors and traffic fleet composition (MOVES 2015). This modeling approach can estimate the per-mile emission rates for the criteria

pollutants (CP) and GHGs from the automobile in terms of CO_2 equivalent emissions. These emissions are then converted to an equivalent monetary value corresponding to 2017 dollars.

The health cost expressed in terms of the present value (PV_{HIC}) of pavement is given by,

$$PV_{HIC} = PV_{GHG} + PV_{CP} \quad (6.1)$$

where PV_{GHG} and PV_{CP} are the present value of impact costs from GHGs and CP, respectively.

6.3.1.2 Environmental Impact Costs

The quantification of environmental impact cost (EIC) is a difficult task. It quantifies the effect of all the activities related to the pavement during its service life on the environment. This includes the climatic change, water quality, noise pollution, and air quality. In this study, the climatic change (EX_{CL}), noise damage (EX_{ND}), water pollution (EX_{WP}) damages due to visibility (VBD), agriculture damage (AGD), materials damage (MD), and effects on forestry (EF) related additional costs are considered as EIC.

The EIC in terms of present value of the pavement (PV_{EIC}) is given by,

$$PV_{EIC} = PV_{CL} + PV_{ND} + PV_{WP} + PV_{VBD} + PV_{AGD} + PV_{MD} + PV_{EF} \quad (6.2)$$

where PV_{CL}, PV_{ND}, PV_{WP}, PV_{VBD}, PV_{AGD}, PV_{MD}, and PV_{EF} are the present value of impact costs from climate change, noise damage, water pollution, damages due to

visibility, agriculture damage, materials damage, and effects on forestry, respectively.

6.3.2 *Life-Cycle Cost Analysis*

The comprehensive LCCA model developed by Praticò *et al.* (2011) for the low volume roads was modified and used in this study to perform LCCA. The model comprised of the agency and user costs associated with initial construction and anticipated maintenance and rehabilitation activities from the projected life-cycle cost. All the expenses related to future activities incurred during the service life of the pavement are calculated in terms of 2017 dollars by converting them to a present value using a discount rate (Inti 2016).

6.3.2.1 Agency Costs

Agency cost (AC) includes all the costs incurred by the operating and maintenance agencies during the projected service life of the pavements. It consists of the cost associated with the raw material collection, construction, maintenance, demolition of the pavement, and engineering administration. These agency cost elements should be estimated for the entire service life of pavement for three different design alternatives. The initial construction cost (C) will be different for all three scenarios due to the different base materials. The rehabilitation cost (R) will also change as the rehabilitation years are different for each case. The agency cost expressed in terms of a present value corresponding to time, T (PV_{ACT}) and is given by:

$$PV_{ACT} = C + \sum_{k=1}^{N} \left(\frac{R_k}{(1+i)^{n_k}} - \frac{S_a}{(1+i)^{n_N}} \right) \quad (6.3)$$

where i is the interest rate, R_t is the rehabilitation cost at time T, n_k is the year in which k^{th} rehabilitation will be performed and S_a is the salvage value of the pavement type under consideration.

6.3.2.2 User Costs

User costs (UC) are mainly the costs associated with the operation and use of vehicles and the time spent by each individual vehicle on the roadway. The main components for calculating user costs are vehicle operating costs (VOC), the value of time (VOT), and crash costs (CC). VOC is primarily associated with the pavement roughness which in turn reflects in the costs associated with fuel consumption, vehicle maintenance, and tire repair and replacement (Islam and Butlar 2012).

VOT mainly consists of the speed reduction and long queues due to lane closure in the work zone area, accidental delays, and detour delays. The estimation of CC is an intricate process. It primarily depends on the severity and location of the accident and the number of fatalities. Usually, CC for the roadway section is calculated based on a rate of accident type per vehicle-miles of travel. Previous studies reported that the presence of a work zone tends to increase the pre-work zone crash rates by 20 to 70 percent (Mallela and Sadasivam 2011).

The time-cost relationship is a significant factor in determining the user cost which affects the social impact of public budget management. The user cost of the pavement in terms of present value (PV_{UC}) is given by,

$$PV_{UC} = PV_{VOC} + PV_{VOT} + PV_{CC} \quad (6.4)$$

where PV_{VOC}, PV_{VOT}, and PV_{CC} are the present value of VOC, VOT, and CC, respectively.

6.3.3 *Present Value and Sustainability Factor*

The ultimate objective of this framework is to select the most sustainable design out of three alternative pavement designs and to quantify the net benefits and total cost with respect to each other. Once all the pertinent costs have been established and discounted to their present value, the cost can be summed to generate the overall present value of the pavement using the following equation,

$$PV = PV_{HIC} + PV_{EIC} + PV_{ACT} + PV_{UC} \quad (6.5)$$

Using the overall PV of each alternative, a sustainability factor (*SF*) is calculated by taking the weighted average of individual and total costs of all the processes during the service life of the pavement. The total sustainability factor (SF_{TOT}) is given by the equation,

$$SF_{\mathrm{TOT}} = PV_{\mathrm{CLS}} + PV_{\mathrm{GR1}} + PV_{\mathrm{GR2}} \quad (6.6)$$

where PV_{CLS}, PV_{GR1}, and PV_{GR2} are the overall present values of pavement section with crushed limestone, 10-cm geocell reinforcement, and 15-cm geocell reinforcement respectively.

The sustainability factor for CLS (SF_{CLS}) is given by,

$$SF_{CLS} = \frac{1}{2}\left(1 - \frac{PV_{CLS}}{SF_{TOT}}\right) \quad (6.7)$$

The sustainability factor for GR1 (SF_{GR1}) is given by,

$$SF_{GR1} = \frac{1}{2}\left(1 - \frac{PV_{GR1}}{SF_{TOT}}\right) \quad (6.8)$$

The sustainability factor for GR2 (SF_{GR2}) is given by,

$$SF_{GR2} = \frac{1}{2}\left(1 - \frac{PV_{GR2}}{SF_{TOT}}\right) \quad (6.9)$$

The sum of individual sustainability factors is 1.

6.4 Case Study

To evaluate the proposed framework, a case study on the reconstruction of a farm-to-market road (FM 1807) in Venus, Texas is analyzed and presented. The test section used for the analysis is shown in Figure 6.2. The current age of asphalt pavement is 10 years and a recent asphalt overlay has been paved on the surface of the existing roadway. In a short span of time, severe longitudinal cracks appeared on the surface of the newly overlaid pavement due to the inadequate strength and stiffness properties of the base and subgrade layers. Therefore, the TxDOT has planned to reconstruct the pavement using a more sustainable base alternative which satisfies the performance objectives. Three alternatives for the base layer were considered in this analysis:

i. Unbounded crushed limestone (CLS),

ii. 10-cm geocell-reinforced RAP (GR1), and

iii. 15-cm geocell-reinforced RAP (GR2).

The major objective of this research is to select the most sustainable and economic design out of three flexible pavement alternatives with an expected service life of 40 years. The crushed limestone for CLS option was assumed to be obtained from a quarry within 96 km (60 miles) of the site location. The RAP material for the geocell-reinforced case was assumed to be milled from the existing pavement and was pulverized to the required gradation at the site. This resulted in considerable cost savings in terms of raw material collection and transportation for GR1 and GR2. The HDPE geocell used for confining RAP material was purchased from a commercial geocell manufacturing company approximately 400 km (250 miles) away from the site. The properties of HDPE geocell, provided by the manufacturer, are listed in Table 3.2.

Figure 6.2 Test site at FM 1807 road at Venus, TX (source: Google Maps, 2018)

Material characterization of both subgrade and base materials was done by performing laboratory tests including Atterberg limits, sieve analysis, and compaction. Large-scale repeated load box tests were also performed to estimate

the strength and stiffness properties of the unreinforced and geocell-reinforced base layer. The M_r of base layers corresponding to CLS, GR1, and GR2 scenarios are 149 MPa (22 ksi), 310 MPa (45 ksi), and 430 MPa (62 ksi), respectively. The subgrade material was classified as lean clay (CL) based on the USCS system and M_r was found to be 11 ksi (76 MPa).

The laboratory test results were used for the flexible pavement design corresponding to an annual average daily traffic (AADT) of 1200 (Liu 2011). The pavement cross-section from the design is shown in Figure 6.4. The traffic data and the summary of the parameters used for the analysis are provided in Table 6.1. Two major maintenances (asphalt overlay) and one rehabilitation were proposed during the service life of the pavement section. The timeline of the construction and major and minor maintenances of the proposed pavement section is shown in Figure 6.4. As compared to CLS and GR1 options, GR2 requires only one major maintenance due to the improvement in the pavement performance due to 15-cm (6-in.) geocell reinforcement. Reinforcing the RAP material with geocell has been proven to enhance the strength and stiffness properties of the RAP by virtue of the three-dimensional honeycomb structure of geocell which offers lateral confinement on the infill material (Pokharel *et al.* 2011, Bortz *et al.* 2012b, Thakur *et al.* 2012a).

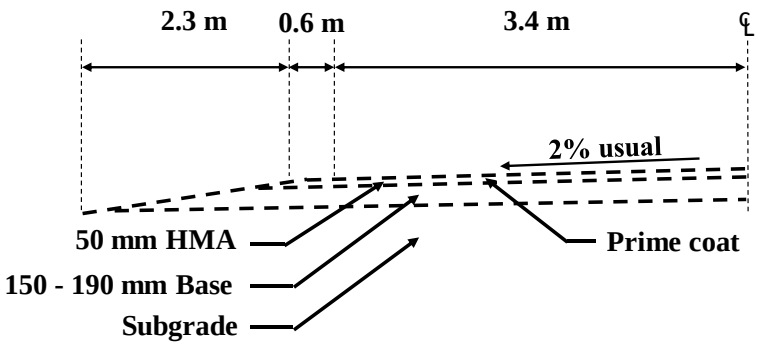

Figure 6.3 Typical cross-section of the pavement used in this study

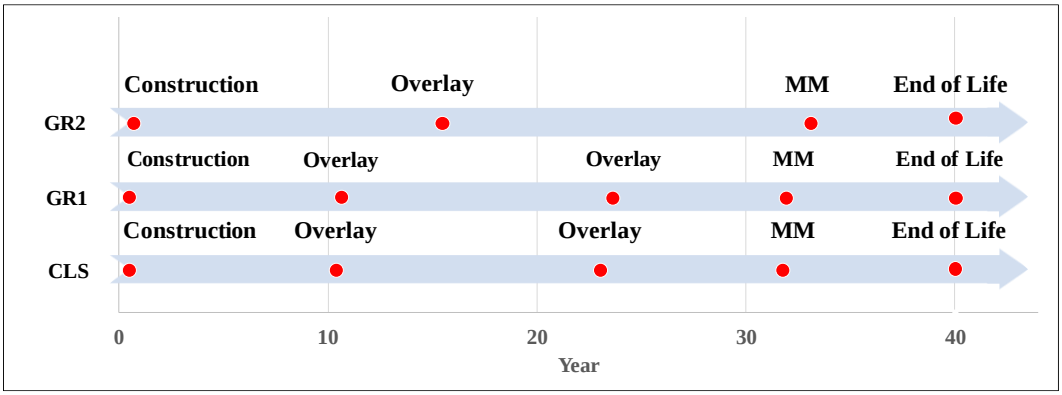

*MM: Major maintenance (Rehabilitation)

Figure 6.4 Pavement maintenance timelines for the three scenarios

Table 6.1 Summary of traffic data and parameters used in the analysis

Description	Values
Annual average daily traffic, AADT	1200
Design period, years	20
Truck %	12
Annual growth of traffic, %	3.5
Design reliability level, %	90
Lane open in each direction under normal/work zone condition	1/two-way lane shift (1/2)

Length of pavement section, km (mile)	1.6 (1)
HMA thickness (CLS/GR1/GR2), mm (in.)	50/50/50 (2/2/2)
Base thickness (CLS/GR1/GR2), mm (in.)	190/150/170 (7.5/6/7)
Width/lane of pavement section, m (ft.)	3.35 (11)
Discount rate, %	3
Analysis period, years	40
Beginning of the analysis period	2018
Maintenance: first overlay, $/SY second overlay, $/SY	8.13/8.13
Rehabilitation, $/SY	9.59

6.4.1 *Health Impact Costs*

In this study, the emissions from the MOVES analysis was converted to equivalent monetary value using the Caltrans estimates of health cost of transportation emissions in metric ton for rural roads (Mallela and Sadasivam 2011) and is shown in Table 6.2. This cost is then multiplied by the ratio of historical cost index to obtain the health impact costs in 2017 dollars. The health impact costs estimated from the MOVES analysis is given in Figure 6.5. It can be observed that the HIC from construction is more than 80% of the total HIC for all the three scenarios. This is due to higher discharge of emissions during the production of raw materials especially the hot mix asphalt (HMA) used in the pavement surface. Emission from the construction equipment and the automobiles in the work zone also contributes to the increased percentage of HIC from construction.

Table 6.2 Caltrans estimates of health impact cost of transportation emissions for rural roads (Mallela and Sadasivam 2011)

Pollutant	$/ton (2010 dollars)	$/ton (2017 dollars)
SO_2	43091.29	50158.3
NO_x	10976.94	12777.2
CO	58.97	68.6
VOC	811.93	945.1
PM_{10}	85275.39	99260.6
CO_{2e}	33.57	39.1

6.4.2 *Environmental Impact Costs*

The EIC related to climatic change, noise damage, and water pollution, estimated by the previous researchers, summarized by Delucchi and McCubbin (2010) is given in Table 6.3. The EIC from all the three factors were estimated corresponding to an AADT of 1200 throughout the service life of the pavement and was found to be $1,800,500 for all the three cases.

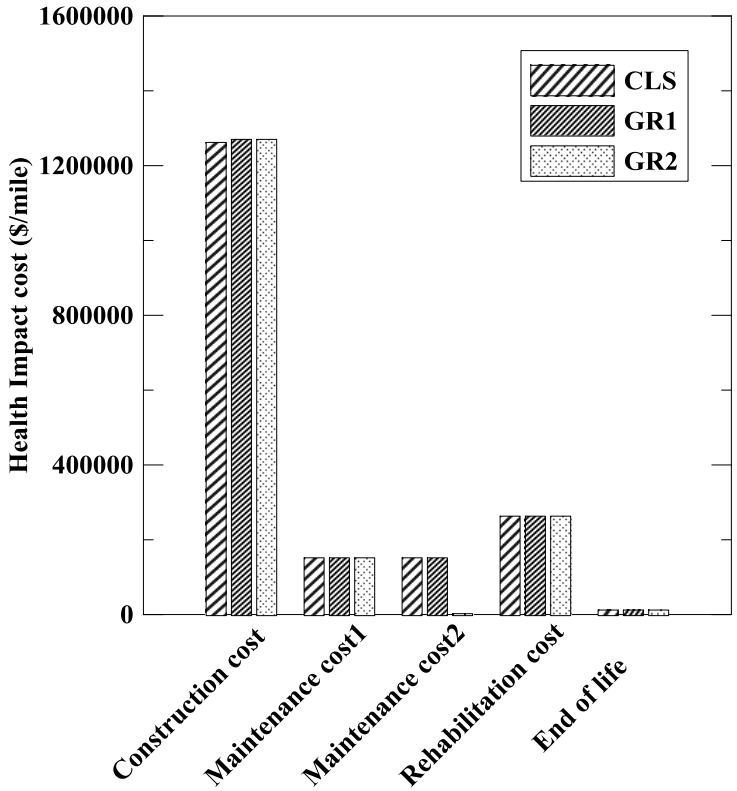

Figure 6.5 Health impact costs of the pavement alternatives

Table 6.3 Estimates of environmental impact cost (year- 2006 cents) from (Delucchi and McCubbin 2010)

Description	Truck (fright) (cents/tm*)	Passenger car (cents/pmt**)	Reference
Climatic change damage cost	0.06	0.06	(Zhang *et al.* 2004)
Noise damage cost	0.05	0 to 3.45	(Delucchi and Hsu 1998, Forkenbrock 1999, 2001)
Water pollution cost	$0.003 to $0.051	0.014 to 0.051	(Delucchi 2000, 2004)

*tm: ton-mile, **pmt: passenger-mile of travel

EIC associated with damage due to visibility, agricultural damage, material damage, and forestry damage was estimated using the research findings by Muller and Mendelsohn (2007). According to Muller and Mendelsohn, the cost of non-

health impacts of air pollution as a percentage of the cost of health impacts for visibility and agriculture are 4% and 2%, respectively. The contribution of material damage and forestry damage to the EIC was observed to be negligibly small (Muller and Mendelsohn 2007). The EIC in terms of the pavement for CLS, GR1, and GR2 options are shown in Figure 6.6.

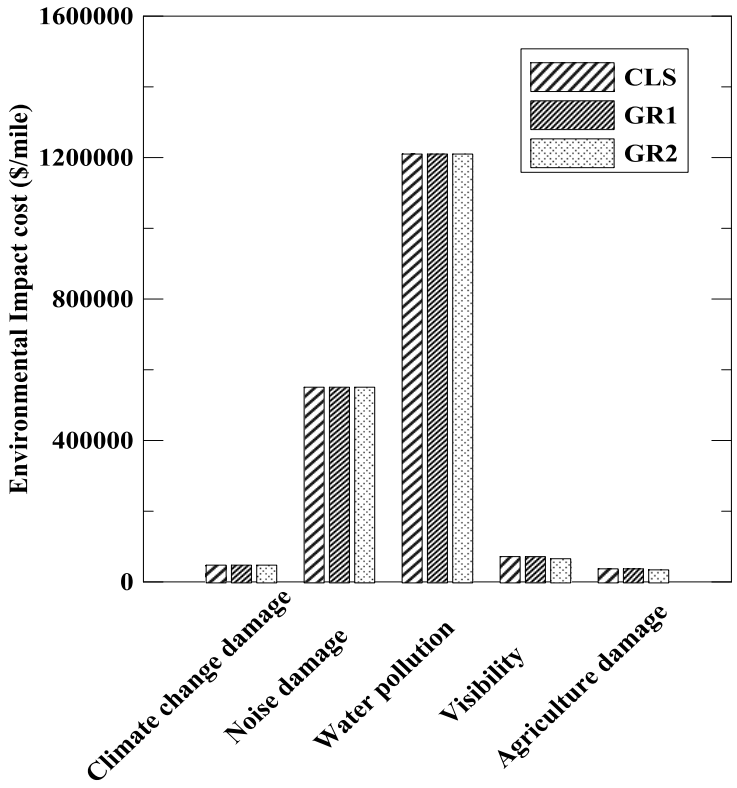

Figure 6.6 Environmental impact costs of the pavement alternatives

EIC for the CLS option was observed to be higher than GR1 and GR2 options as the crushed limestone used in CLS emitted more GHGs and criteria pollutants during its production and transportation. GR1 and GR2 used RAP material as the base material which decreased the emission associated with

manufacturing the material. The onsite recycling strategy was adopted for the RAP base by reusing RAP milled from the existing pavement. This reduced the mass of materials required to be transported to the site thereby reducing CO_{2e} emission levels significantly.

However, the HDPE geocell used in the geocell-reinforced pavement sections greatly contributed to the emission of pollutants due to the presence of carbon black and polyethylene. EIC from the manufacturing process of carbon black and polyethylene were calculated for the 10-cm and 15-cm geocell test sections separately and used in this study. To moderate the emissions during the manufacturing process of geocell, all the machinery was operated on electricity instead of fuel and the wastage from the production was maintained as zero by reusing the scrap in the manufacturing process. For a better understanding of the entire process, the schematic diagram of the manufacturing process of HDPE geocell is given in Figure 6.7.

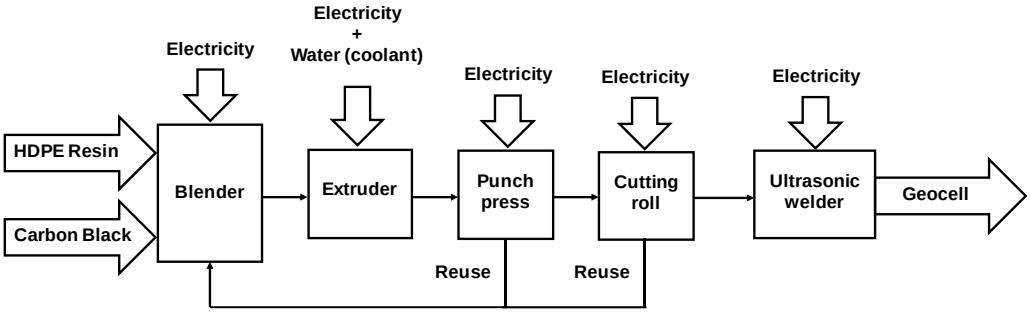

Figure 6.7 Schematic diagram of the manufacturing process of HDPE geocell (source: Geo Products, L. L. C.)

6.4.3 *Agency Costs*

The construction and rehabilitation cost of all the three scenarios were calculated separately using Equation (6.3). For GR1 and GR2, an additional cost of geocell reinforcement was also considered in the construction cost. The salvage value of the pavement after 40 years was assumed to be 30% of the actual cost (MAGPPA 2002) with an annual depreciation rate of 3%. The agency cost during the entire service life of the pavement estimated from the analysis is given in Figure 6.8. The initial construction cost of GR2 was found to be 15% higher than that of GR1 due to the higher price of 15-cm (6-in.) geocell reinforcement. However, the total AC for GR2 was approximately 30% lesser than the GR1 option due to the absence of second major maintenance which resulted from the improved performance of the pavement.

6.4.4 *User Costs*

Vehicle operating cost contributes a major part of UC and is mainly associated with the pavement condition which is a function of the International Roughness Index (IRI). In this study, the initial IRI of the pavement surface was assumed to be 1.2 m/km (76.3 in./mile) and 0.99 m/km (63 in./mile) for the crushed limestone and GRRB, respectively (Jiang and Li 2005, Islam and Butlar 2012). This assumption is based on the fact that the geocell reinforcement improves the strength and stiffness of both the base and subgrade which will further result in a reduced IRI for GR1 and GR2 cases (Thakur *et al.* 2012a).

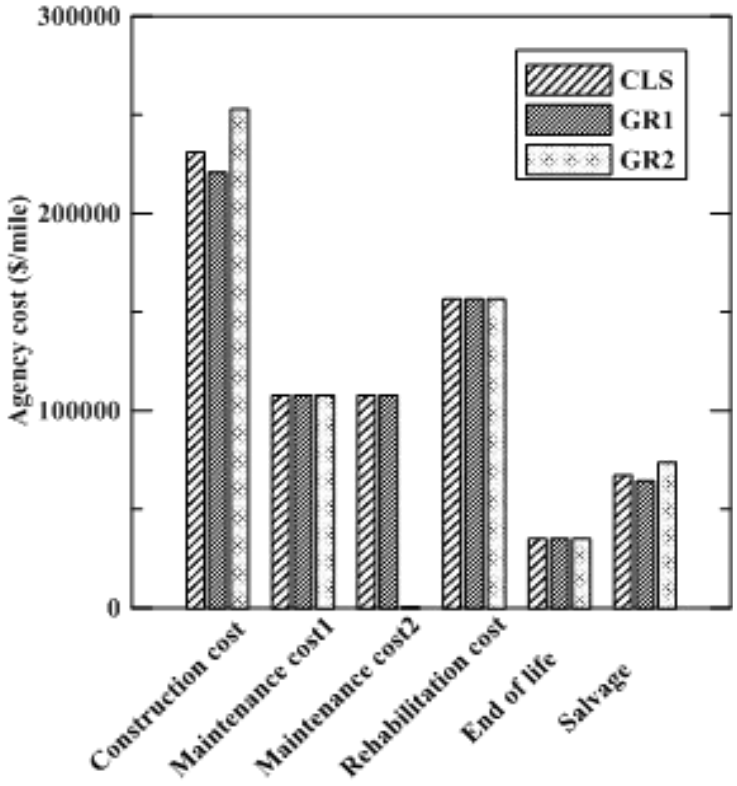

Figure 6.8 Agency costs of the pavement alternatives

Estimation of VOC due to traffic delay is a complex exercise. It depends on work zone length and traffic speed, duration of construction, and traffic delay due to detour and accidents. The FM roadway considered in this study is a two-lane, two-way road. During the construction and maintenance process, only one lane will be opened for the traffic which will be regulated either by a flagman or a temporary traffic signal. This along with reduced vehicle speed on the work zone area will result in traffic congestion and longer queues. To avoid congestion, the vehicles may have to take a detour which will end up with longer routes. As a result, the fuel consumption of the vehicle may increase considerably thereby increasing the VOC.

The average VOC for each additional mile of travel due to detour, estimated by TxDOT for 2017, is $0.582 cents/mile for the passenger vehicle and $1.035/mile for the commercial trucks.

Value of delay time is another important factor affecting the UC. According to TxDOT, the VDT (in 2017) of a personal vehicle and commercial truck is $27.39/hr and $31.36/hr, respectively. This includes the VDT due to reduced traffic speed in the work zone, detour delay, and stoppage delay. From the 2016 crash report by TxDOT, the fatalities in the Venus city was found to be zero out of a total 51 crashes. Also, no vehicle crash incidents were reported in FM 1807 during the last 20 years. Therefore, CC analysis was not performed for this case study.

The user costs estimated during the service life of the pavement is given in Figure 6.9. It can be observed that the user cost due to IRI is significantly higher than all the other factors. This is due to the increase in fuel usage, maintenance cost, tire cost, and vehicle depreciation cost resulted from the deterioration of the pavement. The user cost due to the increase in IRI value of the pavement is slightly lower for the geocell-reinforced case (GR1 and GR2). This is because of the improved resilient behavior of the geocell reinforcement under traffic loading.

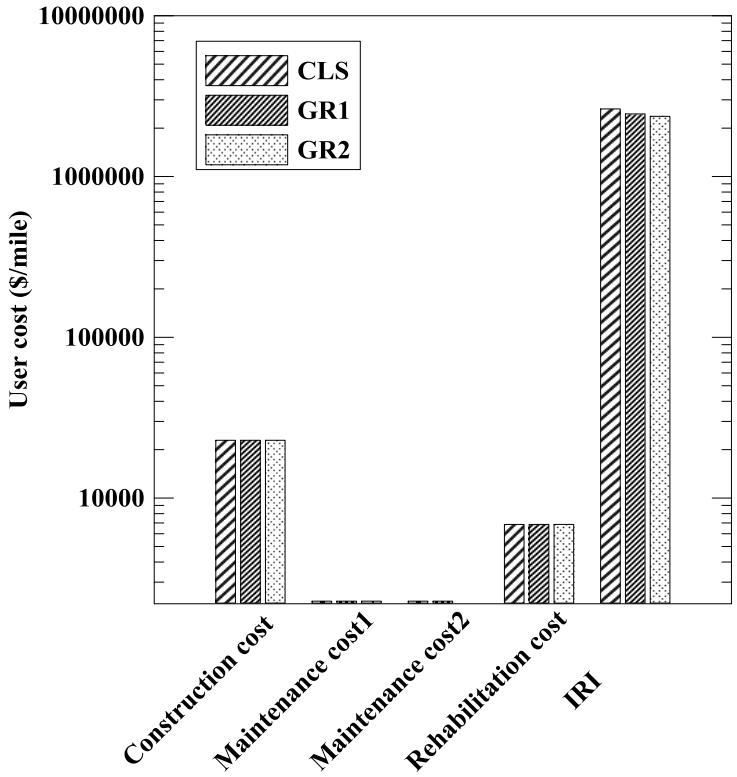

Figure 6.9 User costs of the pavement alternatives

6.4.5 *Present Value*

The overall present value of the pavement by considering all the impact, agency, and user costs using Equation (6.5) is shown in Table 6.4. It was observed that the health and environmental impact costs contribute a major part of the total pavement worth and were approximately about 30% to 40% of the overall present value of the pavement.

6.4.6 *Sustainability Factor*

A sustainability factor has been proposed based on the present value of the pavement infrastructure to quantify the overall sustainability aspects of the

pavement to aid the decision-making in the selection of pavements. The sustainability factors for each alternative was calculated using Equations (6.6) to (6.9) and are found to be 0.33, 0.33 and 0.34 for CLS, GR1, and GR2, respectively. The higher the magnitude of the sustainability factor, the pavement alternative will be more sustainable and vice versa. The results show that the GR2 has a higher sustainability index compared to CLS and GR1. Thus, it can be concluded that the virgin aggregate can be replaced by geocell-reinforced RAP as a sustainable base alternative in the pavement infrastructure.

Table 6.4 Overall present value of the pavement alternatives

Present Value* ($/mile)	CLS	GR1	GR2
PV_{HIC}	1,534,800	1,537,200	1,463,200
PV_{EIC}	1,904,000	1,904,100	1,895,100
PV_{AC}	405,700	392,800	367,700
PV_{UC}	822,800	768,100	742,600
PV	4,667,300	4,602,200	4,468,600

*rounded to nearest hundred.

6.4.7 *Sensitivity Analysis*

The selection of discount rate can be a matter of concern in the life-cycle cost analysis. Adoption of a different discount rate can significantly affect the results of LCCA. For this reason, a sensitivity analysis was performed by varying the discount rate from 1% to 20% keeping all the other parameters constant and the analysis result is shown in Figure 6.10. At lower discount rates, the GR2 option

showed lower total costs compared to CLS and GR2 options. The total cost of all the three scenarios decreased exponentially with an increase in discount rate and was practically equal for a discount rate higher than 10%.

Sensitivity analysis was also performed to study the variation of user costs on AADT as shown in Figure 6.11. The results clearly indicate that the increase in AADT significantly increased user costs. The increase in traffic volume aggravated pavement deterioration which resulted in higher VOC. It can also be observed that the user cost for the GR2 option is considerably less compared to GR1. This resulted from the improved pavement performance due to the geocell reinforcement which in turn reduced the pavement roughness.

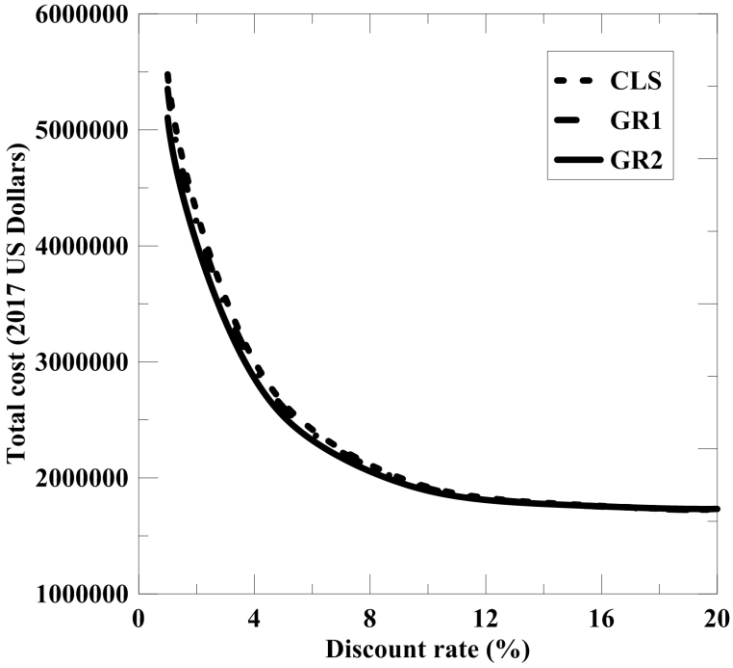

Figure 6.10 Sensitivity analysis on discount rate

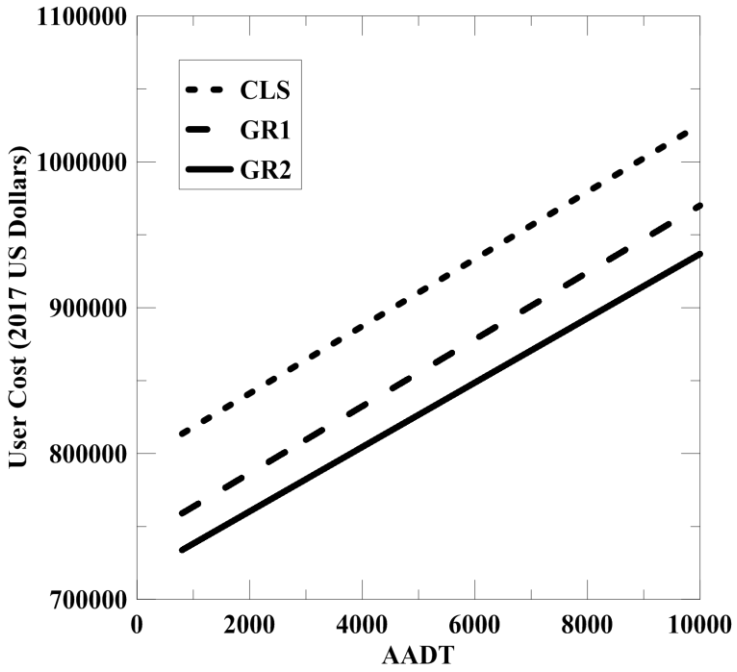

Figure 6.11 Sensitivity analysis on AADT

6.5 Summary

This study highlights the development of an integrated LCA-LCCA framework for the selection of sustainable pavement alternative. A low volume farm-to-market road at Venus, Texas was considered for the analysis. Three potential cases of base alternatives were evaluated: (a) Unbounded crushed limestone (CLS), (b) 10-cm geocell-reinforced RAP (GR1), and (c) 15-cm geocell-reinforced RAP (GR2) by considering health impact costs, environmental impact costs, agency cost, and user costs incurred throughout the service life of the pavement.

The study also focuses on the importance of evaluating the sustainability of pavement infrastructure in terms of the overall present worth of the pavement. The sustainability aspects of each alternative were evaluated separately by considering the impacts of emission, climate change, noise pollution and water pollution from each phase, that includes all the processes involved from raw material production to the end of pavement life along with the agency and user costs incurred over the service period of the pavement section. The results showed that health and environmental impact costs contribute to about 30% to 40% of the overall present value of the pavement in all the three scenarios. This illustrates the importance of considering health and environmental impact costs in the decision making of sustainable pavements.

A sustainability factor has also been proposed based on the present value of the pavement to quantify the overall sustainability aspect of the pavement. Based on the analysis, it can be concluded that the GRRB can be successfully used as a sustainable pavement base alternative for crushed limestone. The use of geocell reinforcement in the base layer can improve the overall performance of the pavement infrastructure both structurally and sustainably when RAP is used as infill material. The LCA-LCCA sustainability framework developed in this study considers only low volume roads and can further be extended to high volume roads. Moreover, since the effect of emissions on health and environment is susceptible to

the type of community and population density of a location, uncertainty analysis of both these parameters are recommended.

Chapter 7

CONCLUSIONS AND RECOMMENDATIONS

7.1 Introduction

The major objective of this research was to quantify the structural support offered by the geocell reinforcement by conducting a series of large-scale static and repeated load box tests on unreinforced RAP base (URB) and geocell-reinforced RAP base (GRRB) layers. The performance of the geocell reinforcement on RAP bases was assessed based on the bearing capacity, M_r, and PD behavior of geocell-RAP composite. Numerical analysis of the GRRB sections was also performed using a finite-difference (FD) approach to evaluate the load transfer mechanism of the geocell reinforcement under static and repeated loading. The numerical models developed were validated using the experimental findings to demonstrate a realistic approach to model geocell-reinforced pavements. Additionally, an integrated LCA-LCCA framework was developed to assess the sustainability of the geocell-reinforced pavement infrastructure.

7.2 Major Conclusions

The summary of the major conclusions from the dissertation research are as follows:

1. The laboratory static load box tests showed a higher performance improvement for RAP when reinforced with HDPE geocell. Geocell reinforcement increased the bearing pressure of RAP at 25% settlement ratio to 1.5 and 2 times for 10-

cm and 15-cm geocell reinforcement, respectively. The improvement in performance can be attributed to the development of additional strength from the lateral confinement offered by the geocell reinforcement.

2. The subgrade modulus, calculated from the pressure-settlement response of URB and GRRB material tests performed in the laboratory, also showed an improvement of approximately 32% to 96% for 10-cm and 15-cm geocell sections, respectively as compared to the URB layer. The increased values of subgrade modulus indicated the existance of structural support offered by the geocell reinforcement at very small deformations.
3. The bearing capacity improvement factor was calculated for 10-cm and 15-cm GRRB and was found to be 1.5 and 1.95, respectively at a settlement ratio of 20%. It was also observed that the bearing capacity improvement factor increased with an increase in settlement ratio for both the cases. This implies that the geocell reinforcement effect is maximum at higher settlements and the improvement is higher with the increased height of geocell. At higher loads, the mobilization of the tensile strength takes place in the reinforcements, which will contribute to the improvement in the performance of the GRRB.
4. The maximum percentage reduction in settlement of RAP base due to geocell reinforcement was about 30% to 75% for 10-cm and 15-cm geocell, respectively. This clearly showed that the presence of geocell reinforcement not

only increased the bearing capacity but also decreased the vertical deformation of the RAP bases significantly.

5. From the large-scale repeated load box tests, it was observed that the HDPE geocell increased the M_r of the base layer by approximately 3 to 4 times and reduced the PD of RAP base by 70% to 80% for 10-cm and 15-cm GRRB, respectively. The improvement in performance was primarily due to the increase in stress distribution angle caused by the lateral distribution of stresses through the interconnected geocell pockets.
6. At the time of repeated loading, the magnitude of elastic deformation of the unreinforced and geocell-reinforced RAP test sections decreased gradually to a constant value after 500 load cycles. Additionally, the M_r and PD values were observed to gradually reach a constant after 500 load cycles. Hence, a minimum number of 500 load cycles is recommended as pre-conditioning cycles for large-scale repeated load box tests.
7. The reduction in RAP base thickness due to geocell reinforcement was quantified by performing pavement design using the *TBR* values obtained from the large-scale repeated load box tests. The analysis results showed a thickness reduction of 0.6 times for 10-cm geocell and 0.5 times for 15-cm geocell reinforcement as compared to URB. The linear elastic analysis of the designed pavement section showed an increase in fatigue and rutting life of GRRB by approximately 8 and 30 times, respectively.

8. Parametric studies on the GRRB evidently showed the effect of various factors such as height of geocell reinforcement, gradation of RAP, and location of loading on the resilient behavior of geocell-RAP composite under repeated loading. The increase in height of geocell reinforcement significantly increased the M_r of reinforced RAP base. Gradation of RAP has also a noticeable effect on the performance of geocell reinforcement. The coarser aggregate in the RAP base layer results in a substantial improvement in the performance of GRRB. This is attributed to the presence of the interlocking mechanism of aggregates with the geocell aperture. The interlocking effect will be absent if more fines are present in the infill material. The effect of location of loading was found to be lesser significant.
9. Three-dimensional numerical models based on FD approach were developed and validated with the experimental results for each loading conditions - one for URB section and the second one for 10-cm GRRB section. The three-dimensional honeycomb shaped geocell reinforcement was modeled separately and integrated into the reinforced model to eliminate composite method errors.
10. The numerical analysis clearly demonstrated the load transfer mechanism of geocell reinforcement. The model successfully captured the beam bending mechanism and the lateral distribution of stresses towards the adjacent cells. In addition, the shear stresses developed on the geocell reinforcement due to the static loading was also quantified. Parametric studies were also performed to

evaluate factors influencing the improvement in the performance of GRRB in terms of bearing pressure when the reinforced test section is subjected to static loading.

11. Numerical simulations were also performed on the unreinforced and geocell-reinforced models under repeated loading conditions by applying 500 load cycles. The variation of cumulative PD was plotted for both unreinforced and geocell-reinforced case and was validated with the experimental results. Significant reduction in the vertical and horizontal stresses was observed on the subgrade surface due to the presence of geocell reinforcement. The model could successfully predict the horizontal and vertical strains developed under repeated loading.
12. An integrated LCA-LCCA framework was developed for the selection of sustainable pavement alternative. A case study was performed on a low volume farm-to-market road at Venus, Texas to demonstrate the framework. The sustainability aspects of each alternative were evaluated separately by considering the impacts of emission, climate change, noise pollution and water pollution from each phase, including all the processes involved from raw material production to the end of pavement life along with the agency and user costs incurred over the service period of the pavement section. The results showed that health and environmental impact costs contribute to about 30% to 40% of the overall present value of the pavement in all the three scenarios. This

illustrates the importance of considering health and environmental impact costs in the decision making of sustainable pavements.

13. A sustainability factor has also been proposed based on the present value of the pavement to quantify the overall sustainability aspect of the pavement. Based on the analysis, it was concluded that the GRRB can be successfully used as a sustainable pavement base alternative for conventional crushed limestone aggregate. The use of geocell reinforcement in the base layer can improve the overall performance of the pavement infrastructure both structurally and sustainably when RAP is used as infill material.

7.3 Future Scope for Research

1. In this research, the experimental studies on the GRRB are limited to large-scale laboratory testing under static and repeated load cases on one type of geocell material, one type of subgrade, and two different gradations of RAP material. A further study is also required on different geocell materials, different gradations of RAP, and different subgrade materials.
2. Since the RAP is a temperature dependent material, additional large-scale laboratory studies are needed on the effect of the temperature dependency of RAP material on the performance of the base layer.
3. Since the current research is mainly focused on laboratory studies, further field implementation of GRRB under real-time traffic loading is required to study the long-term behavior.

4. The elasto-plastic Mohr-Coulomb model with tension cutoff as the failure criterion was used in the numerical study. A further study using an advanced model with more parameters can give more accurate results.
5. The LCA-LCCA sustainability framework developed in this study considered only low volume roads and can further be extended to high volume roads. Moreover, since the effect of emissions on health and environment is highly dependent on the type of community and population density of a location, uncertainty analysis of both these parameters are recommended.

REFERENCES

Acharya, B., 2011. Experimental Study on Geocell-Reinforced Flexible Pavements with Recycled Asphalt Pavement (RAP) Bases under Cyclic Loading. The University of Kansas, Lawrence, KS.

Adams, M.T. and Collin, J.G., 1997. Large Model Spread Footing Load Tests on Geosynthetic Reinforced Soil Foundations. *Journal of Geotechnical and Geoenvironmental Engineering*, 123 (1), 66–72.

Al-Qadi, I. and Hughes, J., 2000. Field Evaluation of Geocell Use in Flexible Pavements. *Transportation Research Record: Journal of the Transportation Research Board*, 1709, 26–35.

Al-Qadi, I.L., Elseifi, M.A., and Carpenter, S.H., 2007. *Reclaimed Asphalt Pavement – A Literature Review*.

Alawaji, H.A., 2001. Settlement and bearing capacity of geogrid-reinforced sand over collapsible soil. *Geotextiles and Geomembranes*, 19, 75–88.

Arulrajah, A., Disfani, M.M., Horpibulsuk, S., Suksiripattanapong, C., and Prongmanee, N., 2014. Physical properties and shear strength responses of recycled construction and demolition materials in unbound pavement base/subbase applications. *Construction and Building Materials*, 58, 245–257.

Attia, M. and Abdelrahman, M., 2010. Modeling the effect of moisture on resilient modulus of untreated reclaimed asphalt pavement. *Transportation Research Record: Journal of the Transportation Research Board*, (No. 2167), 30–40.

Avesani Neto, J.O., Futai, M.M., and Bueno, B.S., 2013. A bearing capacity calculation method for soil reinforced with a geocell. *Geosynthetics International*, 20 (3), 129–142.

Avirneni, D., Peddinti, P.R.T., and Saride, S., 2016. Durability and long term performance of geopolymer stabilized reclaimed asphalt pavement base courses. *Construction and Building Materials*, 121, 198–209.

Ayan, V., Limbachiya, M.C., Omer, J.R., Masoud, S., and Azadani, N., 2014. Compaction assessment of recycled aggregates for use in unbound subbase application. *Journal of Civil Engineering and Management*, 20 (2), 169–174.

Ayers, S., 1992. California Town Rolls Out Pavement Recycling. *City Engineer*.

Banerjee, A., 2017. Response of Unsaturated Soils under Monotonic and Dynamic Loading over moderate Suction States. Doctoral Dissertation, University of Texas at Arlington, Arlington, Texas.

Banerjee, A., Patil, U.D., Puppala, A.J., and Hoyos, L.R., 2018. Suction-controlled repeated load triaxial test of subgrade soil at high suction states. *In*: C.W.W. Ng, A.K. Leung, A.C.F. Chiu, and C. Zhou, eds. *Unsaturated Soils, Proceeding of Seventh International Conference on Unsaturated Soils*. Hong Kong, China: HKUST, 667–672.

Banerjee, A. and Puppala, A.J., 2015. Influence of Rate of Shearing on Strength Characteristics of Saturated and Unsaturated Silty Soil. *In*: *Proc. 50th Indian Geotechnical Conference*. Pune, India.

Banerjee, A., Puppala, A.J., Patil, U.D., Hoyos, L.R., and Bhaskar, P., 2018. A Simplified Approach to Determine the Response of Unsaturated Soils Using Multistage Triaxial Test. *In*: *IFCEE 2018: Advances in Geomaterial Modeling and Site Characterization, GSP 295*. 332–342.

Bathurst, R. and Karpurapu, R., 1993. Large-Scale Triaxial Compression Testing of Geocell-Reinforced Granular Soils. *Geotechnical Testing Journal*, 16 (3), 296.

Bathurst, R.J. and Knight, M.A., 1998. Analysis of geocell reinforced-soil covers over large span conduits. *Computers and Geotechnics*, 22 (3–4), 205–219.

Beckham, W.K. and Mills, W.H., 1935. Cotton-Fabric-Reinforced Roads. *Engineering News Record*, 453–455.

Bennert, T. and Maher, A., 2005. *The development of a performance specification for granular base and subbase material- No. FHWA-NJ-2005-003*.

Bennert, T., Papp, W., Maher, A., and Gucunski, N., 2000. Utilization of Construction and Demolition Debris Under Traffic-Type Loading in Base and Subbase Applications. *Transportation Research Record: Journal of the Transportation Research Board*, 1714, 33–39.

Binquet, J. and Lee, K.L., 1976. Bearing capacity tests on reinforced earth slabs. *International Journal of Rock Mechanics and Mining Sciences & Geomechanics Abstracts*, 13 (3), 31.

Biswas, A., Krishna, A.M., and Dash, S.K., 2016. Behavior of Geosynthetic

Reinforced Soil Foundation Systems Supported on Stiff Clay Subgrade. *International Journal of Geomechanics*, 16 (5), 4016007.

Bleakley, A.M. and Cosentino, P.J., 2013. Improving the properties of reclaimed asphalt pavement for roadway base applications through blending and chemical stabilization. *Transportation Research Record: Journal of the Transportation Research Board*, (2335), 20–28.

Bortz, B. and Hossain, M., 2016. Optimum Properties of Geocell Reinforcement for Sustainable Low-Volume Paved Roads. *In*: *The Roles of Accelerated Pavement Testing in Pavement Sustainability*. Cham: Springer International Publishing, 195–209.

Bortz, B.S., Hossain, M., Halami, I., and Gisi, A., 2012a. Innovative Uses of Quarry Waste and Reclaimed Asphalt Pavement. *In*: *ICSDC 2011*. Reston, VA: American Society of Civil Engineers, 515–523.

Bortz, B.S., Hossain, M., Halami, I., and Gisi, A.J., 2012b. Low-Volume Paved Road Improvement with Geocell Reinforcement. *In*: *Transportation Research Board 91st Annual Meeting*. Washington DC: Transportation Research Board.

Boushehrian, J.H. and Hataf, N., 2003. Experimental and numerical investigation of the bearing capacity of model circular and ring footings on reinforced sands. *Geotextiles and Geomembranes*, 21 (5), 241–256.

Brown, S.F., Kwan, J., and Thom, N.H., 2007. Identifying the key parameters that influence geogrid reinforcement of railway ballast. *Geotextiles and*

Geomembranes, 25 (6), 326–335.

Burmister, D.M., 1943. Theory of stresses and displacements in layered systems and application to the design of airport runways. *Proceedings of Highway Research Board*, 23, 126–148.

Bush, D.I., Jenner, C.G., and Bassett, R.H., 1990. The design and construction of geocell foundation mattresses supporting embankments over soft grounds. *Geotextiles and Geomembranes*, 9 (1), 83–98.

Caltrans, 2011. Using Life Cycle Cost Analysis in Highway Project Development. Preliminary Investigation [online]. *Caltrans Division of Research and Innovation*. Available from: http://www.dot.ca.gov/newtech/researchreports/preliminary_investigations/docs/lcca_preliminary_investigation_11-29-11.pdf. [Accessed 2 Jul 2018].

Camargoa, F.F., Edilb, T.B., and Bensonb, C.H., 2013. Strength and stiffness of recycled materials stabilised with fly ash: a laboratory study. *Road Materials and Pavement Design*, 14 (3), 504–517.

Cardile, G., Moraci, N., and Pisano, M., 2017. Tensile behaviour of an HDPE geogrid under cyclic loading: experimental results and empirical modelling. *Geosynthetics International*, 24 (1), 95–112.

Chan, A.W.C., 2007. Economic and Environmental Evaluations of Life-Cycle Cost Analysis Practice: A Case Study of Michigan DOT Pavement Projects. University of Michigan, Michigan.

Chang, I., Im, J., KharisPrasidhi, A., and Cho, G.-C., 2015. Effects of Xanthan gum biopolymer on soil strengthening. *Construction and Building Materials*, 74 (15), 65–72.

Chen, R.-H., Wu, C.-P., Huang, F.-C., and Shen, C.-W., 2013. Numerical analysis of geocell-reinforced retaining structures. *Geotextiles and Geomembranes*, 39, 51–62.

Chesner, W.H., COLLINS, R.J., and MacKay, M.H., 1998. *User Guidelines for Waste and Byproduct Materials in Pavement Construction*. McLean, VA.

Chester, M. and Horvath, A., 2009. *Life-cycle energy and emissions inventories for motorcycles, diesel automobiles, school buses, electric buses, Chicago rail, and New York City rail.*

Clary, J.A., DeGroot, D.J., and Highter, W.H., 1997. *Structural numbers for reclaimed asphalt pavement base and subbase course mixes: Final Report.* Amherst, MA.

Copeland, A., 2011. High Reclaimed Asphalt Pavement Use, No. FHWA-HRT-11-057 [online]. Available from: https://www.fhwa.dot.gov/publications/research/infrastructure/pavements/11057/11057.pdf [Accessed 9 Aug 2018].

Cosentino, P.J., Kalajian, E.H., Bleakley, A.M., Diouf, B.S., Misilo, J.T., Petersen, A.J., Krajcik, R.E., and Sajjadi, A.M., 2012. *Improving the Properties of Reclaimed Asphalt Pavement for Roadway Base Applications*. Tallahassee,

Florida.

Cosentino, P.J., Kalajian, E.H., Shieh, C.S., Mathurin, W.J.. K., Gomez, F.A., D., C.E., and Treerattakoon, A., 2003. *Developing Specifications for Using Recycled Asphalt Pavement as Base, Subbase, or General Fill Materials, Phase II. Final Report. FL/DOT/RMC/06650- 7754 BC 819.* Florida.

Das, B.M., 2016. Use of geogrid in the construction of railroads. *Innovative Infrastructure Solutions*, 1 (1), 15.

Das, B.M., Puri, V.K., Omar, M.T., and Evgin, E., 1996. Bearing Capacity of Strip Foundation on Geogrid-Reinforced Sand-Scale Effects in Model Tests. *In*: *Proceedings of the Sixth International Offshore and Polar Engineering Conference*. Los Angeles: The International Society of Offshore and Polar Engineers.

Das, J.T., Banerjee, A., Chakraborty, S., and Anand J, P., 2018. A Framework for Assessment of Sustainability and Resilience in Subgrade Stabilization for a High-Volume Road. *In*: *Transportation Research Board 97th Annual MeetingTransportation Research Board, 18-06711*.

Das, J.T., Puppala, A.J., Bheemasetti, T. V., Walshire, L.A., and Corcoran, M.K., 2016. Sustainability and resilience analysis in slope stabilization. *Sustainability and resilience analysis in slope stabilization*, 71, 25–36.

Das, J.T., Samuel, R.A., George, A.M., Chakraborty, S., Bheemasetti, T. V., and Puppala, A.J., 2018. Establishing a Threshold Sustainability Index for a

Geotechnical Construction. *In*: *IFCEE 2018*. Reston, VA: American Society of Civil Engineers, 222–232.

Dash, S., Saride, S., and Sitharam, T., 2003. Behaviour of geocell-reinforced sand beds under circular footing. *Proceedings of the Institution of Civil Engineers-Ground Improvement*, 7 (3), 111–115.

Dash, S.K., 2011. Effect of geocell type on load-carrying mechanisms of geocell-reinforced sand foundations. *International Journal of Geomechanics*, 12 (5), 537–548.

Dash, S.K., Krishnaswamy, N.R., and Rajagopal, K., 2001. Bearing capacity of strip footings supported on geocell-reinforced sand. *Geotextiles and Geomembranes*, 19, 235–256.

Dash, S.K., Rajagopal, K., and Krishnaswamy, N.R., 2007. Behaviour of geocell-reinforced sand beds under strip loading. *Canadian Geotechnical Journal*, 44 (7), 905–916.

Dash, S.K., Reddy, P.D.T., and Raghukanth, S.T.J., 2008. Subgrade modulus of geocell-reinforced sand foundations. *Proceedings of the Institution of Civil Engineers Ground Improvement*, 161 (2), 79–87.

Dash, S.K., Sireesh, S., and Sitharam, T.G., 2003. Model studies on circular footing supported on geocell reinforced sand underlain by soft clay. *Geotextiles and Geomembranes*, 21, 197–219.

Decker, D.S. and Young, T.J., 1996. Handling RAP in an HMA facility. *In*:

Proceedings of the Canadian Technical Asphalt Association. Edmonton, Alberta.

Delucchi, M.A., 2000. Environmental externalities of motor-vehicle use in the US. *Journal of Transport Economics and Policy*, 34, 135–168.

Delucchi, M.A., 2004. *The Annualized Social Cost of Motor-Vehicle Use in the U. S., 1990-1991: Summary of Theory, Data, Methods, and Results*. Davis.

Delucchi, M.A. and Hsu, S.L., 1998. The External Damage Cost of Noise from Motor Vehicles. *Journal of Transportation and Statistics*, 1 (3), 1–24.

Delucchi, M.A. and McCubbin, D.R., 2010. *External Costs of Transport in the US. Handbook of Transport Economics*.

Dong, Q. and Huang, B., 2014. Laboratory Evaluation on Resilient Modulus and Rate Dependencies of RAP Used as Unbound Base Material. *Journal of Materials in Civil Engineering*, 26 (2), 379–383.

Edil, T.B., Tinjum, J.M., and Benson, C.H., 2012. *Recycled Unbound Materials*. St Paul, MN.

Emersleben, A. and Meyer, N., 2008. The use of geocells in road constructions - falling weight deflector and vertical stress measurements. *In*: *EuroGeo 4, Proceedings of the 4th European Geosynthetics Conference*. Edinburgh, Schottland.

Emersleben, A. and Meyer, N., 2010. Verification of the Load Transfer Mechanism of Geocell Reinforced Soil in Large Scale Model Tests and Different In Situ

Test Fields. *In*: *GeoFlorida 2010*. Reston, VA: American Society of Civil Engineers, 1670–1679.

EPA, 2015. *Criteria Air Pollutants. America's Children and the Environment.*

Epps, J.A., 1990. *Cold-recycled bituminous concrete using bituminous materials (No. 160).* Transportation Research Board.

Esmaeili, M., Zakeri, J.A., and Babaei, M., 2017. Laboratory and field investigation of the effect of geogrid-reinforced ballast on railway track lateral resistance. *Geotextiles and Geomembranes*, 45 (2), 23–33.

FHWA, 2002. *Life-Cycle Cost Analysis Primer*.

Forkenbrock, D.J., 1999. External costs of intercity truck freight transportation. *Transportation Research Part A*, 33, 505–526.

Forkenbrock, D.J., 2001. Comparison of external costs of rail and truck freight transportation. *Transport Research Part A*, 35, 321–337.

Gabr, M.A., Dodson, R., and Collin, J.G., 1998. A study of stress distribution in geogrid-reinforced sand. *Geosynthetics in foundation reinforcement and erosion control systems, ASCE Special publication*, 62–76.

Ganne, V.K., 2009. Long-term durability studies on chemically treated Reclaimed Asphalt Pavement (RAP) materials. The University of Texas at Arlington.

Garg, N. and Thompson, M., 1996. Lincoln Avenue Reclaimed Asphalt Pavement Base Project. *Transportation Research Record: Journal of the Transportation Research Board*, 1547, 89–95.

George, A.M., 2015. Numerical Modeling of Geocell Reinforced Beds. Indian Institute of Technology Hyderabad.

George, A.M., Banerjee, A., Anand J, P., and Praticò, F., 2019. An Intergrated LCA-LCCA Framework for the Selection of Sustainable Pavement Design. *Transportation Research Board 98th Annual Meeting, Transportation Research Bard, 19-05948*.

George, A.M., Banerjee, A., Taylor, T., and Puppala, A.J., 2019. Large-Scale Experimental Studies to Evaluate the Resilient Modulus of Geocell-Reinforced Reclaimed Asphalt Pavement Bases. *In*: *Gosynthetics 2019 Conference*. Houston, Texas.

George, A.M. and Saride, S., 2014a. Sustainability of Geogrid Reinforced Flyash Treated RAP Bases in Flexible Pavements. *In*: *International Conference on Sustainable Civil Infrastructure 2014*. Hyderabad, India.

George, A.M. and Saride, S., 2014b. Damage Analysis of Low Volume Roads Constructed with RAP material. *In*: *Indian Geotechnical Conference 2014*. Kakinada, India.

Giroud, J.P. and Han, J., 2004a. Design Method for Geogrid-Reinforced Unpaved Roads. I. Development of Design Method. *Journal of Geotechnical and Geoenvironmental Engineering*, 130 (8), 775–786.

Giroud, J.P. and Han, J., 2004b. Design Method for Geogrid-Reinforced Unpaved Roads. II. Calibration and Applications. *Journal of Geotechnical and*

Geoenvironmental Engineering, 130 (8), 787–797.

Gnanendran, C. T., and Woodburn, L.J., 2003. Recycled Aggregate for Pavement Construction and the Influence of Stabilization. *In*: *Proceedings on Conference of the Australian Road Research Board*. Leederville, Australia, 1755–1768.

Guido, V.A., Chang, D.K., and Sweeney, M.A., 1986. Comparison of geogrid and geotextile reinforced earth slabs. *Canadian Geotechnical Journal*, 23 (4), 435–440.

Guthrie, W.E.S., Cooley, D., and Eggett, D.L., 2007. Effects of reclaimed asphalt pavement on mechanical properties of base materials. *Transportation Research Board, Transportation Research Record, Washington, DC*, (No. 2005), 44–52.

Han, J., Pokharel, S.K., Yang, X., Manandhar, C., Leshchinsky, D., Halahmi, I., and Parsons, R.L., 2011. Performance of Geocell-Reinforced RAP Bases over Weak Subgrade under Full-Scale Moving Wheel Loads. *Journal of Materials in Civil Engineering*, 23 (11), 1525–1534.

Han, J., Yang, X.M., Leshchinsky, D., Parsons, R.L., and Rosen, A., 2008. Numerical Analysis for Mechanisms of a Geocell-Reinforced Base Under a Vertical Load. *In*: *Geosynthetics in Civil and Environmental Engineering*. Berlin, Heidelberg: Springer Berlin Heidelberg, 741–746.

Hanks, A.J. and Magni, E.R., 1989. *The Use of Bituminous and Concrete Material*

in Granular Base and Earth, Materials Information Report MI-137. Downsview, Ontario.

Hansen, K.R. and Copeland, A., 2017. Asphalt Pavement Industry Survey on Recycled Materials and Warm-Mix Asphalt Usage: 2015 — 6th Annual Survey. Information Series 138(6e) [online]. *National Asphalt Pavement Association*. Available from: http://www.asphaltpavement.org/PDFs/IS138/IS138-2015_RAP-RAS-WMA_Survey_Final.pdf.

Hegde, A. and Sitharam, T.G., 2015a. 3-Dimensional numerical modelling of geocell reinforced sand beds. *Geotextiles and Geomembranes*, 43 (2), 171–181.

Hegde, A. and Sitharam, T.G., 2017a. Experiment and 3D-numerical studies on soft clay bed reinforced with different types of cellular confinement systems. *Transportation Geotechnics*, 10, 73–84.

Hegde, A. and Sitharam, T.G., 2017b. Experiment and 3D-numerical studies on soft clay bed reinforced with different types of cellular confinement systems. *Transportation Geotechnics*, 10, 73–84.

Hegde, A.M. and Sitharam, T.G., 2015b. Effect of infill materials on the performance of geocell reinforced soft clay beds. *Geomechanics and Geoengineering*, 10 (3), 163–173.

Hegde, A.M. and Sitharam, T.G., 2015c. Three-dimensional numerical analysis of

geocell-reinforced soft clay beds by considering the actual geometry of geocell pockets. *Canadian Geotechnical Journal*, 52 (9), 1396–1407.

Henkel, D.J. and Gilbert, G.C., 1952. The Effect of Rubber Membranes on the Measured Triaxial Compression Strength of Clay Samples. *Geotechnique*, 3 (1), 20–29.

Holtz, R.D., 2004. GEOSYNTHETICS R&D--THE 'EARLY' DAYS (1960s to Circa 1985). *In*: *Proceedings from the 2004 Symposium Honouring the Research Achievements of Dr. Robert M. Koerner.*

Holtz, R.D., 2017. 46th Terzaghi Lecture: Geosynthetic Reinforced Soil: From the Experimental to the Familiar. *Journal of Geotechnical and Geoenvironmental Engineering*, 143 (9), 3117001.

Hoppe, E.J., D. Stephen Lane, Fitch, G.M., and Shetty, S., 2015. Feasibility of Reclaimed Asphalt Pavement (RAP) Use As Road Base and Subbase Material [online]. *Virginia Center for Transportation Innovation and Research*. Available from: http://www.virginiadot.org/vtrc/main/online_reports/pdf/15-r6.pdf [Accessed 11 Aug 2018].

Hoyos, L.R., Puppala, A.J., and Ordonez, C.A., 2011. Characterization of Cement-Fiber-Treated Reclaimed Asphalt Pavement Aggregates: Preliminary Investigation. *Journal of Materials in Civil Engineering*, 23 (7), 977–989.

Indraratna, B., Hussaini, S.K.K., and Vinod, J.S., 2013. The lateral displacement response of geogrid-reinforced ballast under cyclic loading. *Geotextiles and*

Geomembranes, 39, 20–29.

Inti, S., 2016. A decision making approach for selection of sustainable pavements in Texas by integrating life cycle cost analysis (LCCA), life cycle assessment (LCA) of environmental and social impacts. University of El Paso, Texas.

Islam, S. and Butlar, W., 2012. Effect of Pavement Roughness on User Costs. *Transportation Research Record: Journal of the Transportation Research Board*, 2285, 47–55.

Itasca Consulting Group, I., 2013. *FLAC3D-Fast Lagrangian Analysis of Continua in Three Dimensions, Ver 5.0 User's Guide*. Minneapolis, USA.

Jiang, Y. and Li, S., 2005. Gray System Model for Estimating the Pavement International Roughness Index. *Journal of Performance of Constructed Facilities*, 19 (1), 62–68.

Kandhal, P.S. and Mallick, R.B., 1997. Pavement Recycling Guidelines for State and Local Governments: Participant's Reference Book. Report No. FHWA-SA-98-042. [online]. Available from: https://www.fhwa.dot.gov/pavement/recycling/98042/98042.pdf [Accessed 9 Aug 2018].

Kassim, T.A., Simoneit, B.R.T., and Williamson, K.J., 2005. Recycling Solid Wastes as Road Construction Materials: An Environmentally Sustainable Approach. *In*: *Water Pollution. The Handbook of Environmental Chemistry, vol 1*. Berlin, Heidelberg: Springer-Verlag, 59–181.

Kazerani, B. and Jamnejad, G., 1987. Polymer grid cell reinforcement in construction of pavement structures. Section 1A, unpaved and paved roads. *In*: *Proceedings of Geosynthetic'87*. New Orleans, USA.

Kazmee, H., Tutumluer, E., and Beshears, S., 2017. Using Accelerated Pavement Testing to Evaluate Reclaimed Asphalt Pavement Materials for Pavement Unbound Granular Layers. *Journal of Materials in Civil Engineering*, 29 (2), 4016205.

Kennedy, T.W., Tam, W.O., and Solaimanian, M., 1998. Optimizing Use of Reclaimed Asphalt Pavement with the SuperPave System. *Journal of the Association of Asphalt Paving Technologists*, 67, 311–333.

Kim, W. and Labuz, J.F., 2007. *Resilient modulus and strength of base course with recycled bituminous- Report No.MN/RC-2007-05*. St. Paul, Minnesota.

Koerner, R.M., 1998. *Designing with Geosynthetics*. New Jersey: Prentice Hall.

Koerner, R.M., 2016. Early background and history of geotextiles. *In*: *Geotextiles*. Elsevier, 3–15.

Krishnaswamy, N.R., Rajagopal, K., and Latha, G.M., 2000. Model studies on geocell supported embankments constructed over a soft clay foundation. *Geotechnical Testing Journal*, 23 (2), 45–54.

Kumar, A. and Saran, S., 2001. Isolated strip footings on reinforced sand. *Journal of the Southeast Asian Geotechnical Society*, 32 (3), 117–189.

LaHucik, J., Schmidt, S., Tutumluer, E., and Roesler, J., 2016. Cement-Treated

Bases Containing Reclaimed Asphalt Pavement, Quarry By-Products, and Fibers. *Transportation Research Record: Journal of the Transportation Research Board*, 2580, 10–17.

Lambert, S., Nicot, F., and Gotteland, P., 2011. Uniaxial compressive behavior of scrapped tire and sand-filled wire netted geocell with a geotextile envelope. *Geotextiles and Geomembranes*, 29 (5), 483–490.

Latha, G.M., Rajagopal, K., and Krishnaswamy, N.R., 2006. Experimental and theoretical investigations on geocell-supported embankments. *International Journal of Geomechanics*, 6 (1), 30–35.

Leshchinsky, B.A., 2011. Enhancing Ballast Performance Using Geocell Confinement. *In*: *Geo-Frontiers 2011*. Reston, VA: American Society of Civil Engineers, 4693–4702.

Leshchinsky, B. and Ling, H., 2013. Effects of Geocell Confinement on Strength and Deformation Behavior of Gravel. *Journal of Geotechnical and Geoenvironmental Engineering*, 139 (2), 340–352.

Li, L., Benson, C., Edil, T., and Hatipoglu, B., 2007. Sustainable construction case history: fly ash stabilization of recycled asphalt pavement material. *In*: *86th annual meeting of the Transportation Research Board*. Washington, DC.

Liu, W., 2011. *Flexible Pavement Design System FPS 21: User's Manual*. Texas.

Locander, R., 2009. *Analysis of Using Reclaimed Asphalt Pavement (RAP) as a Base Course Material- Report CDOT-2009-5*. Colarado, USA.

Lu, Q., Mannering, F.L., and Xin, C., 2018. *A Life Cycle Assessment Framework for Pavement Maintenance and Rehabilitation Technologies: An Integrated Life Cycle Assessment (LCA)–Life Cycle Cost Analysis (LCCA) Framework for Pavement Maintenance and Rehabilitation*.

MacGregor, J., Highter, W., and DeGroot, D., 1999. Structural Numbers for Reclaimed Asphalt Pavement Base and Subbase Course Mixes. *Transportation Research Record: Journal of the Transportation Research Board*, 1687, 22–28.

Madhavi Latha, G., Dash, S.K., and Rajagopal, K., 2008. Equivalent Continuum Simulations of Geocell Reinforced Sand Beds Supporting Strip Footings. *Geotechnical and Geological Engineering*, 26 (4), 387–398.

Madhavi Latha, G. and Somwanshi, A., 2009. Effect of reinforcement form on the bearing capacity of square footings on sand. *Geotextiles and Geomembranes*, 27 (6), 409–422.

MAGPPA, 2002. *Capitalization and Depreciation of Infrastructure.*

Maher, M., Gucunski, N., and Papp, W., 1997. Recycled Asphalt Pavement as a Base and Sub-Base Material. *In*: *ASTM Special Technical Publication 1275*. 100 Barr Harbor Drive, PO Box C700, West Conshohocken, PA 19428-2959: ASTM International, 42–13.

Mallela, J. and Sadasivam, S., 2011. *Work Zone Road User Costs – Concepts and Applications*. Washington DC.

Mandal, J.N. and Gupta, P., 1994. Stability of geocell-reinforced soil. *Construction and building materials*, 8 (1), 55–62.

McGarrah, E.J., 2007. *Evaluation of Current Practices of Reclaimed Asphalt Pavement/Virgin Aggregate as Base Course Material. Report No. WA-RD 713.1*. Olympia, WA.

Mehdipour, I., Ghazavi, M., and Moayed, R.Z., 2013. Numerical study on stability analysis of geocell reinforced slopes by considering the bending effect. *Geotextiles and Geomembranes*, 37, 23–34.

Mehdipour, I., Ghazavi, M., and Ziaie Moayed, R., 2017. Stability Analysis of Geocell-Reinforced Slopes Using the Limit Equilibrium Horizontal Slice Method. *International Journal of Geomechanics*, 17 (9), 6017007.

Mengelt, M., Edil, T., and Benson, C., 2000. *Reinforcement of Flexible Pavements with Geocells, Geo Engineering Report No. 00-04*. Madison, WI, USA.

De Merchant, M.R., Valsangkar, A.J., and Schriver, A.B., 2002. Plate load tests on geogrid-reinforced expanded shale light weight aggregate. *Geotextiles and Geomembranes*, 20, 173–190.

Mhaiskar, S.Y. and Mandal, J.N., 1994. "Three dimensional geocell structure: performance under repetitive loads. *In*: *5th International Conference on Geotextile, Geomembranes and Related products*. Singapore, 155–158.

Mhaiskar, S.Y. and Mandal, J.N., 1996. Investigations on soft clay subgrade strengthening using geocells. *Construction and Building Materials*, 10 (4),

281–286.

Michalowski, R.L., 2004. Limit loads on reinforced foundation soils. *Journal of Geotechnical and Geoenvironmental Engineering, ASCE*, 130 (4), 381–390.

Miyata, Y., Bathurst, R.J., and Miyatake, H., 2015. Performance of three geogrid-reinforced soil walls before and after foundation failure. *Geosynthetics International*, 22 (4), 311–326.

Mohammad, L.N., Puppala, A.J., and Alavilli, P., 1995. Resilient properties of laboratory compacted subgrade soils. *Transportation Research Record*, (1504).

Mohammadinia, A., Arulrajah, A., Sanjayan, J., Disfani, M.M., Bo, M.W., and Darmawan, S., 2015. Laboratory Evaluation of the Use of Cement-Treated Construction and Demolition Materials in Pavement Base and Subbase Applications. *Journal of Materials in Civil Engineering*, 27 (6), 4014186.

Mokwa, R.L. and Peebles, C.S., 2005. Evaluation of the Engineering Characteristics of RAP/Aggregate Blends, FHWA/MT-05-008/8117-24 [online]. *Federal Highway Administration*. Available from: https://www.mdt.mt.gov/other/webdata/external/research/docs/research_proj/rap_aggregate/final_report.pdf [Accessed 11 Aug 2018].

MOVES, 2015. *Motor Vehicle Emission Simulator (MOVES) 2014a. User Guide.*

Muench, S. and Dam, T. V, 2014. Pavement Sustainability [online]. *Sustainable Pavements Program (DTFH61-10-D-00042). FHWA.* Available from:

https://www.fhwa.dot.gov/pavement/sustainability/hif14012.pdf. [Accessed 2 Jul 2018].

Mulheron, M. and O'Mahony, M.M., 1990. Properties and performance of recycled aggregates. Highways and transportation. *Highways and Transportation*, 37 (2), 35–37.

Muller, N.Z. and Mendelsohn, R., 2007. Measuring the damages of air pollution in the United States. *Journal of Environmental Economics and Management*, 54, 1–14.

Munzenmaier, A.M., 1994. *City Saves by Using Recycled Asphalt as Base*. El Cajon.

Nair, A.M. and Latha, G.M., 2014. Cyclic loading behaviour of reinforced soil–aggregate bases. *Proceedings of the Institution of Civil Engineers - Ground Improvement*, 167 (2), 88–98.

NAPA, 2009. Black and Green Sustainable Asphalt, Now and Tomorrow. Special Report 200 [online]. *National Ashpalt Pavement Association*. Available from: https://www.asphaltpavement.org/images/stories/sustainability_report_2009.pdf [Accessed 21 Jan 2018].

Noureldin, A.S. and Wood, L.E., 1989. Variations in Molecular Size Distribution of Virgin and Recycled Asphalt Binders Associated with Aging. *Transportation Research Board, Transportation Research Record ,Washington, DC*, (No.1228).

Oliaei, M. and Kouzegaran, S., 2017. Efficiency of cellular geosynthetics for foundation reinforcement. *Geotextiles and Geomembranes*, 45 (2), 11–22.

Omar, M.T., Das, B.M., Puri, V.K., and Yen, S.C., 1993. Ultimate bearing capacity of shallow foundations on sand with geogrid reinforcement. *Canadian Geotechnical Journal*, 30 (3), 545–549.

Ordonez, C.A., 2006. Characterization of cemented and fiber-reinforced RAP aggregate materials for base/sub-base applications. The University of Texas at Arlington.

Osinubi, K.J. and Edeh, J.E., 2011. Reconstituted coal ash stabilization of reclaimed asphalt pavement. *In*: *Geo-Frontiers 2011: Advances in Geotechnical Engineering*. Dallas, TX., 1172–1181.

Osinubi, K.J., Edeh, J.E., and Onoja, W.O., 2012. Sawdust Ash Stabilization of Reclaimed Asphalt Pavement. *Journal of ASTM International*, 9 (2), 1–10.

Page, G.C. and Murphy, K.H., 1987. Hot-mix Recycling Saves Florida $38 Million. *Asphalt, Spring*, 1 (1), 3–4.

Papp, W. J., J., Maher, M.H., Bennert, T.A., and Gucunski, N., 1998. Behaviour of construction and demolition debris in base and subbase applications. *In*: *Proceedings of Geo-Congress: Recycled Materials in Geotechnical Applications.* Reston, VA: American Society of Civil Engineers, 122–136.

Patil, U.D., Banerjee, A., Puppala, A.J., and Hoyos, L.R., 2018. Shear Strength Prediction of Compacted Silty Sand at Peak/Critical State Failure over Wider

Suction Range. *In*: *PanAm Unsaturated Soils 2017, GSP 301*. Reston, VA: American Society of Civil Engineers, 340–349.

Patil, U.D., Puppala, A.J., Hoyos, L.R., and Banerjee, A., 2018. Strength, Stiffness and Radial Anisotropy of Compacted Silty Sand Under Suction-Controlled Axisymmetric Shearing. *Geotechnical and Geological Engineering*.

Patra, C.R., Das, B.M., and Atalar, C., 2005. Bearing capacity of embedded strip foundation on geogrid-reinforced sand. *Geotextiles and Geomembranes*, 23 (5), 454–462.

Pedarla, A., Chittoori, S., and Puppala, A.J., 2011. Influence of mineralogy and plasticity index on the stabilization effectiveness of expansive clays. *Transportation Research Record*, 2212 (1), 91–99.

Pincus, H.J., Omar, M.T., Das, B.M., Yen, S.C., Puri, V.K., and Cook, E.E., 1993. Ultimate Bearing Capacity of Rectangular Foundations on Geogrid-Reinforced Sand. *Geotechnical Testing Journal*, 16 (2), 246.

Pokharel, S.K., 2010. Experimental study on geocell-reinforced bases under static and dynamic loading. University of Kansas.

Pokharel, S.K., Han, J., Leshchinsky, D., and Parsons, R.L., 2018. Experimental evaluation of geocell-reinforced bases under repeated loading. *International Journal of Pavement Research and Technology*, 11 (2), 114–127.

Pokharel, S.K., Han, J., Leshchinsky, D., Parsons, R.L., and Halahmi, I., 2009. Behavior of geocell-reinforced granular bases under static and repeated loads.

In Contemporary Topics in Ground Modification, Problem Soils, and Geo-Support, ASCE, GSP 187, 409–416.

Pokharel, S.K., Han, J., Manandhar, C., Yang, X., Leshchinsky, D., Halahmi, I., and Parsons, R.L., 2011. Accelerated Pavement Testing of Geocell-Reinforced Unpaved Roads over Weak Subgrade. *Transportation Research Record: Journal of the Transportation Research Board*, 2204 (1), 67–75.

Pokharel, S.K., Han, J., Parsons, R.L., Qian, Y., Leshchinsky, D., and Halahmi, I., 2009. Experimental study on bearing capacity of geocell-reinforced bases. *In*: *8th international conference on Bearing Capacity of Roads, Railways and Airfields*. Champaign, IL, USA, 1159–1166.

Potturi, A., Puppala, A.J., and Hoyos, L.R., 2007. Resilient characteristics of cement treated reclaimed asphalt pavement aggregates. *In*: *Presented at 86th Annual Meeting of the Transportation Research Board*. Washington, DC.

Potturi, A.K., 2006. Evaluation of resilient modulus of cement and cement-fiber treated reclaimed asphalt pavement (RAP) aggregates using repeated load triaxial test. The University of Texas at Arlington.

Praticò, F., Saride, S., and Puppala, A., 2011. Comprehensive life-cycle cost analysis for selection of stabilization alternatives for better performance of low-volume roads. *Transportation Research Record: Journal of the Transportation Research Board*, 2204, 120–129.

Puppala, A., Wattanasanticharoen, E., and Hoyos, L., 2003. Ranking of four

chemical and mechanical stabilization methods to treat low-volume road subgrades in Texas. *Transportation Research Record: Journal of the Transportation Research Board*, (1819), 63–71.

Puppala, A.J. and Cerato, A., 2009. Heave distress problems in chemically-treated sulfate-laden materials. *Geo-Strata—Geo Institute of ASCE*, 10 (2), 28.

Puppala, A.J., Das, J.T., Bheemasetti, T. V., and Congress, S.S.C., 2018. Sustainability and Resilience in Transportation Infrastructure geotechnics: Integrating Advanced Technologies for better Asset Management. *Geo-Strata -Geo Institute of ASCE*, 42–48.

Puppala, A.J., Hoyos, L.R., and Potturi, A.K., 2011. Resilient Moduli Response of Moderately Cement-Treated Reclaimed Asphalt Pavement Aggregates. *Journal of Materials in Civil Engineering*, 23 (7), 990–998.

Puppala, A.J., Manosuthikij, T., and Chittoori, B.C.S., 2013. Swell and shrinkage characterizations of unsaturated expansive clays from Texas. *Engineering Geology*, 164, 187–194.

Puppala, A.J., Manosuthikij, T., and Chittoori, B.C.S., 2014. Swell and shrinkage strain prediction models for expansive clays. *Engineering Geology*, 168, 1–8.

Puppala, A.J., Manosuthkij, T., Nazarian, S., and Hoyos, L.R., 2011. Threshold moisture content and matric suction potentials in expansive clays prior to initiation of cracking in pavements. *Canadian Geotechnical Journal*, 48 (4), 519–531.

Puppala, A.J., Pedarla, A., Chittoori, B., Ganne, V.K., and Nazarian, S., 2017. Long-Term Durability Studies on Chemically Treated Reclaimed Asphalt Pavement Material as a Base Layer for Pavements. *Transportation Research Record: Journal of the Transportation Research Board*, 2657, 1–9.

Puppala, A.J., Saride, S., Potturi, A., and Hoyos, L.R., 2009. Resilient Behavior of Cement-Fiber Treated Reclaimed Asphalt Pavement Aggregates. *In*: *Proceedings International Foundation Congress and Equipment Expo, ASCE, GSP 187*. 433–440.

Rajagopal, K., Krishnaswamy, N.R., and Latha, G.M., 1999. Behaviour of sand confined with single and multiple geocells. *Geotextiles and Geomembranes*, 17, 171–184.

Rana, A.S.M.A., 2004. Evaluation of recycled material performance in highway applications and optimization of their use. Texas Tech University.

Rea, C. and Mitchell, J.K., 1978. Sand Reinforcement Using Paper Grid Cells. *In*: *Proceedings, ASCE Spring Convention and Exhibit*. Pittsburgh, PA, 24–28.

Saeed, A., 2007. Appendixes to NCHRP Report 598. NCHRP Web-Only Document 119. [online]. *Transportation Research Board of the National Academies. Washington, DC*. Available from: http://onlinepubs.trb.org/onlinepubs/nchrp/nchrp_w119.pdf [Accessed 9 May 2018].

Saladhi, M., 2017. Experimental Study on Resilient Behavior of Geocell-

Reinforced Recycled Asphalt Pavement Base Layer: Model Development. University of Texas at Arlington.

Sambodh, A., 2017. Mechanical Properties of Soil-RAP-Geopolymer for the Stabilization of Road Base/Subbase. University of Louisiana at Lafayette.

Sandin, C., 2008. Laboratory Evaluation of the Variability of Florida's RAP Materials for Use in Earthwork Applications. Florida Institute of Technology.

Santero, N.J. and Horvath, A., 2009. Global warming potential of pavements. *Environmental Research Letters*, 4 (3), 34011.

Santero, N.J., Masanet, E., and Horvath, A., 2011. Life-cycle assessment of pavements. Part I: Critical review. *Resources, Conservation and Recycling*, 55 (9–10), 801–809.

Santos, R. and Costa, A.A., 2017. Information integration and interoperability for BIM-based life-cycle assessment. *In*: *Integrating Information in Built Environments*. 127–144.

Saride, S., Avirneni, D., Javvadi, S.C.P., Puppala, A.J., and Hoyos, L.R., 2015. Evaluation of fly ash treated reclaimed asphalt pavement for base/subbase applications. *Indian Geotechnical Journal*, 45 (4), 401–411.

Saride, S., George, A.M., Avirneni, D., and Munwar Basha, B., 2017. Sustainable Design of Indian Rural Roads with Reclaimed Asphalt Materials. *In*: *Sustainability Issues in Civil Engineering*. Singapore: Springer, 73–90.

Saride, S., George, A.M., V, V.K., and Puppala, A.J., 2017a. Experimental and

Numerical Evaluation of Reinforcement Mechanism of Geocells. *In*: *Transportation Research Board 96th Annual Meeting*. Washington, DC: Transportation Research Board.

Saride, S., George, A.M., V, V.K., and Puppala, A.J., 2017b. Experimental and Numerical Evaluation of Reinforcement Mechanism of Geocells. *In*: *Transportation Research Board 96th Annual Meeting*. Washington, DC: Transportation Research Board.

Saride, S., Gowrisetti, S., Sitharam, T.G., and Puppala, A.J., 2009. Numerical simulation of geocell-reinforced sand and clay. *Proceedings of the Institution of Civil Engineers - Ground Improvement*, 162 (4), 185–198.

Saride, S., Puppala, A.J., and Williammee, R., 2010. Assessing recycled/secondary materials as pavement bases. *Proceedings of the ICE-Ground Improvement*, 163 (1), 3–12.

Saride, S., Rayabharapu, V.K., and Vedpathak, S., 2015. Evaluation of Rutting Behaviour of Geocell Reinforced Sand Subgrades Under Repeated Loading. *Indian Geotechnical Journal*, 45 (4), 378–388.

Schaefer, V., Stevens, L., White, D., and Ceylan, H., 2008. *Design Guide for Improved Quality of Roadway Subgrades and Subbases.* Ames.

Sekine, E., Muramoto, K., and Tarumi, H., 1994. *Study on properties of road bed reinforced with geocell.* Quarterly Report of RTRI. Japan.

Senior, S.A., Szoke, S.I., and Rogers, C.A., 1994. Ontario's Experience with

Reclaimed Materials for Use in Aggregates. *In*: *International Road Federation Conference*. Calgary, Alberta.

Shadmand, A., Ghazavi, M., and Ganjian, N., 2018. Load-settlement characteristics of large-scale square footing on sand reinforced with opening geocell reinforcement. *Geotextiles and Geomembranes*, 46 (3), 319–326.

Shin, E.C., Das, B.M., Lee, E.S., and Atalar, C., 2002. Bearing capacity of strip foundation on geogrid-reinforced sand. *Geotechnical and Geological Engineering*, 20, 169–180.

Sireesh, S., Sitharam, S., and Dash, S.K., 2009. Bearing capacity of circular footing on geocell-sand mattress overlying clay bed with void. *Geotextiles and Geomembranes*, 27, 89–98.

Sirivitmaitrie, C., Puppala, A., Saride, S., and Hoyos, L., 2011. Combined lime-cement stabilization for longer life of low-volume roads. *Transportation Research Record: Journal of the Transportation Research Board*, (2204), 140–147.

Sitharam, G.T., Sireesh, S., and Dash, S.K., 2007. Performance of surface footing on geocellreinforced soft clay beds. *Geotechnical and Geological Engineering*, 25, 509–524.

Sitharam, T.G. and Hegde, A., 2013. Design and construction of geocell foundation to support the embankment on settled red mud. *Geotextiles and Geomembranes*, 41, 55–63.

Sitharam, T.G., Sireesh, S., and Dash, S.K., 2005. Model studies of a circular footing supported on geocell-reinforced clay. *Canadian Geotechnical Journal*, 42, 693–703.

Smith, R.W., 1980. State of the art hot recycling. *In*: *Proceedings of the National Seminar on Asphalt Pavement Recycling*. Washington, D.C.: Transportation Research Board.

Stroup-Gardiner, M. and Wattenberg-Komas, T., 2013. *Recycled Materials and Byproducts in Highway Applications –Summary Report*. Washington DC.

Suku, L., Prabhu, S.S., Ramesh, P., and Babu, G.L.S., 2016. Behavior of geocell-reinforced granular base under repeated loading. *Transportation Geotechnics*, 9, 17–30.

Suku, L., Prabhu, S.S., and Sivakumar Babu, G.L., 2017. Effect of geogrid-reinforcement in granular bases under repeated loading. *Geotextiles and Geomembranes*, 45 (4), 377–389.

Tafreshi, S.N. and Dawson, A.R., 2012. A comparison of static and cyclic loading responses of foundations on geocell-reinforced sand. *Geotextiles and Geomembranes*, 32, 55–68.

Tafreshi, S.N.M., Darabi, N.J., Mehrjardi, G.T., and Dawson, A., 2016. Experimental and numerical investigation of footing behaviour on multi-layered rubber-reinforced soil. *European Journal of Environmental and Civil Engineering*.

Tafreshi, S.N.M. and Dawson, A.R., 2010. Behaviour of footings on reinforced sand subjected to repeated loading – Comparing use of 3D and planar geotextile. *Geotextiles and Geomembranes*, 28 (5), 434–447.

Taha, R., 2003. Evaluation of Cement Kiln Dust-Stabilized Reclaimed Asphalt Pavement Aggregate Systems in Road Bases. *Transportation Research Record Journal of :Transportation Research Board*, (No. 1819), 11–17.

Taha, R., Al-Harthy, A., Al-Shamsi, K., and Al-Zubeidi, M., 2002a. Cement Stabilization of Reclaimed Asphalt Pavement Aggregate for Road Bases and Subbases. *Journal of Materials in Civil Engineering*, 14 (3), 239–245.

Taha, R., Al-Harthy, A., Al-Shamsi, K., and Al-Zubeidi, M., 2002b. Cement Stabilization of Reclaimed Asphalt Pavement Aggregate for Road Bases and Subbases. *Journal of Materials in Civil Engineering*, 14 (3), 239–245.

Taha, R., Ali, G., Basma, A., and Al-Turk, O., 1999. Evaluation of Reclaimed Asphalt Pavement Aggregate in Road Bases and Subbases. *Transportation Research Record: Journal of the Transportation Research Board*, 1652, 264–269.

Tanyu, B.F., Aydilek, A.H., Lau, A.W., Edil, T.B., and Benson, C.H., 2013. Laboratory evaluation of geocell-reinforced gravel subbase over poor subgrades. *Geosynthetics International*, 20 (2), 47–61.

Tavakoli Mehrjardi, G., Ghanbari, A., and Mehdizadeh, H., 2016. Experimental study on the behaviour of geogrid-reinforced slopes with respect to aggregate

size. *Geotextiles and Geomembranes*, 44 (6), 862–871.

Thakur, J.K., 2013. Geocell-Reinforced Unpaved and Paved Roads with Recycled Asphalt Pavement (RAP) Bases: Experimental Study and Damage Model Development. The University of Kansas.

Thakur, J.K. and Han, J., 2015. Recent Development of Recycled Asphalt Pavement (RAP) Bases Treated for Roadway Applications. *Journal of Transportation Infrastructure Geotechnology*, 2 (2), 68–86.

Thakur, J.K., Han, J., and Parsons, R.L., 2013. Creep Behavior of Geocell-Reinforced Recycled Asphalt Pavement Bases. *Journal of Materials in Civil Engineering*, 25 (10), 1533–1542.

Thakur, J.K., Han, J., Pokharel, S.K., and Parsons, R.L., 2012a. Performance of geocell-reinforced recycled asphalt pavement (RAP) bases over weak subgrade under cyclic plate loading. *Geotextiles and Geomembranes*, 35, 14–24.

Thakur, J.K., Han, J., Pokharel, S.K., and Parsons, R.L., 2012b. A Large Test Box Study on Geocell-Reinforced Recycled Asphalt Pavement (RAP) Bases over Weak Subgrade under Cyclic Loading. *In*: *GeoCongress 2012*. Reston, VA: American Society of Civil Engineers, 1562–1571.

Verma, B.P. and Char, A.N.R., 1986. Bearing Capacity Tests on Reinforced Sand Subgrades. *Journal of Geotechnical Engineering*, 112 (7), 701–706.

Walls III, J. and Smith, M.R., 1998. Life-cycle cost analysis in pavement design-

interim technical bulletin (No. FHWA-SA-98-079) [online]. Available from: https://www.fhwa.dot.gov/infrastructure/asstmgmt/013017.pdf. [Accessed 2 Jul 2018].

Wang, J., Liu, F.Y., Wang, P., and Cai, Y.Q., 2016. Particle size effects on coarse soil-geogrid interface response in cyclic and post-cyclic direct shear tests. *Geotextiles and Geomembranes*, 44 (6), 854–861.

Webster, S.L., 1979a. *Investigation of Beach Sand Trafficability Enhancement Using Sand-Grid Confinement and Membrane Reinforcement Concepts, Report GL-79-20 (1)*. Vicksburg, MS.

Webster, S.L., 1979b. *Investigation of beach sand trafficability enhancement using sand-grid confinement and membrane reinforcement concepts, Report GL-79-20 (1)*. Vicksburg, Mississippi.

Webster, S.L. and Watkins, J.E., 1977. *Investigation of construction techniques for tactical bridge approach roads across soft ground (No. WES-TR-S-77-1).* Vicksburg, Mississippi.

Wen, H., Warner, J., and Edil, T., 2008. Laboratory comparison of crushed aggregate and recycled pavement material with and without high-carbon fly ash. *In*: *87th annual meeting of the Transportation Research Board*. Washington, DC.

Wen, H., Warner, J., Edil, T., and Wang, G., 2010. Laboratory Comparison of Crushed Aggregate and Recycled Pavement Material With and Without High

Carbon Fly Ash. *Geotech.Geol. Eng*, 28 (4), 405–411.

Wesseloo, J., Visser, A.T., and Rust, E., 2009. The stress–strain behaviour of multiple cell geocell packs. *Geotextiles and Geomembranes*, 27 (1), 31–38.

Wilburn, D.R. and Goonam, T.G., 1998. *Aggregates from natural and recycled sources: Economic assessments for construction applications - a materials flow analysis. USGS Circular, 1176*. Reston, VA.

Williams, B.A., Copeland., A., and Ross, T.C., 2018. Asphalt Pavement Industry Survey on Recycled Materials and Warm-Mix Asphalt Usage: 2017, Information Series 138 [online]. Available from: http://www.asphaltpavement.org/PDFs/IS138/IS138-2017_RAP-RAS-WMA_Survey_Final.pdf [Accessed 9 Aug 2018].

Wright, Jr., F., 2001. Recycled Materials Policy, Federal Highway Administration [online]. *FHWA, Washington, DC.* Available from: https://www.fhwa.dot.gov/legsregs/directives/policy/recmatpolicy.htm. [Accessed 9 May 2018].

Wu, Z., 1999. Structural performance of cold recycled asphalt pavements. *In*: *Transportation Scholars Conference Compendium of Student Papers*. Ames, IA.

Yamamoto, K. and Otani, J., 2002. Bearing capacity and failure mechanismof reinforced foundations based on rigid plate-finite element formulation. *Geotextiles and Geomembranes*, 20, 367–393.

Yang, N. and Wang, R., 2015. Sustainable technologies for the reclamation of greenhouse gas CO2. *Journal of Cleaner Production*, 103, 784–792.

Yang, X., 2010. Numerical analysis of geocell-reinforced granular soils under static and repeated loads. The University of Kansas, Lawrence, KS.

Yang, X., Han, J., Parsons, R.L., and Leshchinsky, D., 2010. Three-dimensional numerical modeling of single geocell-reinforced sand. *Frontiers of Architecture and Civil Engineering in China*, 4 (2), 233–240.

Yang, X., Han, J., Pokharel, S.K., Manandhar, C., Parsons, R.L., Leshchinsky, D., and Halahmi, I., 2012. Accelerated pavement testing of unpaved roads with geocell-reinforced sand bases. *Geotextiles and Geomembranes*, 32, 95–103.

Zhang, A., Boardman, A.E., Gillen, D., and Waters, W.G., 2004. *Towards Estimating the Social and Environmental Transportation in Canada*. The University of British Columbia, Vancouver, Canada.

Zhang, L., Zhao, M., Shi, C., and Zhao, H., 2010. Bearing capacity of geocell reinforcement in embankment engineering. *Geotextiles and Geomembranes*, 28 (5), 475–482.

Zhang, Y., McKechnie, J., Cormier, D., Lyng, R., Mabee, W., Ogino, A., and MacLean, H.L., 2010. Life Cycle Emissions and Cost of Producing Electricity from Coal, Natural Gas, and Wood Pellets in Ontario, Canada. *Environmental Science & Technology*, 44 (1), 538–544.

Zhou, H. and Wen, X., 2008. Model studies on geogrid-or geocell-reinforced sand

cushion on soft soil. *Geotextiles and Geomembranes*, 26 (3), 231–238.

Biographical Information

Anu Muthumala George was born on October 4, 1990, in Cochin, Kerala, India. She graduated from Government College of Engineering, Kannur (GCEK), Kerala, India, with a Bachelor's degree in Civil Engineering in May 2012. After working in College of Engineering, Vadakara as an Assistant Professor, she pursued Master's in Civil Engineering with a specialization in Geotechnical Engineering from Indian Institute of Technology (IIT) Hyderabad, India. In IIT Hyderabad, she examined the effect of geocell reinforcement on improving the performance of weak sand beds using finite-difference models.

In 2015, she joined the doctoral program in the Department of Civil Engineering at the University of Texas at Arlington. She studied the effect of geocell reinforcement on RAP bases subjected to monotonic and repeated loading by performing experimental and numerical studies, under the guidance of Prof. Anand J. Puppala. She successfully defended her dissertation in November 2018.